TECHNISCHE
UNIVERSITÄT
MÜNCHEN

ANNUAL REPORT 2003
ZWE FRM-II

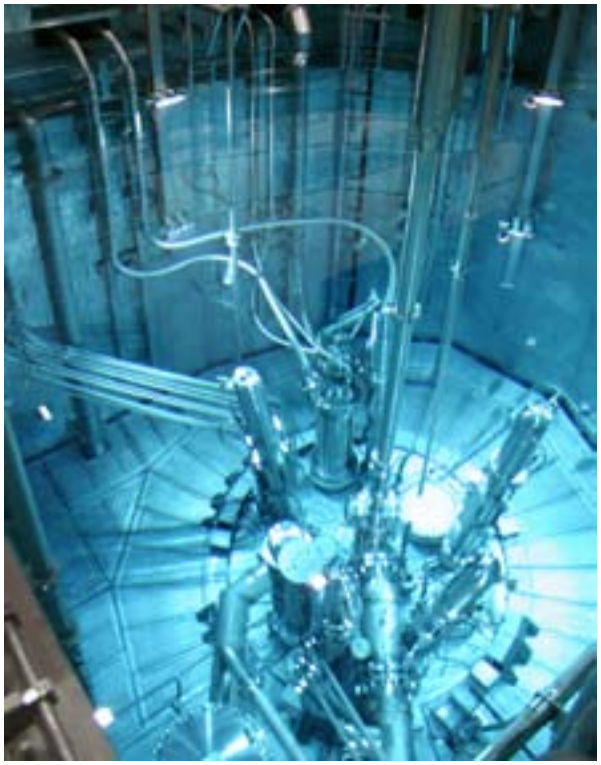

Contents

Director's Report

The Nuclear Start-up of the FRM-II

After a very long and difficult procedure the FRM-II obtained its license for the nuclear start-up and operation (3rd license) in May 2003 from the Nuclear Licensing Authority, the Bavarian State Ministry of State Development and Environment (StMLU), now renamed to Bavarian State Ministry of Environment, Health and Consumer Protection (StMUGV). The first draft for this license was submitted already in August 2000 and had to be agreed upon by the Federal Ministry of Environment and Reactor Safety (BMU). The final list of questions from this federal ministry was answered in January 2003 by Siemens/TUM and finally opened the way for the license. The 3rd license includes instructions for running the facility and the condition to develop a fuel element with reduced enrichment in ^{235}U.

The event of issuing the nuclear license for FRM-II has been celebrated by a visit of the Bavarian Prime Minister, Dr. Stoiber, the Bavarian Minister of Science and Art, Mr. Zehetmair and the Bavarian Minister of Environment, Dr. Schnappauf on June 4th at FRM-II.

With the 3rd license we immediately initiated the delivery of the heavy water for the moderator, the first fuel elements and the converter plates. We received the heavy water in June 2003 and the fuel elements in July 2003 as well as the primary neutron source for the nuclear start-up. The heavy water was filled safely into the storage tank. The fuel elements were inspected and measured by EURATOM and IAEA on its ^{235}U content one day after delivery.

Prior to the nuclear start-up a general inspection of all reactor components was required, since the starting of the systems in 2001 was too far away due to the long licensing procedure. The general contractor Siemens had to reestablish its working team for the nuclear start-up. The systems were also checked in respect to their long-term operational behavior and were improved accordingly.

The nuclear start-up from first criticality to full power will start in early 2004 and end with a continuous run at 20 MW in June 2004. Important steps are the calibration of the shut-down and control rods, the shut-down safety proofs, the power density distribution measurements, the neutron flux measurements, the power calibration and control and tests of the cooling systems. During this program the various special facilities such as Cold Source, Hot Source, Converter, irradiation facilities and silicon doping device will also be taken into operation. First neutrons will also be available to take into operation most of the 19 beam position instruments, currently under construction. It is expected that 14 of these instruments including the positron source will receive their first users with the start of the second fuel cycle. The nuclear start-up program ends with the burn-up of the first fuel element. Based on a report on the experience with the first fuel element the licensing authority is in the position to permit the routine operation of the FRM-II which will start with the 2nd fuel cycle.

Within the 6th frame work programme of the EU a **N**eutron **M**yon **I**ntegrated **I**nfrastructure **I**nitiative NMI 3 has been granted to the most powerful neutron and myon centers in Europe. FRM-II takes part and will welcome its first EU supported users in 2004.

The German Federal Ministry for Science and Technology starts with April, 1st 2004 a new 3 years period of grants devoted to facilitate the access of university groups to neutron and synchrotron facilities. University groups involved in the instru-

mentation of FRM-II will largely profit from this programme.

Construction work on the FRM-II site never ends. With help of the Bavarian investment programme in science and technology, HighTech Offensive Bayern, a center for industrial applications of the FRM-II neutrons is currently under construction. In Autumn 2004 the first industrial users will settle in the new labs and offices.

The use of polarized neutrons will be an essential tool for neutron research in the future. As a central service for the instruments a facility to produce polarized ^{3}He gas as filter medium for polarized neutron beams has been ordered in May 2003. A key ready system will be delivered in April 2004 at the site of the FRM-II with a capacity of 30bar·liters per day.

With the issue of the nuclear license our advisory boards have also changed. On October 9th, the "Projektbegeleitender Beirat", our advisory board during the constructions phase met for the last time. Prof. Dr. Tasso Springer who has led this board since 1994 has been honored by the Karl-Max-von-Bauernfeind medal. At the same time the new advisory board, now called Strategierat did have its constitutive meeting under the presidency of Prof. Dr. Gernot Heger.

Erich Steichele presenting neutron guides at the FRM-II

At the end of October 2003 Dr. Erich Steichele retired after 37 years of work devoted to neutron research at the Technische Universität München. Major projects of Eric Steichele have been a neutron time-of-flight diffractometer for high resolution studies and the development of neutron guide systems and neutron optical devices. At the FRM-II he worked from the very beginning on the design of the secondary sources and beam tubes as well as on the neutron guide system. For the new instrumentation he worked on the radiography stations and the reflectometer where he designed and realised the first twisted neutron guide. We wish him all the best for a long and prosperous retirement.

We commemorate the death of Jürgen Didier (Framatom/ANP) on Febuary, 2nd 2004. He was involved already in the concept and planing of the FRM-II and took over the responsibilities as project leader in 1994 until 2002. We appreciated him as a very competent and always friendly minded partner. Even in complicated negotiations he was willing to find a good compromise leading to a reliable solution without loosing his fundamental humor. We will keep pleasant memories of Jürgen Didier with building of our reactor.

Jürgen Didier

Guido Engelke Winfried Petry Klaus Schreckenbach

16.1.03 The group of french reactor operateurs (OEA) visits the FRM-II

10.3.03 Parliamentary group from CSU with Dr. M Mayer(MP) and J. Singhammer(MP)

4.4.03 A. Berg(MP) visits the FRM-II

7.4.03 J. Singhammer(MP) visits the FRM-II

20-22.5.03 Jahrestagung Kerntechnik in Berlin

4.6.03 Bavarian Prime minister Dr. E. Stoiber arrives at the FRM-II

4.6.03 Bavarian Prime minister Dr. E. Stoiber and Prof. W. Petry

4.6.03 W. Schnappauf, bavarian minister for environment, during his talk at the FRM-II

4.6.03 H. Zehetmair, minister of science, talks at the FRM-II

4.6.03 Prof. Dr. W. A. Herrmann (President of the TUM)

1.10.03 B. Bigot (Haut Commissaire à l'Energie Atomique), Reg.Dir. B. Schmid (StMWFK) and Min.Dir. Dr. H. Schunck (BMBF) visit the FRM-II

30.10.03 Production of the internal safety instruction film

9.10.03 Prof. Hermann awards Prof. T. Springer with the Karl-Max-von-Bauernfeind medal for his long-standing support of FRM-II

30.10.03 The FRM-II building in October 2003

1 Central Services

1.1 Detector and Electronics Laboratory

K. Zeitelhack [1], **A. Kastenmüller** [1], **S. Egerland** [1], **D. Maier** [1], **M. Panradl** [1]

[1] ZWE FRM-II, TU München

Corresponding to the progressive commissioning of the scientific instruments at FRM-II the main tasks in 2003 were to give service and assistance. In parallel a few research and development projects could be pursued and the upgrade of the laboratory infrastructure continued.

Detectors

For most of the neutron scattering instruments we took care of inspection and adjustment of detectors and readout electronics purchased. An important part of this job was the quality control of 605 squashed ^{3}He-detectors (filling gas: ^{3}He/CF_4 97/3; p=10 bar) installed at the *TOF-TOF*-spectrometer. Developed with Eurisys-Mesures these detectors show an improved charge collection due to the CF_4 admixture. This should result in a better homogeneity and improved TOF-resolution for thermal neutrons. Fig. 1 shows the pulse height spectrum of thermal neutrons from a ^{252}Cf-source recorded with the new detector type 120NH40RTF using fast readout electronics (0,5 μs shaping) in comparison to a conventional Dextray type 90NH40Rec squashed series detector.

The detectors were delivered in 5 batches within the period of a year. Quality control included verification of mechanical dimensions using a semi-automatic measuring bench designed by our group and recording of pulse height spectra using thermal neutrons from a ^{252}Cf-source for every single detector.

All detectors kept within the mechanical specifications and revealed good homogeneity in gas gain and energy resolution independent of the batch. The relative deviation (1σ) in gain of the complete detector ensemble was determined to 2.4 %. Three detectors showing a significant deviation could be proven to be leaky and were replaced.

Instrument Control and Readout Electronics

Installation and commissioning of components for instrument control or detector readout systems took a center stage in 2003. Commissioning

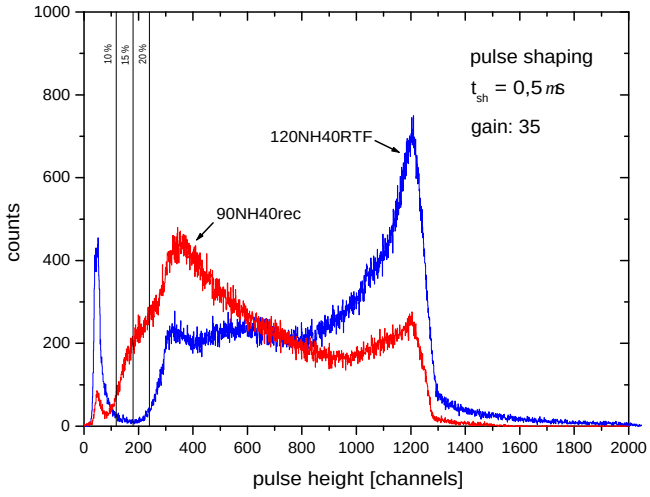

Figure 1.1: Comparison of the pulse height spectrum of thermal neutrons recorded with a 120NH40RTF and a conventional 90NH40Rec detector

of the remote controlled bias and HV-supply system for the *TOFTOF* detectors and completion of slow control components for the Intense Positron Source *NEPOMUC* or the experimental site for very cold neutrons *MIRA* comprising a vacuum & dosimetry interlock, remote bias and magnet power supply, fieldbus integration, pressure valve and motion control were some major issues. Beside these projects the assistance to instrument scientists in all technical questions related to electronics was a main task.

Several neutron scattering instruments have been equipped with our FRM-II standard readout electronics developed for ^{3}He- and ^{235}U-fission detectors. It consists of a amplifier/w-discriminator unit with variable shaping time, a remote controlled 3HE 19"-crate for bias and HV supply and instrument specific PCI/cPCI data aquisition boards [1]. Meanwhile, we developed a whole family of detector data acquisition boards for counting, Time-of-Flight measurement or pulse height analysis in neutron scattering experiments. These boards consist of a commercial PCI/cPCI or VME carrier board [2] and an appropriate M-module designed for the application required. The M-module types available are

- a counter/timer/ratemeter module. It carries four 32-bit counters with opto-isolated inputs that can be set as master/slave and operated in absolute, preset, timer or ratemeter mode. In addition, it provides 2 programmable I/O channels
- a multichannel scaler module (MCS). It provides 8 input channels, 1 μs - 32 s dwell time, 8 ms - 150 h time span (8k full memory depth), 32 bit memory capacity. It can be operated in internal or external trigger mode. Start of time span can be delayed to Trigger from 0 - 18 h
- a multichannel analyzer module (MCA). It provides 4 input channels and a 12 bit peak-sensing ADC. It can be operated in gated or self triggered mode. A prototype module has been successfully tested

Control software and drivers are available for FRM-II instrument software TACO or LABVIEW.

[1] Zeitelhack K., Kastenmüller A., Maier D., Panradl M. *annual report*.
[2] MEN mikro-elektronik, Germany.

1.2 Project HELIUS – Polarized ^{3}He for Neutron Instrumentation

S. Masalovich [1], **G. Borchert** [1], **W. Petry** [1]

[1] ZWE FRM-II, TU München

Polarized nuclei of helium-3 possess very high spin-dependent neutron absorption efficiency over a wide range of neutron energy. Neutron spin filters (NSF) based on a dense hyperpolarized ^{3}He gas may compete in polarization efficiency with such common devices as magnetized single crystals, supermirrors or soller guides. Although these latter are rather simple in operation, their applications are strongly limited by acceptable neutron energy and scattering angle range. By contrast, the broadband neutron spin filter can be sized and shaped in such a way that it will meet just about all practical needs. Until recently, the main disadvantage of this technique was a limited possibility to produce highly polarized ^{3}He gas. However, the progress achieved during last years in this area nearly eliminates this limitation. At present the ^{3}He setups at the University of Mainz (Germany) and at the ILL (Grenoble, France) feature a production rate 30 bar·litre/day for highly polarized ^{3}He gas with polarization of around 65%. Both setups utilize the direct optical pumping of metastable ^{3}He atoms in ^{3}He plasma at about 1 mbar. After

subsequent compressing, the polarized gas at a pressure of a few bars may be collected in a detachable cell of a given size and shape and then transported to a neutron instrument. Experiments performed at the ILL showed a high efficiency of NSFs over a wide range of experimental conditions.

On July 2002 the expert's meeting "Realization of a ^{3}He facility at the FRM-II" has been held at Garching. The main outcome of this meeting was a general agreement about the necessity of a ^{3}He polarization facility at the FRM-II. A way to obtain such a facility was seen in a close cooperation with partner laboratories at Mainz and Grenoble.

Fig. 1.2 shows the most general scheme of the production of a polarized ^{3}He gas and delivering this gas for neutron experiments.

This scheme can be divided into three levels:

- production of dense polarized ^{3}He gas (^{3}He facility)
- delivery of this gas to neutron experiments without losing a polarization (transportation)
- the use of a polarized gas in neutron experiments with proper environment conditions (neutron experiments)

The most crucial part in this scheme is certainly the production of polarized gas. At present this facility is under construction in Mainz and expected delivery time is April-May 2004.

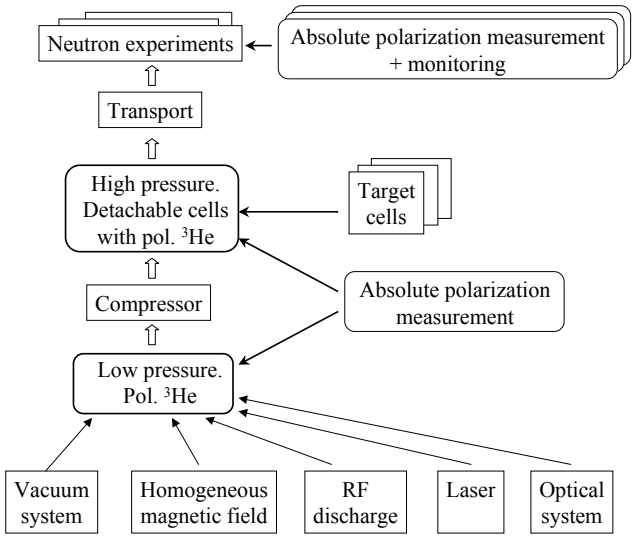

Figure 1.2: General scheme of the production of polarized ^{3}He gas

During last year all necessary preparations were made at the FRM-II to provide this facility with required infrastructure:

- the construction of a special "nonmagnetic" laboratory for the ^{3}He setup is started at the local area,
- the laboratory for the cells preparation is built and partly equipped.

In the context of the agreement for cooperation Dr. Masalovich (TU München) stayed for ten months at the Johannes Gutenberg University of Mainz where he learned the theory of the optical pumping and practice of the production of a polarized gas. During his visit a new method for the precise measurement of a dense gas polarization has been proposed in a close cooperation with the University of Mainz. The first test measurements showed good results. This work will be continued in the next year.

During two-month stay at the ILL (Grenoble, France) Dr. Masalovich was able to learn the practice of polarized ^{3}He production there as well as NSFs application for neutron instrumentation. Polarized gas transportation to a neutron experiment site and magnetic shielding for polarized gas at an experimental site were of particular interest. This visit and knowledge transfer became feasible due to the goodwill of the ILL and financial support from the European Community. In general, this visit is considered to be a first step in a new close collaboration between the Technical University of Munich and the Institut Laue-Langevin.

After construction and installation of the ^{3}He facility and preparation of necessary infrastructure the first neutron spin filters is expected to be available in summer 2004.

1.3 IT-Network Services

Jörg Pulz [1], **Felix Zöbisch** [1], **Jakob Mittermaier** [1], **Roman Müller** [1], **Joseph Ertl** [1], **Sebastian Roth** [1], **Sebastian Krohn** [1], **Christoph Herbster** [1], **Jörn Beckmann** [1]

[1] ZWE FRM-II, TU München

Overview

Due to a significant growth of the network, central servers had to be replaced and changes in the architecture of the network where done. Major efforts and achievements of this year were:

- Integration of the Reactor Operations Network and the Scientific Network into one FRM-II Network
- LDAP Server as method for unified access to user information
- New Mail-Servers
- New FTP-Server
- Terminal-Server Farm put into operation
- Cabling of instrument networks
- Updated version of the Taco-Box distribution
- Setup and testing of a Document- and Workflow-Management System

The FRM-II network is separated into subnetworks. Each instrument, administration, reactor crew and the servers have their own subnet. Guests will be able to connect their laptops to a special network which will allow Internet access but limits the access to internal networks for non-authenticated users. The separation of the individual networks is done by means of Access Control Lists (ACLs) on the central router. The connection between the FRM-II network and the Internet is provided by a two-stage firewall. Public accessible services are placed in the Demilitarized Zone (DMZ) between both firewall stages. The architecture of the FRM-II network is shown in Fig. 1.3.

Unified Access to User Information

Different Operating Systems require different protocols to store and exchange User Information. With a common username different passwords have to be set

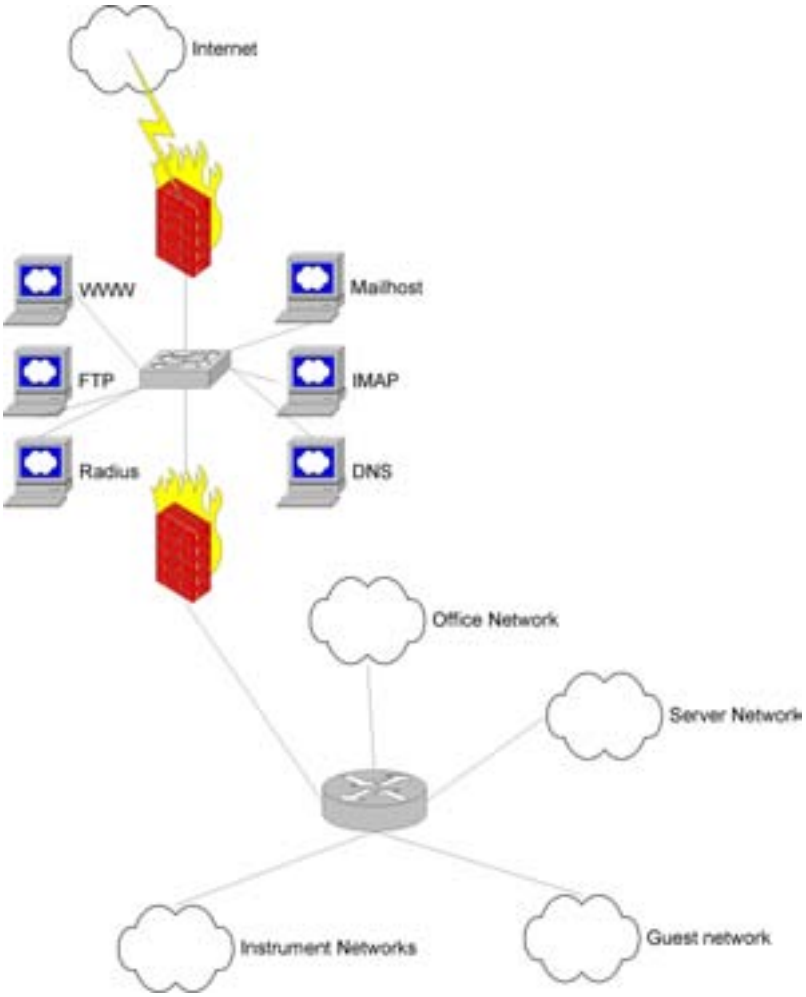

Figure 1.3: Architecture of the FRM-II network.

for individual systems. Up to now this was done by the GeNUA User-Manager, a set of Perl Scripts running on Unix systems. For a new server the scripts had to be changed.

In order to construct a robust multi-platform User Management System, LDAP was chosen as the central information repository. For redundancy one Master Server holds the information and distributes them on Slave Servers. The Slave Servers offer read-only access and replace the Master Server in case of failure. To add new information or to change already stored information access to the Master Server is necessary. LDAP offers password protection and is able to limit access to parts of the directory based on role and user information. We decided to use OpenLDAP [1].

New Servers for FTP and Email

For older Unix systems, were NIS is still required, NIS maps are created for the LDAP repository.

Furthermore the LDAP system is used for authentication purposes using the Samba [2]systems (access of Windows machines to Unix servers) and Radius [3](external connections).

As already mentioned in section 1 the old Mail Server was not able anymore to handle the user load. The old Server was based on the Post Office Protocol (POP) where users download their Email from the server and store the Email on their local machine. This is impractical for users working on more than one machine and also a security issue, as POP sends passwords unencrypted over the network. Therefore IMAP was chosen as the protocol for the new Mail Server. IMAP stores the Mail on the server and allows users to create subfolders which could also be shared with other users. As the Email is stored on the server a central backup is possible and the user can access his or her Email from all computers inside the network.

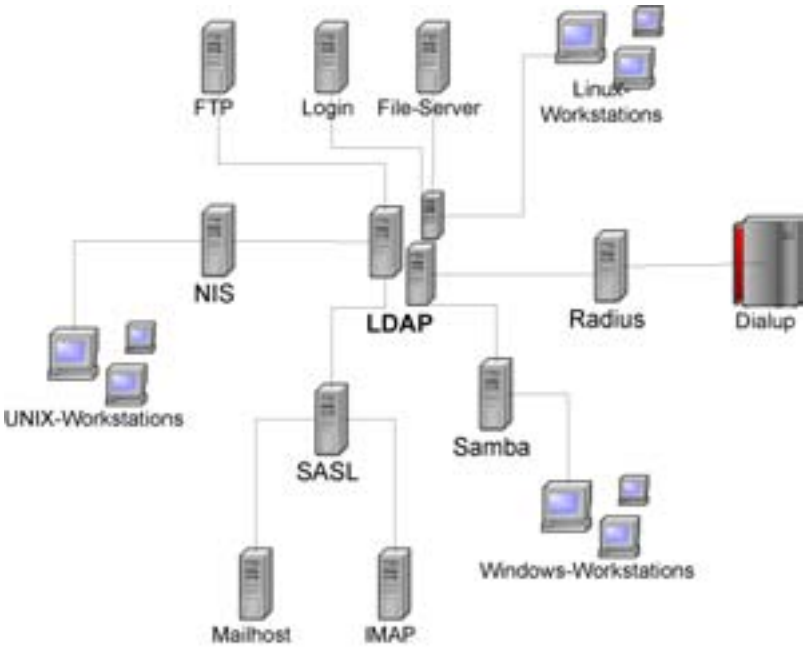

Figure 1.4: Hierarchy of User Information Systems and Protocols

Major concern with Email nowadays are malicious content and spam. To cope with this the new server was equipped with Virus and Spam Filtering functionalities. Mail processing is shared between two servers. The server for incoming messages is “mailhost”. On this machine Postfix handles Email. The Add-on Amavis [4] connects Sophie [5] as virus scanner with Postfix. Sophie is a daemon process which uses the Sophos library to check incoming mails. After the virus check is passed, SpamAssasin [6] performs header analysis, text analysis, consults blacklists and the Razor signature database to filter out unsolicited bulk Email. Messages which have passed the tests are handed over to Postfix for further processing. If it was sent from a FRM-II computer Postfix finally checks with the LDAP Server if the user exists and rewrites the “From” field in the Mail Header accordingly. If the Emails final destination is inside the FRM-II network it is handed over to the IMAP Server for further processing.

On the IMAP server Sendmail first checks with the LDAP Server, if the recipient exists and forwards the Email to the Cyrus IMAP Server. Users can collect their Email directly from Cyrus

IMAP, if they have an IMAP Client and reside inside the FRM-II network. Users from, outside can use the Webmail interface provided by Squirrel Mail [7]. Squirrel Mail offers full HTTPS access to IMAP servers and allows to manage Sieve Scripts on the Mail Server. A function to change the user password in the LDAP repository is also included. Authentication of users is via regular IMAP login. The Apache Web Server (with modules) offers direct authentication by means of the LDAP Server. In Fig. 1.5 the blue arrows show the way, an Email takes through the different programs. The red arrows show authentication requests of the different servers and the green arrows show user information requested from the central LDAP repository.

On our mail servers the data transfer is limited to 10 MB per Email. To exchange larger files with external partners an FTP server was built. FTP is not a secure protocol and transfers passwords unencrypted. To prevent users from sending their passwords unencrypted through the Internet, our FTP server only accepts authenticated logins from inside the FRM-II network and anonymous logins only from the Internet. Every upload is virus checked and reported to the admins. Files in the incoming and outgoing section are removed automatically after 7 days.

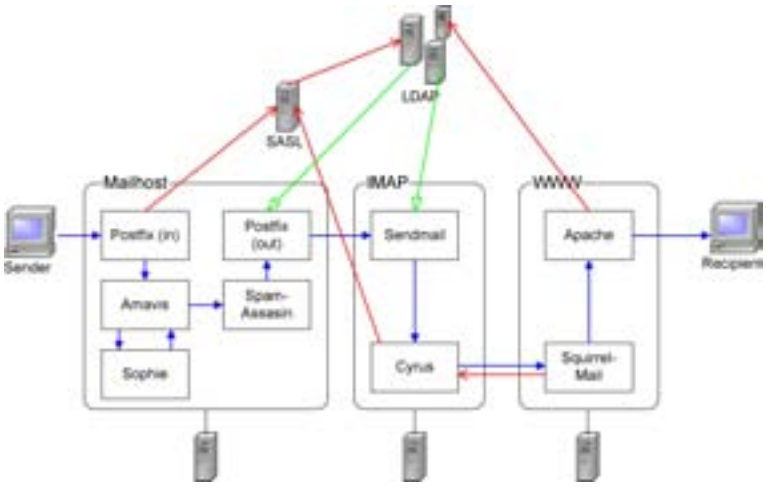

Figure 1.5: The Mail system at FRM-II. Blue arrows show the way an Email takes through the server hierarchy. The red arrows show Authentication requests and the green arrows show User Information provided.

Roll-out of the Windows Terminal Server Farm

The configuration and idea behind a Windows Terminal Server was already explained in last years report. Just as a reminder, our server farm consist of three dual-Xeon 2 GHz servers with 4 GB RAM with Citrix MetaFrame XPa. Standard Software is installed on all three machines. User can either connect a full desktop session or open single applications. If the user requests just an application a scheduler decides to which of the three servers the user is connected. In case of full desktop sessions the user can decide to which of the servers he wants to connect. Clients for MetaFrame XPa are available for all major operating systems like Windows, Linux, MacOS and IRIX. The client is able to map local drives and printers to the server.

The Terminal Server Farm was widely accepted by users. Not only Linux users, but also many Windows users installed the client and started to use software on the server. This profoundly reduced software installation requests on user machines. As a second effect software costs where also reduced. Expensive scientific software was placed on the server farm and could be used there by all interested users. Also non-standard graphics software, which is only needed to view or convert files received from coworkers, is restricted to terminal server usage.

Although the Terminal Server Farm was a huge success some problems occurred during the roll-out phase. Not all software was able to run on MetaFrame servers.

In conclusion the roll-out of the Terminal Server Farm was a success. Though the break even is not yet reached, user numbers are increasing while support requests are decreasing. By providing a standard TeX environment to all users, the Terminal Servers even helped to produce this report with less effort than last year.

Realization of Instrument Subnetworks

By providing an individual broadcast domain to each instrument, interactions between instrument control software should be kept to a minimum. The networks are designed in a way, that they can operate independently from the FRM-II network, in case of failure. Each instrument networks contains a switch and the instrument control hardware required. In addition it is highly recommended to install an instrument server. This server provides basic services like DNS, DHCP or File Sharing (NFS or CIFS). Acquired data will be temporarily stored on the instrument server, a failure of the central FRM-II file server will therefore not influence instrument operation. The same holds true for DNS and DHCP, in addition the local servers help to reduce network traffic by keeping local traffic local. If no additional tasks should be performed by this server, a mid-class PC (P-III 1 GHz or above) is sufficient.

The Taco-Box Linux Distribution

The Taco-Box Linux distribution for embedded instrument control devices has been renewed this year. The idea is to place small devices running Taco next to the hardware to be controlled. One application for this is to provide Ethernet connection for devices with just a serial port. Our Taco-Box Linux Distribution is derived from SuSE 7.2. Together with Taco it fits on 6 disks, occupying 10 to 12 MB after installation. So far we have used the Taco_box distribution on JumpTec and ICP Wafer computers. The first disk contains the boot image, the next two disks Tacobox A and B contain the major operating system, disk 4 contains SSH and SSL, disk 5 the kernel and disk 6 the Taco system itself. Installation could either be done with monitor and keyboard, but the latest release also supports a serial console for installation. After installation the system could be accessed either by keyboard, serial console or remotely via ssh. The Taco-Box Distribution supports NE1000, NE2000, Cirrus Logic CS8900 and CS8920 network cards, multi-port serial interface cards and the PC104 bus.

Details about the Taco-Box Linux distribution and disk images can be found on the FRM-II website.

Planing of a central Document- and Workflow-Management System

In conjunction with the planing and construction of FRM-II large amounts of paper have been created and must be stored. Furthermore paper files might get misplaced or damaged. The idea is to store all legal required information about the FRM-II and its operation in an electronic storage. Such Document Management Systems (DMS) are already in use and become more popular with eGovernment projects. Such systems may not only be used to store documents but to also define a work-flow for repeating tasks.

As a pilot study the first step is to bring a system for electronic distribution and storage of snail mail and for electronic procurement into operation. Requirements for such a system are, that it is possible to use it from Linux and Windows clients and that the server should also run under Linux. We decided to use the Software Fabasoft, which is already in use at major Austrian Government offices.

Incoming mail is first scanned and then electronically forwarded to the recipient. The scanned document can be put into an electronic file or passed on. Order forms can be filled in on the system and electronically passed on for approval. The defined workflow then processes the order and passes it on to all persons who need to approve it. Finally the approved order comes back to the issuing user. The user then can implement the order and also passes on the approved form to the administration. When the administration receives the bill the ordering user has to approve the bill and the administration pays it. The whole process is done electronically. If the supplier needs the order on paper, it is possible to create a printout of a standard order form from the system, but the rest of the ordering process is filed electronically.

A pilot system for 50 users is installed and training of pilot users takes place in the moment. The roll-out of the order processing workflow will take place at the beginning of next year. After 6 month the process will be

evaluated and a decision on further steps taken.

[1] Zeilenga K., Chu H., Masarati P. OpenLDAP. http://www.openldap.org/.
[2] Tridgell A., et al. The Samba Project. http://www.samba.org/.
[3] Project F. S. The FreeRADIUS Server. http://www.freeradius.org/.
[4] Bricart C., Link R. AMaViS – A Mail Virus Scanner. http://www.amavis.org/.
[5] Hrustica V. Sophie. http://www.vanja.com/tools/sophie/.
[6] Dinter T. V., Findlay D., Hughes C., Mason J., Quilan D., Sergeant M., Stretz M. S. SpamAssasin. http://au.spamassassin.org/index.html.
[7] Castello R., et al. Squirrel Mail – Webmail for Nuts. http://www.squirrelmail.org/.

1.4 The Neutron Guides at FRM II

Ch. Schanzer[1], **E. Kahle**[2], **G. L. Borchert**[2], **D. Hohl**[3], **S. Semecky**[4]

[1] Physikdepartment E 21, TU München
[2] ZWE FRM-II, TU München
[3] D. Hohl, Technische Dienstleistungen, München
[4] S. Semecky, Kommunikationstechnik, München

During the year 2003 the construction of the neutron guides (NG) at FRM II was accomplished. It comprises the following tasks:

1) The adjustment of the NG was performed by means of theodolites reaching high mechanical tolerances. Maximum displacement of two consequent glass elements is less than 10μm, at complex positions, as junctions, less than 20μm, angular mismatch less than 15arcs and less than 45arcs in horizontal and vertical direction, respectively.

Figure 1.6: The tunnel wall, seen from the casemate side after completion. The vacuum tubes sticking out of the steel plates are connected with the high speed shutters. At their exit the vacuum tight NG follow, which are supported by the steel bars (first one is brown).

2) In section 0 and section 1 of the FRM II the NG are enclosed in stainless steel tubes equipped with conventional vacuum fittings. These sections have been checked for vacuum tightness of less than $2 \cdot 10^{-2}$ mbar. In section 2 of FRM II (NG hall and casemate) the glass NG have to be vacuum tight, except NL 2b. Therefore all consequent glass tube elements were glued together. The final element was equipped with an Al window that withstand the vacuum pressure and is transparent for neutrons.

3) All NG in the NG hall have been jacketed by 7cm thick lead plates.

4) The three openings in the tunnel wall where the NG NL1 to NL6 pass through have been closed. To reach the maximum shielding a sandwiched structure

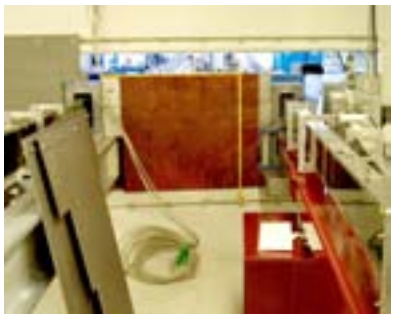

Figure 1.7: Closing the 80cm thick casemate wall towards the NG hall. Between the lead jacketed NG and the high density concrete blocks (brown) are visible the light-grey steel containers, filled with concrete, which are precisely fitted into the remaining gaps. On the left side the steel plates for final closure can be seen.

of materials was used. Starting from the casemate side, we introduced one layer of 10cm lead, one layer of borated PE, 16cm thick. The remaining 155cm of depth were filled with Röbalith type 4 bricks (density 3.2g/cm^3). As the NG pass at skew directions through the openings the bricks were cut so that they fit precisely in the gaps. All bricks are arranged in a way so that no through-running slits occur. Remaining slits at the borders were closed with lead wool. From outside the openings were covered with steel plates (see Fig. 1.6).

5) The openings in the casemate wall were closed with high density (4.5g/cm^3) concrete units. To scope for the skew directions of the individual NG stainless steel containers were produced that fit precisely in the prismatic gaps (see Fig. 1.7). They were filled with the high density concrete and inserted into the gaps. Remaining slits at the borders were closed with steel plates or lead wool. Finally the openings were covered on both sides with steel plates. In Fig. 1.8 and Fig. 1.9 the completed wall between casemate and NG hall is shown. A final overview of the NG hall is depicted in Fig. 1.10.

Figure 1.8: the completed casemate wall. The individual NG running through the casemate pass the wall towards the NG hall.

Figure 1.9: The accomplished wall of the NG hall. On the final steel cover several shock sensors of the safety system are visible. All NG are jacketed by the (blue) lead plates.

6) The high speed shutters of NL1 to NL6 have been installed completely and integrated into the central control system. In a first test it was observed that the accuracy of the used vacuum sensors was not sufficient for a reliable operation. After some systematic tests they all were replaced by another high accuracy type. Now the complete shutter system works in the expected way. For three NG we installed the corresponding instrumental shutters.

Finally all tasks have been completed successfully so that the instruments can make full use of the NG facility, provided neutrons are available.

Figure 1.10: A general view of the NG hall. The completed NG run to their instruments or end at the position where in next future the corresponding instruments will be built.

1.5 Progress Report of the Sputtering Device for Supermirrors

C. Breunig [1], **Prof. Dr. G. Borchert** [1], **A. Urban** [1]

[1] ZWE FRM-II, TU München

Production of Supermirrors

For conducting the thermal neutrons from the source to various experiments the research-reactor is equipped with 437 meters of neutron guides, produced by two companies, partly in cooperation with the sputtering-team of the FRM II. As this team operates a self made sputtering device, part of the supermirrors i.e. glass-plates with thin multilayers consisting of increasing alternating layers of titanium an nickel in a magnetron sputtering process were produced there. Finally the glass-plates were glued together to build a rectangular vacuum tight neutron guide. To check the performance our supermirrors are measured at the neutron beam of BENSC in Berlin. After concluding 75 sputtering processes which means an amount of 11,7 m^2 super mirrors of quality 2.0 and 1.8 m^2 of quality 2.5 from January up to the end of February in 2003, the sputtering device was dismantled.

Rebuilding the facility

Apart from the fact that the laboratory was renovated and joint with a neighboring room some important modifications at the sputtering device itself were started. To fill the conditions of getting optimal atmosphere and clean circumstances the slide vane rotary vacuum pumps were installed in the basement under the laboratory for keeping the atmosphere oil-free. Additionally there was installed a complete cleanroom cabin (purity class 1000) with a direct air lock to the sputtering device for encamping, preparing and cleaning the glass before the sputtering process.

Apart from these modifications of the surrounding area of the sputtering plant some new features were mounted directly at the installation itself. The most obvious innovation is a third vacuum chamber fitted directly to the main chamber where the sputtering-procedure takes place.

Figure 1.11: Sputtering facility

In this sluice the cleaned glass-plates will be prepared for the subsequent process by using a infrared substrate-heating in order to detract last water oddments. Furthermore for guaranteeing a dirt-free surface, the glass is cleaned by a fluorescing plasma to debar last impurities. One more positive effect of this new sluice is, that the process itself is accelerated because pumping times can be reduced and parallel procedures are possible. Another innovation was done inside the main vacuum vessel, the new drive train consisting of a link-age for facilitate consistent speed and ensure the drive-train-unit maintenance-free. For the whole process control a new Labview system is installed, enabling a fast and simple communication with the device.

With the beginning of the year 2004 the production will be restarted with improved quality.

1.6 Sample Environment

J. Peters [1], **H. Kolb** [1], **A. Schmidt** [1], **A. Pscheidt** [1], **J. Wenzlaff** [1]

[1] ZWE FRM-II, TU München

In 2003 the main activities were focused on further development of our closed cycle refrigerators and high temperature equipment.

Closed Cycle Cryostat

Extensive tests were done on our new sample tube closed cycle refrigerator CCR2 resulting in an improved performance. Features are the compact design and easy handling. The initial cool down time from room temperature to 3.5 K now is about 4 hours. Three additional cryostat's will be ready for use early 2004. Sample holders allowing temperatures from 3.5 K up to 700 K are available. Sample cool down times are about 1 hour depending on initial temperatures. In co-operation with the Walther Meissner Institute, Garching, ^{3}He/^{4}He dilution inserts are under construction. Appropriate gas handling systems are being mounted actually. In co-operation with the FRM II software team, an automatic cool down procedure was successfully tested.

Magnet

After completing the design review our cryogen free superconducting split coil magnet is under construction at ACCEL Instruments GmbH. The magnet will provide a vertical symmetric magnetic flux of 10 T, a split of 30 mm and a room temperature bore of 100 mm. Delivery is planed early 2004.

High Temperatures

In co-operation with Paul Scherrer Institute (PSI), a FRM-II type high temperature furnace built for the structure powder diffractometer (SPODI) was successfully tested with neutrons in April 2003. SPODI instrument responsible R. Gilles and co-workers accomplished SANS measurements on Ni-base superalloys at temperatures up to 1700 K.

An IR-radiation furnace allowing temperatures up to 1700 K, providing a 40 mm beam window and a horizontal access of 360° is under development. The furnace can be evacuated or operated using diverse atmospheres. Heating is done via four commercially available

Figure 1.12: Top loading Closed Cycle Cryostat CCR2

reflectors equipped with 150 W halogen lamps. To achieve highest temperatures the sample size is restricted to the the filament dimensions (3 x 5 mm). First tests are very promising.

High Pressure

A co-operation with the Bayerisches Geoinstitut Bayreuth has been initiated for the developement of a diamond anvil cell suitable for neutron scattering experiments.

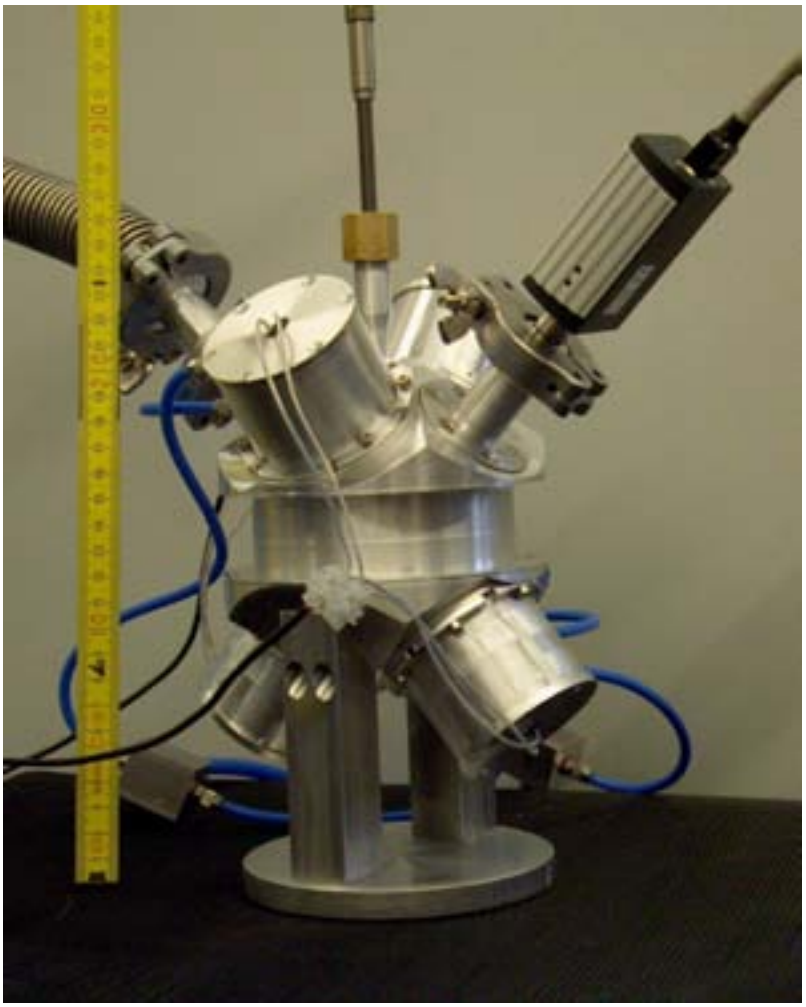

Figure 1.13: IR-furnace

1.7 Software Group

J. Krüger[1], **S. Praßl**[1], **H. Gilde**[1], **S. Roth**[1], **U. Graseman**[1], **S. Huber**[1], **A. Fuchs**[1], **M. Salfer**[1], **S. Kreyer**[1], **J. Beckmann**[1]

[1] ZWE FRM-II, TU München

The main activities of the software group of the FRM-II in 2003 were on the following fields:

- Improvement of the basic TACO system in close cooperation with the ESRF
- Improvement of current TACO servers
- Development of a database driven system for creation and management of TACO devices and servers
- Enhancement of the TACO LabView server
- Enhancement of the "TACO-box" in collaboration with the IT/Network service group
- Recoding of the openDaVE software

TACO basic system

In 2003 software groups of the ESRF[1] and FRM-II decided to put the TACO system on Sourceforge[2]. The main advantage is to get an infrastructure for developing and improving the TACO system. In view of error handling and future extension. The first step was to merge the code bases of the ESRF and FRM-II into a common one. Into this merge a new designed database server entered, which may use the "old" GDBM[3] as well as the "new" mySQL[4] database. The mySQL database gives the user much more flexibility for changing resources.

In addition to the current systems we adopted the code to run also on a FreeBSD system which allows to use the TACO system also on BSD based systems like Mac OS X.

TACO servers

During the last year we improved and stabilised the existing TACO basic servers. Some new basic servers were written, especially servers which provide the communication through several bus systems and several communication protocols.

The following servers belong to this group:

RS232

With the help of this server one may communicate directly with a connected device. That way one may send a request or command to the device and get the answer from it. The communication is not restricted to ASCII commands, it can also be used for binary communication protocols. An additional feature is the possibility to send series of communication requests, without interruption.

Server for ModBus Protocol Göttingen

Server for GPIB

This new server was developed for the communication over the GPIB interface. The first version of this server was based on the developments of the Linux-GPIB[5] group on Sourceforge, which restricted the possible selection of GPIB cards. However, this library supports most of the standard cards.

In a next step the server was extended to the National Instrument High-Performance Ethernet-to-GPIB-Controller NI GPIB-ENET/100. This controller will be used by the PUMA experiment. Due to the library compatibility of the free implementation to the NI library it was only necessary to bind the NI library to get a running system.

This server has the same set of commands as the RS232 server. Thus one may change the communication path without changing the software (tested on the LakeShore 340 controller, with RS232 and GPIB communication interface).

Server for Profibus DP

Based on the server developed at the ZEL at the FZ Jülich[6] we have completely rewritten the server for the Profibus DP. The reason for the rewrite was to extend the server by some new commands for reading and writing

- bits
- words (short int's in C/C++)
- double words (long's in C/C++)
- floats
- double floats

directly to the Profibus DP. The advantage of direct writing or reading these types directly is to avoid the conversion of the data on the client side resulting in simpler use of the Profibus DP.

As the old server uses the OIC (Objects In C) model, and all servers at the FRM-II are written in C++ we decided to rewrite this server.

In addition to the communication TACO servers we developed some servers for more specialised tasks.

Temperature controller like Eurotherm 2404 and LakeShore 340:

Both servers provide the same set of commands so it will be possible to use the same client for both servers. This allows the user to use parts of software developed by other users.

Vacuum gauge Leybold IT90 and and Vacuum gauge controller ITR23

Both devices provide the same set of TACO commands. Thus the client software does not need to support both. The device may also be used as analogue input devices. This is a standard device client class for all devices which give analogue inputs to the experiment control software.

Turbo molecular pump controller NT20

This device only gives some information about the status of the pump controller. The controller

does not accept any commands from the serial line.

Motor control of the HeiDi experiment

The HeiDi experiment uses a SIEMENS PLC S7 for controlling the motors and encoders of the sample table and the detector. The S7 is connected to the computer by a Profibus DP interface. This server exports right now 4 motor and 4 encoder devices to access all four axes. It will be extended by a device to control all axes simultaneously.

TACOdevel

This project is a database driven system for developing and managing the TACO devices and servers. With the increasing number of TACO devices and servers one gets problems with the TACO commands of the servers.

TACO implies the following rules:

- Devices belong to classes with the same set of commands.
- Commands are only numbers
- Servers export devices

The problem of this philosophy is that there is no way to check the rules. Therefore we use a mySQL database to store the commands of all devices as well as the information which server may export what devices. From this database one may create a code frame into which the current implementation of the commands of the devices has to be coded. This framework allows us to speed up the development of new TACO servers because the coding of the setup of a server is taken by the framework.

Another advantage of TACOdevel is the consistency of all TACO clients. The number of client classes is drastically reduced because only for one type of device a client class exists. Usually the control software needs mainly the following types of devices:

- **analogue outputs**
  like motor positions, voltages, temperatures.
- **analogue inputs**
  like encoder positions, voltages, temperatures.
- **digital inputs**
  like counter presets, timer presets, switches.
- **digital outputs**
  like counter values, limit switches, timer values.

Each device, additionally to its basic functionality, needs some commands for setup etc. Therefore we divide these basic groups into subgroups, summarizing devices with same functionality like temperature controllers, motors, or temperature sensors. These classes inherit the functionality of their base classes.

Thus, the first step of developing a TACO device for a new hardware reduces to look for a similar device in the database and to integrate this device into the new server. After this, the basic code has to be generated from the database. Afterwards the real implementation of the server device starts. Usually the client is ready then.

TACO binding to LabView

Based on the development by Andy Götz from the ESRF we developed a new TACO server to interface LabView. We looked for a possibility to integrate this powerful control software. Because some commercial products, especially sample environments like high field magnets, are controlled by LabView programs. LabView is shipped with some powerful mechanisms to execute external (native) codes. One of these mechanisms allows developers to invoke external library function calls from within LabView. This port was used at the ESRF, and we used it to access the LabView controls and indicators. With our extension it is possible to integrate LabView VI's (virtual instruments) into a LabView TACO server.

The access to LabView with the help of our solution is kind of generic and should work with most VI's.

Additionally we tested the network transparency of LabView (the LabView Control may run on a different computer than the TACO LabView server).

TACO box

"TACO box" is a small floppy disc based linux distribution derived from a SuSE 7.2 distribution, which can be installed on an embedded PC with reduced functionality. It provides only those features necessary to run a TACO system including the database and some simple TACO servers like RS232.

The main application of such servers is the TACO binding of sample environments, like high temperature ovens, or cryostats. With the help of such embedded controllers add these sample environments can be added into the experiment control software very easily. The hardware is added by plugging in a network cable, and the software by importing the TACO devices.

Reengineering of openDaVE

In the first half of the year the old openDaVE was rewritten by one of its creators, U. Graseman. It was shown, that some of the first implementation details were clumsy implemented. The system contained some restrictions which were not very helpful in practice.

These restrictions are removed in the new implementation.

It changes the design to a less restrictive system. The data flowing between the modules may be data in the old sense, commands, events or whatever. So the system became more flexible than the old one.

[1] http://www.esrf.fr.
[2] http://taco.sourceforge.net.
[3] http://www.gnu.org/software/gdbm.
[4] http://www.mysql.org.
[5] http://linux-gpib.sourceforge.net.
[6] http://www.fz-juelich.de/zel.

1.8 NICOS – The ease of getting TACO servers

T. Unruh [1], **C. Geisler** [1]

[1] ZWE FRM-II, TU München

Since the development of the first version of the network based instrument control system NICOS in 2001 it is advanced to an accepted frontend for the TACO system at FRM–II. Besides the NICOS client especially the NICOSMethods which have been described in the FRM–II annual report 2002 are intensely used. NICOS is currently used at 4 instruments at FRM–II: The polarised cold neutron three–axis spectrometer PANDA, the thermal three–axis spectrometer PUMA, the MIRA reflectometer for very cold neutrons and the time–of–flight spectrometer TOFTOF.

In 2003 some new features have been added to NICOS. The most important add–on which will be described in the following is a generic TACO server (nicmTACO) which allows to export NICOS methods as TACO servers at the push of a button.

These TACO servers are fully functional and are running outside the nicos environment. The user has just to set two parameters in the configuration editor GUI. No resource files are needed, no special konwledge of the TACO internals are required to write a class that can be exported as a TACO device. The nicmTACO system mainly consists of three components: The nicmServer and nicmClient classes and a ServerFactory script. The fundamental class nicmServer creates and embeds an instance of a nicos method, reads its configuration and provides access to its public commands. The ServerFactory script instantiates one or more nicmServers and exports them as device on the TACO system. The nicmClient class instance can be used to communicate with a given TACO server; furthermore, if that specific device is not yet exported via TACO, it takes care during its init process, that the neccessary server is started automatically.

The only visible difference for the user is as mentioned before, that he has to change the server parameter of his device from ’nicos’ to ’TACO’ and

give a valid TACO name for that particular device in the form ⟨domain⟩/⟨family⟩/⟨member⟩ using the configuration editor. The resulting client instance is equivalent to a pure nicos method with respect to the use of public commands. Some additional functionality is available, which is also helpful for development and debugging purposes as e.g. an automatic server–restart procedure and a logging mechanism.

The current state of development is, that any derivative of the Xable or HWGeneric classes can be exported as a TACO server. Grouping via XOGroup works too. The controller derivative is currently under 'heavy testing' and is most likely available in a stable version in spring of 2004.

Another remarkable feature of nicmTACO is, that there is no more need to write resource files to get the server parameters into the TACO database. The nicmServer init process creates all database information on–the–fly out of the configuration, which the user generates using the configuration editor. You can run the nicmTACO system nearly without any restrictions outside from NICOS. Only a python installation (version $>$ 2.1.0) is needed: Just import the nicmClient or ServerFactory module, instantiate a nicmClient class with the key of the configuration of your device and run the start() command with that key as parameter, respectively, and your server is up! The only drawback of using nicmTACO outside the NICOS context is that some functionality requiring direct access to a running NICOS daemon may (in the current state of development) not work.

1.9 Radiation Protection

H. Zeising[1]

[1] ZWE FRM-II, TU München

Research Reactor FRM-II

On the day of 02.05.2003 the TU-München received the 3rd partial license according to §7 Atomic Energy Act (AtG) from the Bavarian State Ministry for State Development and Environment for the operation of the high flux neutron source Munich (FRM-II). The license also encompasses the handling of nuclear fuel and other radioactive substances and has the stipulation of immediate execution.

Prior to this an intensive appraisal was undertaken by the Federal Ministry for the Environment, Nature Conservation and Nuclear Safety (BMU), who brought in not only the Reactor Safety and Radiation Protection Commissions, but also external outside experts. The appraisals were concluded with positive results.

Due to the direct execution, directly after reception of the license for operation and handling the delivery of the heavy water (D_2O), which is the moderation medium needed for the

Figure 1.14: The inspection of the screw cap of a cask filled with heavy water.

operation of the reactor, and the delivery of the first two fuel rods and the two converter plates for the beam tube converter facility (SKA) were initiated. In addition, the primary start-up neutron source was installed in the moderator tank.

Delivery and filling in of the heavy water (D_2O)

The heavy water moderation medium bought for FRM-II, which was kept in storage in Cadarache in France, had already been used in a French research reactor, after which it was cleaned and detritiated. It still has a tritium activity of about 2×10^{10} Bq/l.

The amount of heavy water needed for FRM-II is about 20 m^3 and was transported to Garching in two charges, packed for transport in 105 stainless steel casks with a volume of 200 l.

The first delivery with 52 casks took place on 05.06.2003 and proceeded smoothly. On the second transport with 53 casks on 13.06.2003, two leaks were detected on the screw caps of two casks during the radiation safety‘s incoming components inspection. Since the critical value for the contamination of radioactive transport was exceeded, the leaks had to be reported to the atomic controlling institution. The amount of heavy water which leaked out was about 5 ml. This small amount of leaked water drew an extensive control- and review procedure after it in order to found the cause of the leakage. The procedure was not yet concluded at the end of the year 2003.

In the time period from the beginning of October until the middle of November 2003 the required amount of heavy water was filled from the casks into the D_2O system of FRM-II. From the viewpoint of radiation protection extensive safety precautions were necessary. Tritium is a low energy beta particle emitter which causes practically no external radioactive exposition. However, when handling open tritium, precautions must be taken in order to avoid dose-relevant incorporations of the personnel. One must pay attention that the tritium concentration in the air of the room where the casks are opened and filled into the system stays at a low level.

After completion of each work campaign the participating persons had to deliver urine samples which were analysed by the official evaluating Office, the "Messstelle für Radiotoxikologie" at the Bavarian Environ-

Figure 1.15: Pulling out of a fuel rod from a transportation container in the truck lock of FRM-II.

mental Protection Agency in Kulmbach, in order to find the tritium activity in the body and calculate the resultant personal doses. The internal radiation dose was not higher for any single person than a few microsieverts. The collective dose for the entire filling in of the heavy water was about 60 microsieverts. There were no unplanned events during the filling.

One can say that the filling in of the heavy water proceeded very satisfactorily.

Delivery and storage of the fuel rods and converter plates

The fuel rods and the converter plates for the beam tube converter facility (SKA) are manufactured in France. The delivery from France proceeded under strict conditions using a so-called safety vehicle (SIFA) to FRM-II in Garching.

The first two fuel rods and a converter plate were delivered on 10.07.2003. Due to reasons pertaining to technical authorization of transport, the second converter plate was delivered extra on 23.07.2003.

The fuel rods as well as the converter plates contain uranium with an Uranium-235 enrichment of about 93 % by weight, so-called HEU (highly enriched uranium).

The delivery, unloading and the storage of the two fuel rods and the two converter plates in the fuel element repository was planned well and proceeded without any problems.

Special radiation protection measures were not necessary during the unloading. The fuel rods and the converter plates with the firmly integrated uranium showed only a minor dose rate. The dose rate was only about 20 microsievert per hour.

Just one day later on 11.07.2003 a first inspection of the stored nuclear fuel was conducted by the IAEA and Euratom. It took place without any complaints.

The installation of the primary start up neutron source, Cf-252

In order to start up the reactor and to permit the smooth regulation using the control rod, one has to have a certain neutron flux at one´s disposal even before criticality is reached. This is achieved through use of a Cf-252 source. The Cf-252 decays to a small part through spontaneous fission and sends out neutrons at the same time. The primary start up source for FRM-II has an activity of 1.2×10^{10} Bq with a neutron emission rate of 1.4×10^{9} per second. The neutron source was manufactured in England, delivered to Garching on 25.04.2003 and on 01.12.2003 it was installed in the moderator tank of FRM-II.

Because of the relatively short half-life of Cf252 of 2.645 years it is essential to have a further secondary start up source available for later start ups. This is made possible through use of a secondary start up source which is made up of antimony and beryllium. Through activation of the antimony (Sb-123) during the operation of the reactor to Sb-124 and the resulting high energy gamma radiation through a (γ,n) reaction of the Be-9 to Be-8 or rather, two alpha particles, the required neutrons are generated.

Instruments and Experiments

In the year 2003 further proposals regarding the design of instruments and experiments were talked through and discussed with the submitters.

As a result, the assembly of the approved instruments proceeded quickly.

Information brochure "All around safe!"

In July 2003 an information brochure was completed, required according to paragraph §53 of the Radiological Protection Ordinance, which informs the public about precautions to fight damage at the onset of significant safety-related incidents at FRM-II.

The brochure with the title "All around safe!" was sent via bulk mail to all households of the communities within a 2 km perimeter to FRM-II.

Other interested parties can obtain the brochure at the public relations office of FRM-II at all times or online from http://www.frm2.tum.de/publikationen.

2 Diffractometers

2.1 BIODIFF – Monochromatic Single Crystal Diffractometer for Biological Macromolecules

A. Ostermann [2], **F.G. Parak** [1]

[1] Physik Department E17, TU München
[2] ZWE FRM-II, TU München

It is planned to install a monochromatic single crystal diffractometer at the thermal beam tube SR5a at the FRM-II. Monte-Carlo simulations (McStas) have been carried out to optimize all components of the instrument. This diffractometer

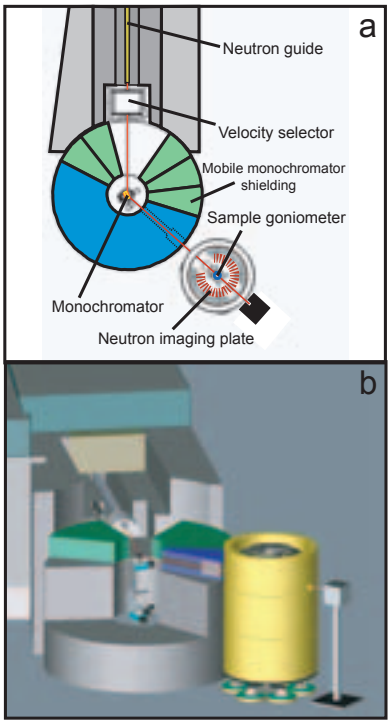

Figure 2.1: Schematic view of the planed diffractometer. (a) Top view. Only a part of the neutron guide is shown. (b) 3-dimensional view.

Monte-Carlo simulations (McStas) have been carried out to optimize all components of the instrument. This diffractometer will be dedicated to the structure determination of proteins and other biological macromolecules in the temperature range between 20K and 300K.

Hydrogen atoms play an important role in biological macromolecules. They mediate hydrogen bridges and take part in non-bonding interactions such as electrostatic and van der Waals forces. They are essential for the stabilization of the defined 3-dimensional structure of proteins and thus contribute to the complex energy landscape of this molecules. Hydrogen atoms in polarized bonds play critical roles in enzymatic catalysis. They are involved in hydrogen bonds in the substrate binding and are essential in proton transfer reactions during the catalysis. The knowledge about amino acid protonation states in the active center of proteins is often crucial for an understanding of the molecular reaction mechanism. Another point of interest is the hydration structure around proteins. This hydration structure has a great influence on the dynamic properties of proteins[1, 2].

The planned diffractometer should allow the determination of hydrogen atom positions and mean square displacements in proteins. For a detailed data analysis it is important that high resolution data sets can be collected[3, 4]. The planned diffractometer is specially designed for the data collection of crystals with large units cells ($\geq$ 100Å·100Å·100Å). Due to the large unit cells of protein crystals the total diffracted intensity is distributed over a large number of Bragg reflections and is therefore weak. For this reason a low background and a small horizontal and vertical divergence is essential for this instrument.

Instrument design

To optimize all components Monte-Carlo simulations (McStas) of the whole beam path, including the scattering process at the sample crystal, have been carried out. An overview over

the main components of the instrument is shown in figure 2.1.

Neutron guide

The geometric design and coating of the neutron guide are determined by the monochromator characteristic and therefore by the target value of the divergence at the sample position. To achieve a low background, the instrument will be installed at a 8.7 m neutron guide. The planned neutron guide consists of 5 channels (channel width = 5.2 mm) and is slightly curved (R = 1800 m) to avoid a direct sight to the beam tube entrance. This will suppress the background of fast neutrons and γ-radiation. Due to the small divergence at the sample position a coating with ^{58}Ni is sufficient. The guide will be slightly vertical focussing with an entrance height of 96 mm and an exit height of 57.5 mm. The total guide width is 30 mm.

Velocity selector

The next component in the beam path is a lamella velocity selector (Dornier). This selector is used as a higher order filter for the monochromator (pyrolytic graphite) and will allow a continuous wavelength choice within the wavelength range of interest ($\lambda = 2.0 - 4.0$Å). The velocity selector combines a very efficient energy cut–off (spectral band width $\Delta\lambda/\lambda = 35\%$) with a high transmission of 87.5% – 85%. Due to the energy cut-off the selector is also a essential component for the background reduction.

Wavelenght (Å)	Hor. divergence FWHM (°)	Vert. divergence FWHM (°)	$\Delta\lambda/\lambda$ FWHM (°)
2.0	0.71	0.72	2.1
2.75	0.68	0.83	1.8
3.5	0.64	0.90	1.3
4.0	0.62	0.90	1.1

Table 2.1: Results of Monte-Carlo simulations for the divergence and wavelength distribution at the sample position (2mm x 2mm).

Monochromator unit

The diffractometer will be able to operate in the wavelength range of $\lambda = 2.0 - 4.0$Å. However, in its standard configuration, the diffractometer use will neutrons of approx. 2.75Å to cover a large area of the reciprocal space ($d_{min} \simeq 1.45$Å). As monochromator a flat highly oriented pyrolytic graphite monochromator (PG(002), mosaicity = 0.4°–0.5°) will be used. Pyrolytic graphite shows in the wavelength range of 2.0 - 4.0Å a high reflectivity of 63% – 80%. Since the distance between the monochromator and the sample position is rather small ($\leq$ 1.7 m) no focussing geometry will be used to keep the divergence within the desired range. The planed monochromator has a width of 75 mm with a height of 35 mm. The thickness is 2 mm. This flat monochromator is a easy and inexpensive solution. Furthermore the background will be reduced since apart the monochromator there is nearly no supporting material in the direct beam.

For the cylindrical monochromator shielding different types of heavy concretes with densities up to 6.3 g/cm^3 will be used. The outer diameter will be 1940 mm. The shielding will allow a continuous usage of of $2\Theta_M$-angles between 30°and 75°. A flight tube consisting of B_4C/resin and lead between the monochromator and the diffractometer will be used as a first collimation unit.

Diffractometer

For the detector of the diffractometer a neutron imaging plate (NIP) will be used. Due to the large dynamic range and the very high spatial resolution ($\leq$200μm) neutron imaging plates are the best choice for diffraction experiments, especially in the case of large unit cells. The neutron imaging plates are mechanical flexible and thus can be easily adapted for the desired geometry. Neutron imaging plates are already successfully used for the diffractometers BIX-3/4 (reactor JRR3M, Japan) and LADI/VIVALDI (Institut Laue-Langevin, France).

To cover a large solid angle range the NIP will have a upright cylindrical geometry. The sample is placed in the middle of the cylinder. The vertical cylindrical design allows a high flexibil-

ity concerning the sample environment. For the NIP-cylinder radius one has to consider the beam divergence at the sample position (compare table 1). Monte-Carlo simulations of the planed instrument show that a radius of 230 mm is the best choice. The total covered horizontal solid angle is ±145°. The total NIP-area is 1160 mm (width) by 550 mm (height) and will be realized in two pieces.

The NIP readout device is composed of a semiconductor laser and a photomultiplier. During the readout procedure the NIP-cylinder is rotated at high speed while the reader moves from one side to the other. Finally, any remaining signal is erased using a halogen lamp. The time for readout and erasing will last about 5 minutes. To shield the NIP against a potential neutron- and γ-background from the reactor hall the diffractometer is covered by cylindrical shielding of B_4C/resin and lead.

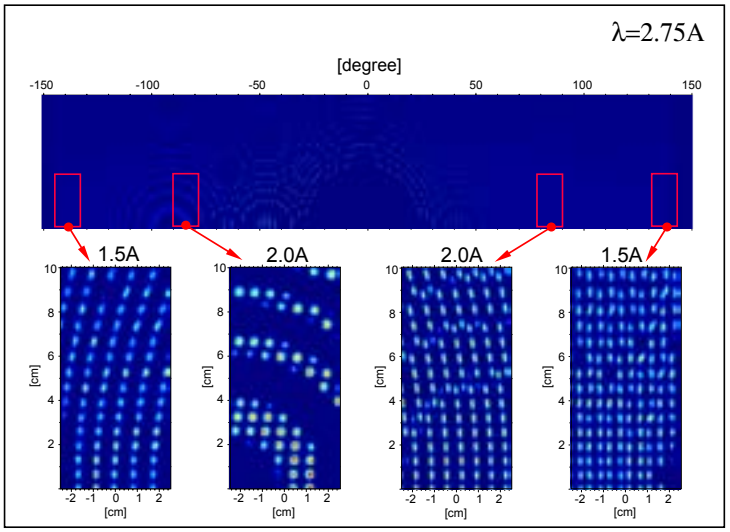

Figure 2.2: Monte-Carlo simulation of Bragg reflections from a sample crystal. Only the upper half of the neutron imaging plate is shown. Detailed views are shown for a resolution of d=2.0Å and d=1.5Å. Unit cell: 100Å·100Å·100Å, $\alpha = \beta = \gamma = 90°$; crystal mosaicity = 0.1°; neutron imaging plate spatial resolution: 0.4mm x 0.4mm.

Results of Monte-Carlo simulations of the scattering process at a sample crystal with unit cell dimensions of 100Å·100Å·100Å are shown in Fig. 2.2. With a wavelength of 2.75Å it is possible to measure crystals with such a large unit. With a wavelength > 3.0Å it will even be possible to measure crystals with larger unit cells. A big advantage of this instrument is the possibility to adapt the wavelength to the unit cell of the sample crystal.

[1] Bon C., Lehmann M. S., Wilkinson C. *Acta Cryst. D*, **55**, (1999), 978–987.
[2] Chatake T., Ostermann A., Kurihara K., Parak F. G., Niimura N. *Proteins*, **50**, (2003), 516–523.
[3] Ostermann A., Tanaka T., Engler N., Niimura N., Parak F. G. *Biophys. Chem.*, **95**, (2002), 183–193.
[4] Engler N., Ostermann A., Niimura N., Parak F. G. *Proc. Natl. Acad. Sci. USA*, **100**, (2003), 10243–10248.

2.2 HeiDi – Single Crystal Diffractometer at the Hot Source

M. Meven [1], **F. Hibsch** [1], **G. Heger** [2]

[1] ZWE FRM-II, TU München
[2] RWTH Aachen, Institut für Kristallographie

The single crystal diffractometer HEiDi uses beam line SR-9 in the experimental hall of the FRM-II. This beam tube is the only one that is connected to the hot source of the reactor. HEiDi uses the higher flux of neutrons with shorter wavelengths (in comparison to thermal neutrons) to observe a larger area of the reciprocal space Q ($|Q| = \sin\Theta_{max}/\lambda$). The gain in observable Bragg re-

flections yields a significant enhancement in detailed structural investigations. Examples for this important application for scientific cases after the launch of FRM-II are structural investigations on high T_c superconductor [1], structural phase transitions with atomic or molecular order/disorder character [2], anharmonic behaviour and the important role of hydrogen bonds, e.g. in ferroelectrics of the KDP family. Due to the bandwith from $\lambda = 0.3$Åto $\lambda = 1.1$Åit is also possible to investigate the quantitative description of the wavelength dependent extinction effect, e.g. for TOF Laue techniques at spallation sources [3]. An overview of the instrument is shown in picture 2.3.

Details of the instrument and its applications were presented on the german conference for crystallographers, DGK 2003, in Berlin and at the ECNS conference in Montpellier.

In 2003 the following components of the instrument were completed: The three primary beam collimators (manufactured at the HMI in Berlin) were mounted in the beam shutter of SR-9. They define the horizontal divergence of the primary beam (15', 30', 60'). They are needed for the choice of the best compromise between good resolution and high intensity.

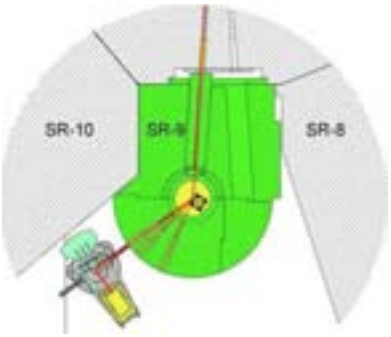

Figure 2.3: Overview

Figure 2.4: Instrument in experimental hall

The position of the biological shielding was tested and realigned to the direction of beam tube SR-9B. Two beam shutter were integrated in front and behind the monochromator pit. In picture 2.4 the biological shielding with open monochromator pit and the diffractometer unit itself with open detector shielding (to mount the single detector) are shown.

One Cu-(220) and one Cu-(420) crystal were cut into slices at the FZ Jülich to mount them on the focussing units of the monochromator. Recently the alignment of the slices was successfully tested at the single crystal diffractometer SV28 (DIDO, FZ Jülich). A picture of one focussing unit with a mounted Cu crystal is shown in picture 2.5.

Another focussing unit for the Ge-(311) crystal was delivered at the end of 2002. The thermoplas-

tic crystal treatment in Risoe has been found to be the best way to get suitable Ge monochromator crystals. This third monochromator unit should be ready at the end of 2004.

Concerning the optional 2D-detector a small (200*200 mm^2 sensitive area) ^{3}He wire chamber with high pressure (about 8 bar) was found to be the most suitable technique for our needs. The complete system should be ready in spring of 2004.

In summary all major components of the instrument are now available. After the final tests and fine tuning of the instrument during the first reactor period we expect this instrument to be ready for many scientific cases in structural science.

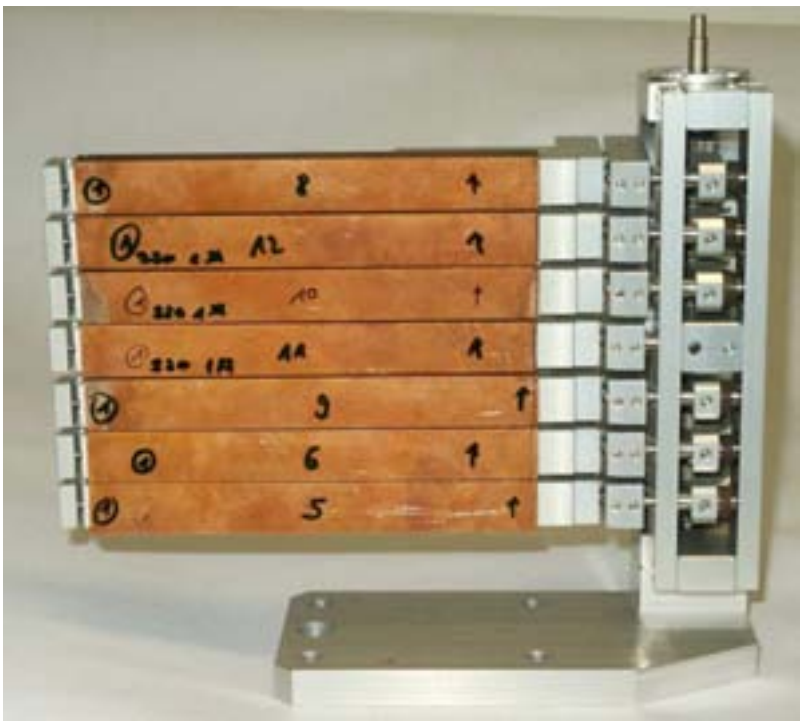

Figure 2.5: Focussing unit with mounted Cu-(220) crystal

[1] Braden M., Meven M., Reichardt W., Pintschovius L., Fernandez-Diaz M., Heger G., Nakamura F., Fujita T. *Phys. Rev. B*, **63**, (2001), 140510.
[2] Schiebel P., Hoser A., Prandl W., Heger G., Schweiss P. *J. Phys. I France*, **3**, (1993), 987.
[3] Jauch W., Schultz A., Heger G. (1987).

2.3 MatSci-R – Materials-Science Reflectometer

J. Major [1], **J. Franke** [1], **A. Rühm** [1], **U. Wildgruber** [1], **H. Dosch** [1]

[1] Max-Planck-Institut für Metallforschung Heisenbergstr. 3, D-70569 Stuttgart, Germany

Within the framework of an initiative of the Max Planck Society for the Advancement of Science (MPG) 'Materials Science at the New Neutron Source FRM-II', this instrument is built and will be operated by the Max-Planck-Institut für Metallforschung (Stuttgart). An overview of the instrument has been presented in the 2002 annual report of the FRM-II.

By now the design is completed and most hardware components are built and ready for installation at the cold neutron guide NL-1 in the neutron-guide hall of the FRM-II. The monochromator shielding (Fig. 2.6) is in place and the neutron guide is operational. The monochromator (Fig. 2.7) is ready to be tested in the neutron beam.

The length of the monochromator is determined by the width of the neutron guide (60mm) and the monochromator Bragg angle for 2 Å neutrons (17.34°). During commissioning of the instrument up to eleven HOPG (highly oriented pyrolytic graphite) plates (approx. 66 mm × 21.5 mm × 2 mm) will be used. Each crystal is directly mounted to a geared

Figure 2.6: Monochromator shielding at the cold neutron guide NL-1 in the FRM-II guide hall with sliding front wall (including the rotating drum) in place.

down miniature ARSAPE stepping motor (Faulhaber, Schönaich, Germany) with an angular step size of 0.0005°. Later the single plates can be replaced with stacks of three HOPG plates introducing a small angular offset between three the individuals to achieve a better match between the angular acceptance of monochromator and primary beam divergence and thus increase the intensity of the monochromatic beam. The HOPG monochromator "crystals" are lowered from above in the "white" beam of NL-1. Nl-1 has a cross section of 120 mm × 60 mm (h×w). Due to the low beam-center line, we are planning to use the upper half of the beam to extract monochromatic neutrons.

Furthermore, the monochromator device will rotate with respect to the incoming beam when the sample table is moving up or down. This assures maximum monochromatic intensity at the center of a 'liquid mode' sample even at large angles of incidence. The motor controllers (MPI design) to move the monochromator crystals, the slit systems, etc. are compact rack mountable units (19″ × 2 rack units) which can be equipped with up to three 'Sixpack', 'Quadpack', or 'Monopack' modules (Trinamic, Hamburg, Germany). The fieldbus interface is an RS485 system (with optional CAN protocol). Most of the other control hardware (larger stepper motor controllers, angular and linear encoders, temperatures sensors, etc.) is integrated via the 'Profibus-DP' protocol and additional gateways to other fieldbus systems if necessary.

Currently all 'crystals' are characterized by means of gamma-ray diffraction (MPI, Stuttgart). This is necessary because the overall mosaicity of the HOPG plates varies significantly. Furthermore, depending on the geometrical cross section of the monochromatic beam, different parts of the 'crystals' will be used. This requires to measure the dependency of the mosaic spread along the 'plates' in order to be able to optimize the monochromator device numerically. The variation of the mosaic spread for the eleven center crystals is between 0.37° (fwhm) and 0.71° (fwhm). Although this variation is within the specifications (0.8° ± 0.2°) of the purchased HOPG-ZYB (Advanced Ceramics, a GE company, USA), it is so large that additional Monte Carlo Ray tracing calculations are necessary to optimize the arrangement of all HOPG plates within the monochromator. This is especially important for shorter wavelengths where the spatial neutron flux distribution at the exit of NL-1 is particularly complex due to the curved design of the guide with different '*m*-value' for both side walls.

Figure 2.7: The MatSci-R monochromator gallows.

Detector electronics (GKSS, Geesthacht, Germany) and active anti-vibration hardware (Halcyonics, Göttingen, Germany) will be put into operation in January 2004. The final assembly of the reflectometer will start in February 2004.

2.4 REFSANS – Neutron Optics of the Reflectometer REFSANS for Comprehensive Investigations on the Air/Liquid Interface

R. Kampmann [1], **M. Haese-Seiller** [1], **V. Kudryashov** [1,3], **Ch. Daniel** [2], **V. Deriglazov** [3], **B. Toperverg** [3], **A. Schreyer** [1], **E. Sackmann** [2]

[1] GKSS Forschungszentrum, Institut für Werkstoffforschung, D-21502 Geesthacht, Germany
[2] Physik Department E22, TU München
[3] Petersburg Nuclear Physics Institute, Gatchina, 188350, Russian Federation

Introduction

REFSANS is a time-of-flight (TOF) instrument with three double disc choppers which allow setting the wavelength resolution in the broad range of $0.25\,\% < \Delta\lambda/\lambda < 15\,\%$ to meet the different experimental demands comprising high and low resolution reflectometry and small-angle scattering at grazing incidence (GI-SANS) [1–3]. The instrument is being built at the end of the cold neutron guide NG-2b with 12 mm high and 170 mm wide beam cross-section. This unusually broad beam is used to install radially collimating neutron optics to substantially improve the GI-SANS capability of REFSANS.

Neutron optical design

REFSANS is equipped with novel Neutron guide elements (NGE) which allow continuing the beam of NG-2b through REFSANS (upper channels in Fig. 2.8a and b), collimating the beam vertically while maintaining the horizontal divergence (lower channel in Fig. 2.8b), reflecting the beam from top to bottom (or vice versa) onto the sample surface by means of the upper channels of NGE's-3, -4, -7, and -8 (Fig. 2.8 and upper chart in Fig. 2.9). A further possibility for declining the beam at an angle of ≈ 180 mrad is provided by a special bender (see beam B4 in upper chart of Fig. 2.9). Finally, the lower channels of NGE-3 and -4 (Fig. 2.8a) may be moved into the beam to separate and pre-collimate 13 partial beams which are focused in the detector plane at a

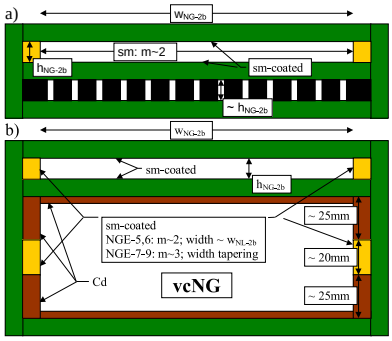

Figure 2.8: Cross-sections of neutron guide elements (NGE) of REFSANS, perpendicular to the beam direction (a: NGE-3 and -4; b: NGE-7 and -8).

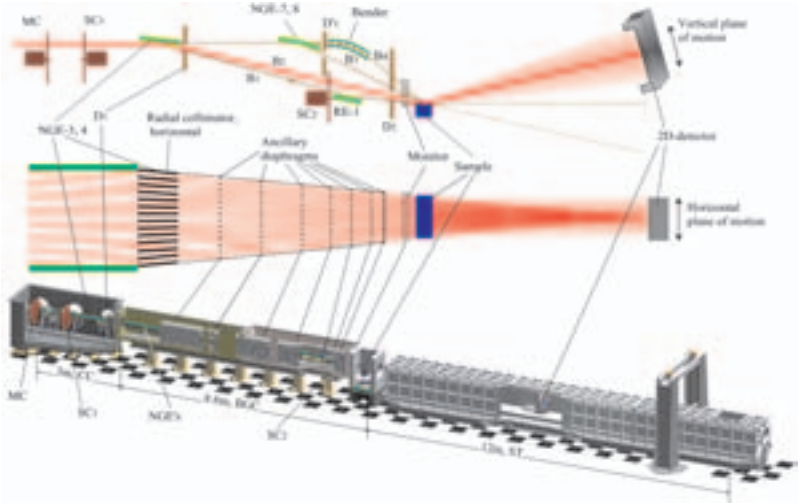

Figure 2.9: Schematic view of REFSANS and its neutron optics, details are mentioned in the text.

Figure 2.10: Neutron optical body in the beam guide chamber with the mechanics for vertically aligning a NGE and an ancillary diaphragm.

distance of ≈ 9 m from the sample. The separation of the latter is maintained in the beam guide chamber over ≈ 8 m by ancillary diaphragms with comb-like apertures (Fig. 2.9, central chart and Fig. 2.10).

The intensity of such radially focused beams hitting a sample with a size of ≈ 60 mm ×60 mm has been calculated on the basis of the brilliance of the cold source of FRM-II and accounting for the expected transmission of the chopper, the neutron optics and the radially collimating system [3]. An excellent peak intensity is calculated for the case of a resolution in momentum transfer of $\Delta q/q \approx 14\,\%$ (Fig. 2.11).

It is pointed out that this results on the one hand from the excellent transmission of the 3-double-disc chopper which is close to that of a 10 % selector and on the other hand from focussing of 13 beams in the detector plane. This altogether results in an intensity which would be expected if 13 modern SANS facilities at a high flux reactor would be arranged in focussing and grazing incidence geometry.

Due to this very high beam intensity at grazing incidence REFSANS is expected to offer new GI-SANS perspectives. Today's measuring times could be decreased by an order of magnitude and time dependent GI-SANS studies will become feasible. All investigations may be performed at the air-water interface with horizontally aligned samples and may be combined with further measurements of the specular reflectivity to characterise comprehensively vertical and horizontal surface structures.

The intensity may be further increased by almost one order of magnitude by increasing the vertical beam divergence (Fig. 2.11). This can easily achieved by guiding the 13 partial beams in the upper channels of the neutron guide elements in the beam guide chamber (Fig. 2.8 and 2.9). This geometry will especially allow of measuring extremely weak diffuse surface scattering from very small lateral structures and of following the tails of diffuse surface scattering patterns.

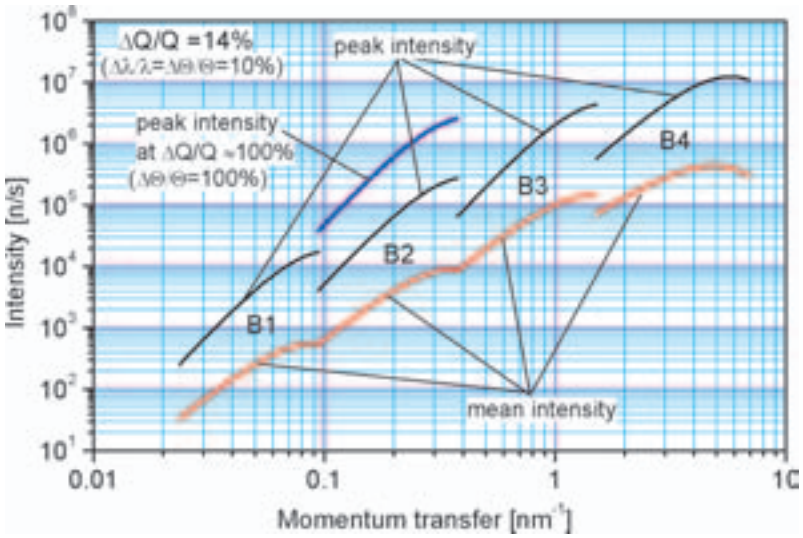

Figure 2.11: Calculated peak and time averaged beam intensities I_{peak} and I_{mean} of 13 beams horizontally focused in the detector plane (details in the text).

Acknowledgements

The great contribution of the technical department of GKSS to constructing and manufacturing of REFSANS components is gratefully acknowledged. The development of REFSANS has been supported by the German Federal Ministry of Education, Research, and Technology (BMBF) under Contracts 03-KA5FRM-1 and 03-KAE8X-3.

[1] Kampmann R., Haese-Seiller M., Marmotti M., Burmester J., Deriglazov V., Syromiatnikov V.,

Okorokov A., Frisius F., Tristl M., Sackmann E. *Applied Physics A*, **74**, (2002), 249–251.
[2] Kampmann R., Haese-Seiller M., Kudryashov V., Deriglazov V., Tristl M., Daniel C., Toperverg B., Schreyer A., Sackmann E. *Applied Physics A*. In press.
[3] Kampmann R., Haese-Seiller M., Kudryashov V., Deriglazov V., Tristl M., Schreyer A., Sackmann E. *Nuclear Instruments and Methods A*. Submitted.

2.5 2D-multi-wire neutron detector with a large sensitive area and high spatial resolution for SANS and reflectometry

R. Kampmann [1,2], **M. Marmotti** [2], **M. Haese-Seiller** [1], **V. Kudryashov** [1,3]

[1] GKSS Forschungszentrum, Institut für Werkstoffforschung, D-21502 Geesthacht, Germany
[2] DENEX Detektoren für Neutronen und Röntgenstrahlung GmbH, D-21339 Lüneburg, Germany
[3] Petersburg Nuclear Physics Institute, Gatchina, 188350, Russian Federation

Introduction

A two-dimensional position-sensitive multi-wire gaseous detector for small-angle neutron scattering (SANS), reflectometry and high-resolution diffractometry has been developed at the GKSS research centre in cooperation with DENEX GmbH. The counter with a sensitive area of $500 \times 500\,\mathrm{mm}^2$ has been designed to be used in the reflectometer REFSANS being built at the new high flux reactor FRM-II [1].

Figure 2.12: REFSANS detector being tested at SANS-2 at GKSS

Design and performance of the detector

The REFSANS detector is a ^{3}He and CF_4 filled multi-wire proportional counter (MWPC) with delay line read-out, its design is based on that of detectors with smaller active areas developed previously at GKSS [2, 3]. REFSANS needs a detector which meets requirements both of reflectometers and SANS instruments [1]:

- Sensitive area: $500 \times 500\,\mathrm{mm}^2$;
- Spatial resolution: $\approx 2\,\mathrm{mm} \times 2\,\mathrm{mm}$;
- Wavelength range: $0.3\,\mathrm{nm} < \lambda < 3\,\mathrm{nm}$;
- Read-out: fast, ToF-application;
- Background: very low;
- γ-sensitivity ε_γ: extremely low ($\varepsilon_\gamma \ll 10^{-6}$).

All electrodes are made of tungsten wires with a distance of 2 mm. Drift electrodes limit the detection volume which has a depth of 3 cm to achieve a high detection probability p at rather low ^{3}He partial pressure. The anode is located in the centre of the detection volume. Its distance to the pick-up electrodes is only 5 mm to achieve high capabilities for both good position resolution and high local count rates.

One prototype of REFSANS detector was manufactured and characterised with neutrons. It has been filled with only 0.8 bar ^{3}He and 1 bar CF_4 for use in the SANS-2 at the GKSS Research Centre (Fig. 2.12).

The detection probability was measured with a well collimated neutron beam at SANS-2 in comparison with an almost black ^{3}He counter tube. A detection probability larger than 50 % over the range for $0.5\,\mathrm{nm} < \lambda < 1.8\,\mathrm{nm}$ with a maximum of $\approx 58\,\%$ at $\lambda = 1.0\,\mathrm{nm}$ was found (Fig. 2.13). This detection probability is close to the ideal one which is calculated by accounting for the losses in the detector window (20 mm thick Al-alloy)

and the dead volume between the window and the first drift electrode (thickness: ≈ 2 mm).

The γ-efficiency was measured without changing the setting of the analogue electronics. Radioactive sources were positioned at short distance ($\approx$ 10 cm) in front of the detector. Extremely low γ-sensitivities of $\varepsilon_\gamma \ll 10^{-7}$ were measured (Fig. 2.13).

After these tests the detector was mounted in the evacuated scattering tube of SANS-2 / GKSS. An isotropic scatterer was set in the beam at a distance of ≈ 3 m from the detector which was covered by a Cd-mask (≈ 20 cm in front of its window) with a grid of holes with distances of 50 mm. A spatial resolution of ≈ 3 mm $\times$ 3 mm together with an excellent linearity was found [3].

Summary

Due to its large sensitive area ($500 \times 500\,\mathrm{mm}^2$), its spatial resolution of ≈ 3 mm $\times$ 3 mm and its low γ-sensitivity ($\varepsilon_\gamma \ll 10^{-7}$) the prototype detector meets already central requirements of the REFSANS detector and it is an excellent detector for a SANS at a monochromatic beam. For the use in REFSANS the detection probability will be further increased by changing the electrode design to avoid any dead volume behind the detector window. Furthermore, the spatial resolution will be improved to ≈ 2 mm $\times$ 2 mm by increasing the partial pressure of CF_4. The REFSANS detector has been licensed by GKSS to DENEX.

Acknowledgments

The support of M. Pauls, H. Eckerlebe and K. P. Pranzas during tests of the REFSANS detector at SANS-2 / GKSS is gratefully acknowledged. The development of REFSANS has been supported by the German Federal Ministry of Education, Research, and Technology (BMBF) under Contracts 03-KA5FRM-1 and 03-KAE8X-3.

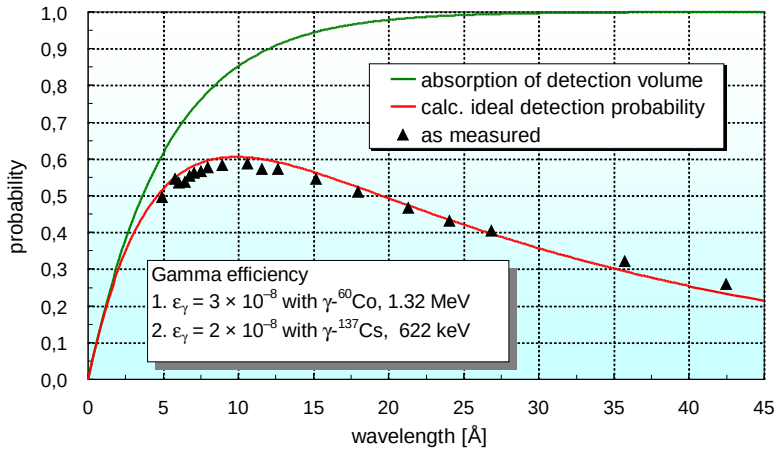

Figure 2.13: Neutron detection probability and γ-efficiency of the prototype REFSANS detector.

[1] Kampmann R., Haese-Seiller M., Marmotti M., Burmester J., Deriglazov V., Syromiatnikov V., Okorokov A., Frisius F., Tristl M., Sackmann E. *Applied Physics A*, **74**, (2002), 249–251.

[2] Marmotti M., Burmister J., Haese-Seiller M., Kampmann R. *Nuclear Instruments and Methods A*, **477**, (2002), 347–352.

[3] Kampmann R., Haese-Seiller M., Marmotti M., Burmester J., Deriglazov V., Syromiatnikov V., Okorokov A., Frisius F., Tristl M., Sackmann E. *Applied Physics A*, **74**, (2002), 252–254.

2.6 RESI – The Single Crystal Diffractometer

B. Pedersen [1], **G. Seidl** [1], **W. Scherer** [2], **F. Frey** [3]

[1] ZWE FRM-II, TU München
[2] Inst. f. Physik, Universität Augsburg
[3] Sektion Kristallographie, Geodepartment, LMU, München

Introduction

The thermal single crystal diffractometer RESI has been designed to record strong and weak scattering in large portions of Q-space with high resolution. Hence RESI is optimized for both (i) chemical problems requiring fast scanning of the reciprocal space and (ii) crystallographical demands, where non-Bragg scattering is of major importance.

This can be achieved by a flexible setup with different interchangeable monochromators, goniometers and detector systems.

Status

RESI is now in the final testing phase. All essential components, which are needed to operate RESI in the standard modus, have been installed and tested during the last year.

Also new developments, such as the construction of a 511-Ge monochromator could be finished in 2003. The 511-Ge monochromator crystals, consisting of stacks of soldered and bent wafers, were processed by Risø and delivered in the meantime. The effective mosaic has been optimized in the same way as for the copper crystals by MonteCarlo-simulations to get an optimum flux/resolution ratio [1]. The final characterisation is planned for spring time next year upon availability of neutrons.

The goniometer software has passed all tests, and is now ready for operation. It is based on the Collect™ package by Bruker-Nonius and allows easy determination of cell parameters and orientation matrices, calculation of optimised scans to cover the reciprocal space and is complemented by an advanced and user-friendly integration software for Bragg peaks.

The second goniometer is designed and in the final assembly stage (see Fig. 2.14). It allows the usage of heavier sample environments (e.g. furnances, cryostats) in combination with the image plate detection system.

Outlook

During the next year we will install the heavy goniometer and start to operate RESI to perform the “hot” test of the instrument and first measurements to characterise the instrument.

The analyzer option, which allows the separation of inelastic and elastic contributions, is scheduled for installation for fall 2004.

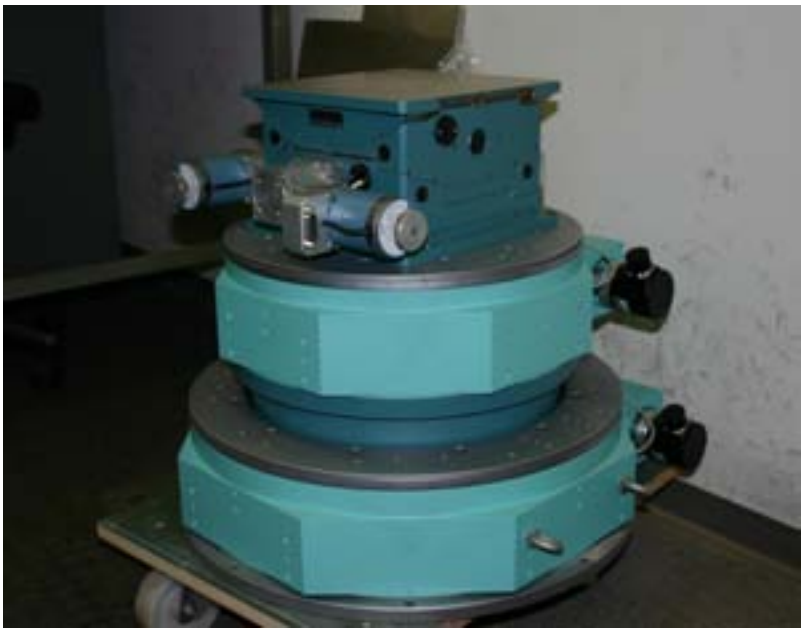

Figure 2.14: The goniometer for heavy sample environment

[1] Pedersen B., Seidl G., Scherer W., Frey F. . *FRM-II Annual Report*, 16–19.

2.7 SPODI – Structure Powder Diffractometer

R. Gilles [1], **M. Hoelzel** [2], **M. Schlapp** [2], **B. Krimmer** [2], **H. Boysen** [3], **H. Fuess** [2]

[1] ZWE FRM-II, TU München
[2] Fachbereich Materialwissenschaft, Technische Universität Darmstadt
[3] Ludwig-Maximilians-Universität München

The design and status of the new **S**tructure **PO**wder **DI**ffractometer (SPODI), currently being built up at the new neutron source FRM-II in Garching near München is reviewed. Based on an optimization of the components by Monte Carlo simulations, new features include supermirror neutron guides, a very high monochromator take-off angle and an array of position sensitive detectors. This concept aims at an optimum compromise of improved resolution, higher intensity, better profile shape and lower background. The design of new instruments can benefit from recent theoretical and technical progress as well as new ideas. In order to be able to solve complicated structures reliably by powder diffraction, not only a high resolution and intensity are essential. One also requires good peak profiles that can be described as perfectly as possible. For strongly overlapping reflections, uncertainties in the exact shape can lead to a wrong distribution of the intensities. Moreover, such knowledge virtually increases the resolution of the instrument far beyond that given by the widths of the peaks. Similar arguments hold for a good peak to background ratio which can be achieved not only by a low background, but also by narrow tails of the peaks. Finally, such good peak shapes should be maintained up to large scattering angles 2θ. Based on these considerations computer simulations have been used to optimize each single component and additionally their interaction along the instrument. The resulting concept together with test measurements of single components at neutron sources have been described in references [1–5]. The instrument SPODI is shown in Fig. 2.15.

Figure 2.15: Side-view on instrument SPODI with shielding of the neutron guide & monochromator and detector in the foreground

During his visit at the FRM-II on the occasion of the granting of the third partial license, the Bavarian Minister-President Dr. Edmund Stoiber participated in a presentation about the Structure Powder Diffractometer SPODI (Fig. 2.16). Under development is the construction of a small-angle scattering apparatus in forward direction to characterize the structure and the size distribution of powder samples. Monte Carlo simulations have been carried out to optimize this additional feature [6]. Other applications such as the determination of particle morphology, texture analysis and investigations on the crystallinity of samples are planned with the image plate system of this SANS option.

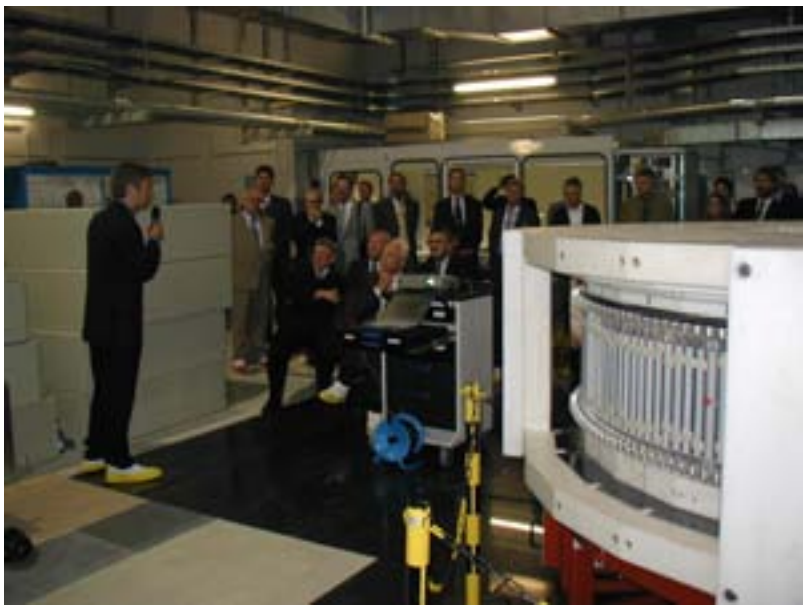

Figure 2.16: The Bavarian Minister-President Dr. Edmund Stoiber visits the instrument SPODI

[1] Gilles R., Artus G., Saroun J., Boysen H., Fuess H. *Physica B*, **276-278**, (2000), 87.
[2] Gilles R., Artus G., Saroun J., Boysen H., Fuess H. In: *Proc. HERCULES X EuroConference* (Grenoble, 2000).
[3] Gilles R., Krimmer B., Saroun J., Boysen H., Fuess H. *Mat. Sci. For.*, **378-381**, (2001), 282.
[4] Gilles R., Krimmer B., Boysen H., Fuess H. *Appl. Phys. A 74 (Suppl.)*, **74**, (2002), 148.
[5] Hoelzel M., Gilles R., Schlapp M., Boysen H., Fuess H. (2003). Submitted to *Physica B*.
[6] Schlapp M., Hoelzel M., Gilles R., Ioffe A., Brueckel T., Fuess H., von Seggern H. (2003). Submitted to *Physica B*.

2.8 STRESS-SPEC – Materials Science Diffractometer

M. Hofmann [1], **G. Seidl** [1], **R. Schneider** [2]

[1] ZWE FRM-II, TU München
[2] Hahn-Meitner-Institut, Berlin

Introduction

The Materials Science diffractometer Stress-Spec is situated at the thermal beam tube SR3 and will be primarily used for residual stress analysis and texture measurements of new materials and engineering components. Its main characteristics have been described elsewhere [1, 2] and here only the developments of last year will be reviewed.

Test phase at HMI Berlin

In cooperation with the Hahn-Meitner-Insitut, Berlin the secondary part (monochromator lift, sample table, detector and electronics) of the materials science diffractometer STRESS-SPEC has been moved to the BER-II reactor and installed at beam port D1S/E7 during the last year. This allowed to test and optimize those components, to gain experience with new calibration and alignment procedures and to run first experiments.

For instance in one of the first measurements the relaxation of residual stresses in cold rolled crank shafts under different mechanical load conditions was investigated in cooperation with Volkswagen AG (P. Lemke, HMI, Diploma thesis 2003). Other examples included experiments to study magnetoviscosity effects in some ferrofluids materials like nanocrystalline $CoFe_2O_4$ (E. Steichle, TUM), temperature dependent residual stress analysis in SiC reinforced AlSi metal composites (U. Göbel, Siemens AG) and residual stress analysis in as cast Al bars (T. Hanss, UTG-TUM). Also investigated was a prototype rocket nozzle fabricated by Astrium GmbH (figure 1) using a carbon fibre reinforced ceramic composite material (J. Rebelo Kornmeier, TUM). Here the main interest was focussed on whether and how residual stress due to different thermal expansion of the materials when heated can be relieved by micro cracks in the matrix material. This is in turn could help to counteract failure or fatigue of the component and extend its life time under working conditions.

In course of this test phase some parts of the equipment were modified due to the experience gained using the diffractometer in real life conditions. As an example a new detector slit system has been installed with regard to reproducibility of the slit positioning and sturdiness. Also a new high capacity Eulerian cradle (sample load up to 50 kg) has been designed at the HMI, which will be available in early summer 2004 for routine operation at FRM-II. In addition most of the electronics and mechanical systems could be tested and the data acquisition software has been adapted and upgraded.

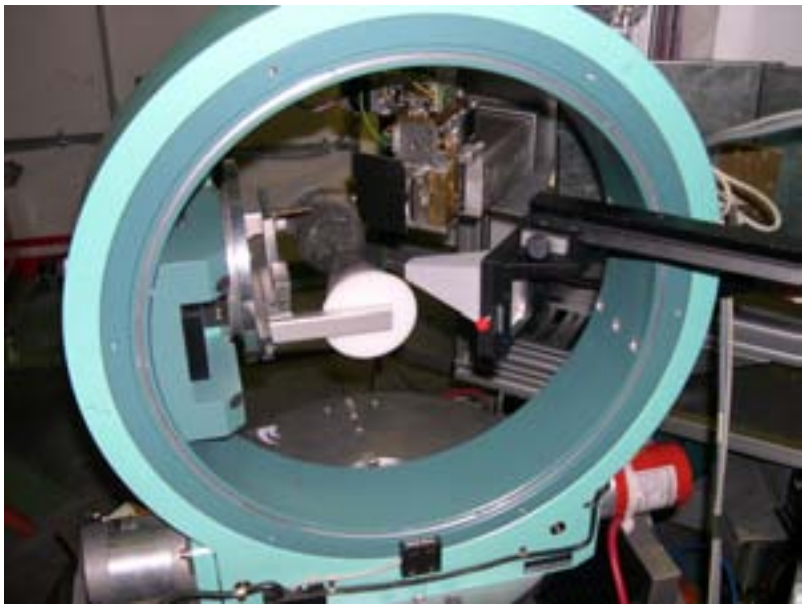

Figure 2.17: Example of a typical measurement setup at Stress-Spec.

FRM-II and outlook

While the diffractometer was in Berlin work continued on the shielding at FRM-II, with development and installation of new fast shutter systems, new primary beam slits and mobile block system electronics. With delivery of the focussing device for the Ge(511)-monochromator early Winter 2003, two monochromators will now be available at startup of the reactor FRM-II. As a third monochromator option we will install a PG(002)-monochromator, which will be mainly used for texture analysis and high intensity measurements. This monochromator will be available in spring 2004. It is forseen to transfer the diffractometer back from HMI Berlin to the beam port SR3 at the FRM-II reactor in January 2004.

[1] Mayer H. M., Pyzalla A., Reimers W. *Mat. Sci. Forum*, **29**, (2000), 347–349.
[2] Hofmann M., Seidl G. A., Schneider R. *Ann. Report FRM-II*.

3 Spectrometers

3.1 MIRA – Very Cold Neutrons for New Methods

R. Georgii [1], **N. Arend** [2], **P. Böni** [2], **H. Fußstetter** [1], **D. Lamago** [1], **G. Langenstück** [1], **H. Wagensonner** [1]

[1] ZWE FRM-II, TU München
[2] Physik-Department E21, TU München

The instrument MIRA (see JB 2002) in its current configuration provides neutrons in the wavelength range 8 to 15 A using a mica monochromator. The instrument has been designed for being able to measure a great variety of phenomena with very cold neutrons. The reflectometer for mesoscopic structures is equipped with a polarised option. Neutrons will be polarised using a switchable transmission multilayer polarizer. Then a field of approximately 50 Gauss provided by permanent magnets will guide the polarised beam to the sample. Here the standard FRM sample environment (cryostats, cryomagnets and ovens) can be used. At last the neutrons are again guided by a magnetic field to the detector. Currently a ^{3}He detector is being used. A 2-dimenisenional position sensitive detector with 20 x 20 cm sensitive area and a resolution of about 1 mm has been bought from GKSS and is currently tested a the reactor in Geesthacht. It will be available early next year.

Figure 3.1: The reflectometer option of MIRA without the detector and the magnets for the guide field.

The instrument setup for this option has been successfully installed (see Fig. 3.1). It is fully operational, with the exception of the analysing possibility, which will be added early next year. The instrument control software exits, but is still on a very basic level. Nevertheless first reflectivity measurements could be performed. A simple evaluation software has been developed and will be available after testing with real data also early next year.

3.2 Phonon Lifetime Measurement Using the NRSE-TAS Technique

T. Keller [1], **K. Buchner** [1], **R. Golub** [2], **K. Habicht** [2], **H. Klann** [1], **F. Mezei** [2], **M. Ohl** [1], **B. Keimer** [1]

[1] Max-Planck-Institute for Solid State Research, Stuttgart
[2] Hahn-Meitner-Institut, Berlin

Introduction

The NRSE-TAS spectrometer at the FRM-II is a combination of the *resonance spin echo* (NRSE) and the *triple axis* (TAS) spectroscopy techniques. This instrument will allow the determination of the energies and lifetimes of dispersive excitations, including both phonons and magnons, over the entire Brillouin zone. The design [1] of the NRSE-TAS at the FRM-II (Fig. 3.2) is based on a prototype instrument set up at BENSC, Berlin [2]. At this instrument we first demonstrated the spin-echo phonon-focusing technique [3]. As an example for this technique we show here the determination of lifetimes of transverse acoustic phonon modes in Pb at temperatures between 5-300 K at low q values. To correct for instrumental resolution effects, an analytical resolution function for the NRSE-TAS technique [4] has been developed.

The polarization P measured by a combination of a spin echo and a TAS instrument is given by

$$P \propto \int S(\mathbf{Q},\omega)\,T(\mathbf{k}_i,\mathbf{k}_f)\exp[i\phi(k_i,k_f)]\,d^3k_i\,d^3k_f \tag{3.1}$$

where $S(\mathbf{Q},\omega)$ is the scattering function, $T(\mathbf{k}_i,\mathbf{k}_f)$ is the transmission probability of the TAS spectrometer. $\phi = \phi_i - \phi_f$ is the total Larmor precession angle for neutrons passing precession field regions before and after the sample.

Mezei showed [5] that in order to measure phonon linewidths, the spin echo instrument has to be tuned both to the phonon energy ω_0 and group velocity $\nabla_q\omega_0(q_0)$. With our resonance spin echo technique, this tuning is achieved by rotating the RF spinflippers bounding the precession regions thus that the normal vectors on the coil surfaces satisfy the condition

$$\mathbf{n}_{i,f} \parallel [(\hbar/m)\mathbf{k}_{I,F} - \nabla_q\omega_0(\mathbf{q}_0)] \tag{3.2}$$

The RF $\nu_{i,f}$ applied to the coils in the first and second arm is tuned to the ratio

$$\frac{\nu_i}{\nu_f} = \frac{k_I^2}{k_F^2}\,\frac{\hbar\mathbf{k}_I - m\nabla_q\omega_0(\mathbf{q}_0)}{\left|\hbar\mathbf{k}_F - m\nabla_q\omega_0(\mathbf{q}_0)\right|} \tag{3.3}$$

$\mathbf{k}_{I,F}$ are the mean wavevectors. For non-dispersive excitations ($\nabla_q\omega_0(\mathbf{q}_0) = 0$) the tuning conditions (eqs. 3.2, 3.3) require to set the field boundaries perpendicular to the neutron beam and to set the frequency ratio to $\nu_i/\nu_f = (k_i/k_f)^3$.

If we assume the scattering

Figure 3.2: The NRSE-TAS spectrometer at the FRM-II

law $S(\mathbf{Q},\omega)$ to be independent of $\mathbf{Q}$ in that part of the dispersion surface which is located within the TAS resolution ellipsoid, we can integrate over the momentum components in eq. (1) and obtain

$$P(\tau) \propto \int S(\Delta\omega)T(\Delta\omega)\exp(-i\tau\Delta\omega + i\phi_0)d(\Delta\omega) + c.c. \tag{3.4}$$

In a high resolution spin-echo experiment the energy resolution $T(\Delta\omega)$ is usually much broader than $S(\Delta\omega)$,thus $T(\Delta\omega)$ can be considered to be constant over the integration range. Then eq. 3.4 directly yields the cosine Fourier transform of the line. For a *Lorentzian* lineshape with half-width-at-half-maximum Γ the polarization follows a simple exponential decay

$$P(\tau) \propto \exp(-\Gamma\cdot\tau) \tag{3.5}$$

τ is the *spin echo time*

$$\tau = \frac{A_{1,2}}{\mathbf{k}_{I,F}\cdot\mathbf{n}_{i,f}[(\hbar/m)\mathbf{k}_{I,F}^2 - \mathbf{k}_{I,F}\nabla_q\omega_0(\mathbf{q}_0)]} \tag{3.6}$$

where $A_{i,f} = (2\pi m/\hbar)\nu_{i,f}L_{i,f}\cos\theta_{i,f}$, $L_{i,f}$ are the lengths of the precession regions and $\theta_{i,f}$ are the inclination angles of the RF coils. Note that τ is identical to the correlation time t which is the fundamental variable in the time dependent *van Hove* density-density correlation function.

If the energy width of $S(\Delta\omega)$ is comparable to or broader than $T(\Delta\omega)$, eq. 3.5 gets much more complicated. In this case its easier to determine the linewidth with a standard TAS scan.

Experiment

Inelastic neutron scattering experiments were performed at the cold triple-axis spectrometer V2 (FLEX) at the BER-II research reactor, HMI, Berlin. This instrument can optionally be equipped with an NRSE setup [3]. The spectrometer was configured in the $SM=-1$, $SS=-1$, $SA=+1$ scattering senses with fixed $k_I = 1.7\text{Å}^{-1}$. The PG monochromator was vertical focussing, the analyzer (PG) was flat. A tunable PG filter [6] was installed to suppress second order contamination.

In order to satisfy the spin-echo conditions (eqs. 3.2, 3.3) the slope of the dispersion has to be known. This quantity has been obtained from a Born-von- Kàrmàn fit to published dispersion data [7, 8]. Typical coil tilt angles were $\theta_{1,2} \simeq 30$, typical frequency ratios $\nu_1/\nu_2 \simeq 1.2$.

For each phonon mode and temperature the TAS was set to the nominal $(\mathbf{Q},\omega)$ values where it was kept fixed during spin-echo scans. The polarisation was measured for at least four different values of the spin echo time τ per phonon and temperature (Fig. 3.3). Within statistical error our measurements are in agreement with a single exponential decay (eq. 3.5). Thus we find no evidence for possible deviations from Lorentzian lineshapes.

To correct for resolution effects, we used an analytical resolution function for the NRSE-TAS instrument [4] taking into account instrumental parameters and sample properties (mosaicity and curvature of the dispersion surface). Like in quasielastic spin echo experiments [9], the measured polarization $P_{\text{exp}}(\tau)$ can be written as a product of a resolution term $P_{res}(\tau)$ and the Fourier transform of the scattering law:

$$P_{\text{exp}}(\tau) = P_{\text{res}}(\tau) \times \int S(\Delta\omega)\exp(-i\tau\Delta\omega)d(\Delta\omega) \tag{3.7}$$

The resolution calculation was tested for a phonon at very low q and low temperature, which is expected to have zero linewidth on our resolution scale. Thus the polarisation should be constant ($P(\tau) = 1$). The experimental data in Fig. 3.4 shows a decaying polarisation, which results both from sample mosaicity η_S and curvature of the dispersion surface. For increasing q, the curvature of the dispersion surface gets smaller, the influence of the mosaicity stays nearly constant. For longitudinal phonons (not studied in the present experiment), the depolarizing effect of η_S enters only in second order and is negligible

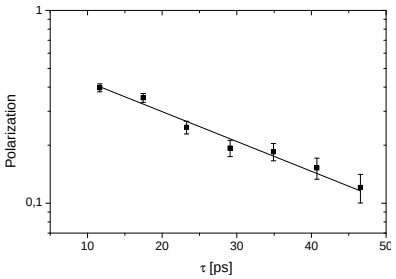

Figure 3.3: Polarization *vs.* spin echo time τ for the [2 0.1 0] TA phonon in Pb, T = 200 K. The line is a fit to an exponential decay.

on our resolution scale, but variations of the lattice spacing $\Delta d/d$ become a first order effect and have to be considered.

In 3.6 the corrected linewidths of our measurements are compared to the TOF experiment of Furrer and Hälg [8] to demonstrate the enhanced resolution of the NRSE-TAS technique.

Since lattice defects are not expected to contribute to the measured linewidths only electron-phonon and phonon-phonon interaction remain. *Ab initio* calculations provided by the MPI Stuttgart [10] show that the electron-phonon contribution to

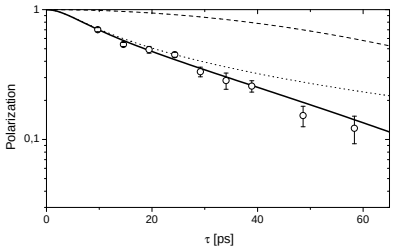

Figure 3.4: [0.025 0.025 0] TA phonon in Pb, T = 50 K. Calculated depolarization resulting from sample mosaicity (dotted) $\eta_S = 4.2'$ (FWHM), curvature of the dispersion surface (dashed) and the combined effect of both (solid). Open circles: experimental data of a linewidth measurement performed at BENSC.

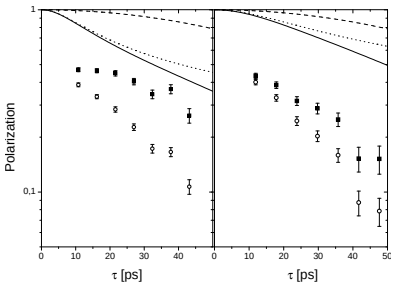

Figure 3.5: Calculated depolarization due to sample mosaic (dashed), curvature of the dispersion surface (dotted) and the combination of both (black line). Experimental raw data (circles) and normalized data (squares). Left: [2 0.05 0] TA phonon at T = 300 K. Right: [2 0.1 0] TA phonon at T = 300 K.

the phonon linewidths is negligible. Furthermore we have measured the linewidth of the [0.1 0 0] TA mode at temperatures above and below T_C. No change in linewidth was experimentally observed.

Zoli [11] has calculated linewidths for Pb based on a pseudopotential model and obtains much larger values than observed in our measurement (Fig. 3.6). He obtained the harmonic constants from a fit to experimental phonon dispersion data and macroscopic elastic

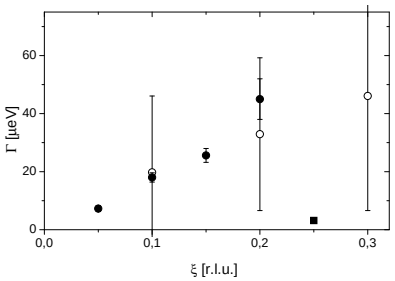

Figure 3.6: Phonon linewidths of the [ξ00] TA mode in Pb. Solid circles : NRSE experiment (this work) ; red open circles : TOF experiment, Furrer and Hälg, 1970

constants. Anharmonic constants were obtained from a fit to the linear coefficient of thermal expansion and the thermodynamic Grüneisen-parameter. There is of course general doubt over the accuracy of the anharmonic parameters obtained from a pseudopotential model. The fact that the interatomic potential in the fcc metals is of long range implies a large number of parameters. Furthermore an approach with only two-body forces is not possible since the macroscopic elastic constants do not satisfy the second-order Cauchy relations. In the last years however there is a growing number of publications with ab initio models of the interatomic interaction which can provide the Fourier transforms of the higher order derivatives of the interatomic potential. No such calculations are published for Pb.

Conclusions

Using the NRSE technique on a cold TAS we have sucessfully applied the phonon-focusing technique to dispersive phonon modes in single crystalline lead. The broadening of the one-phonon peaks resulting in Lorentzian linewidths could be measured with high accuracy superior to conventional neutron scattering techniques used in previous experiments. Phonon linewidths were extracted by taking mosaicity and curvature of the dispersion explicitly into account with a resolution function based on the Gaussian approximation of the TAS transmission function. The result of the linewidth measurement supports

the disagreement between the pseudopotential theory of Pb and previous experiments.

[1] Keller T., Habicht K., Klann H., Ohl M., H. Schneider B. K. *Appl. Phys.*, **A74 [Suppl.]**, (2002), 332.
[2] Keller T., Gähler R., Kunze H., Golub R. *Neutron News*, **6**, (1995), 16.
[3] Keller T., Habicht K., R.Golub. In: Mezei F., Pappas C., Gutberlet T. (Editors), *Lecture Notes in Physics* (Springer, 2003).
[4] Habicht K., Keller T., Golub R. *J. Appl. Cryst.*, **36**, (2003), 1307.
[5] Mezei F. *Inelastic Neutron Scattering* (IAEA, Vienna, 1978).
[6] Vorderwisch P., Hautecler S., Mezei F., Stuhr U. *Physica B*, **213-214**, (1995), 866.
[7] Brockhouse B., et al. *Phys. Rev.*, **128**, (1962), 1099.
[8] Furrer A., Hälg W. *Phys. Stat. Sol.*, **42**, (1970), 821.
[9] Mezei F. (Editor). *Neutron Spin Echo* (Springer, 1980).
[10] Bose S. MPI Stuttgart, private communication.
[11] Zoli M. *J. Phys. Cond. Mat.*, **3**, (1991), 6249.

3.3 PANDA – The Cold Neutron Three-axes Spectrometer

P. Link [1], **D. Etzdorf** [1], **N. Pyka** [1,3], **M. Rotter** [2], **R. Schedler** [2], **R. Sprungk** [2], **E. Kaiser** [2], **C. Wetzig** [2], **M. Dörr** [2], **S. Sahling** [2], **M. Loewenhaupt** [2]

[1] ZWE FRM-II, TU München
[2] Inst. f. Festkörperphysikphysik, TU Dresden
[3] now at: MOWO Maschinenbau GmbH, Berlin

Personal

30th of April this year Dr. N. Pyka left FRM-II and the PANDA project for a position in industry. Since 1st of May Dr. Peter Link is the new instrument responsible.

Project status and progress

During the year assembly of the components of both, secondary spectrometer as well as the primary spectrometer has been continued. The final positioning of the neutron channel in front of beam port SR2 was a major milestone for the primary spectrometer achieved in august. This included optical adjustment of all neutron optical devices (collimators, neutron guide and variable horizontal aperture) inside the channel. All devices have been fully integrated in the instruments remote control software and are ready for operation. Further all crystal holders for double focussing Heusler and PG002 monochromators and analysers have been manufactured and delivered. Concerning the sample environment we note the delivery and successful test of the Oxford 15T vertical magnet system including an adapted Kelvinox ^{3}He-^{4}He dilution refrigerator. The tests after delivery had been performed at PANDA experiment

Figure 3.7: The focussing mechanics for the Heusler crystal analyser (foreground) and monochromator (background)

Figure 3.8: 15T vertical magnet on the PANDA sample table

with the non-magnetic sample-table of PANDA (Fig.3.8). The system reached a maximum field of 14.5T and a lowest temperature of about 30mK (as specification from Oxford Instruments). The cryomagnet is available on PANDA at start of routine operation.

Outlook

During the year 2004 the assembly of the main parts of PANDA should be completed and the spectrometer will be aligned and characterised with neutrons before routine operation may start finally.

3.4 PUMA – The Thermal Three Axes Spectrometer at SR7

K. Hradil [1], **H. Schneider** [1], **G. Eckold** [1], **P. Link** [2], **J. Neuhaus** [2]

[1] Institut für Physikalische Chemie, Universität Göttingen
[2] ZWE FRM-II, TU München

Scientific design

Within a cooperation of the Physical Chemistry Department of the Georg-August University of Göttingen and the Physical Department of the Technical University of Munich the thermal three-axes spectrometer PUMA is installed at the beam tube SR7. The concept of the instrument is an optimal utilisation of the beam using focusing techniques, reduction of background and higher-order contamination using a velocity selector. Thus the instrument is designed to be well adapted with regard to resolution, intensity and background for the planned experiments.

The instrument is particularly intended for the study of collective excitations like phonons and magnons. Due to its flexibility it will also be well suited for the investigation of disordered materials, i.e. diffuse and superorder

scattering, critical phenomena, or for time-resolved experiments on non-equilibrium systems. Fig. 3.9 shows the actual setup of the instrument.

Current status

The detailed technical design of the instrument is given at http://www.frm2.tum.de/puma. This report reviews briefly the progress of the components in 2003. The main components for the single detector option of the instrument are in place. The activities within this year were focused on the mechanical alignment of the spectrometer and the test of the interplay of different components. The software control system is being developed and need to be completed in the near future in combination with the first tests with neutrons.

Background and high order contamination at PUMA will be reduced by the use of a velocity selector before the monochromator built by Astrium. Due to some technical problems the design of the selector had to be changed and could not be delivered as scheduled. The container of the selector is rebuilt and the selector discs are dynamically balanced by Astrium. The first tests under real conditions can be performed beginning of next year and the selector can be delivered in the first quarter of the year.

The horizontal divergence of the neutron beam can be defined by remotely controlled Soller collimators before (20', 40', 60') and after (10', 20', 30', 45', 60') the monochromator. Between sample, analyser and detector the corresponding collimators have to be changed by hand.

PUMA is equipped with a monochromator changer for four different crystals each with a maximum effective area of about 460 cm^2. PG(002), Cu(220), Cu(111) and Si(311) are foreseen. While the silicon monochromator consists of a single bent perfect wafer, the other ones are made from more than 100 small mosaic crystals that are mounted on a doubly focussing device. A rocking curve study of the PG(002) and Cu(220) crystals by gamma-rays exhibits a mosaicity of around 30'. The double bend apparatus was designed within a cooperation of the mechanical workshop of the university of Göttingen (IPC) and the FRM-II and is currently being tested and aligned in the workshop of IPC. In the first quarter of 2004 the device equipped with PG(002) crystals will be installed at PUMA, tested mechanically and aligned optically. The installation of the Cu(220) monochromator is forseen afterwards. The Si(311) monochromator, built by Swiss Neutronics, is aimed for delivery beginning of next year. So in fact, PUMA can provide two different monochromators during its commissioning phase. The characteristics of both monochromators will be tested with neutrons after start-up of FRM-II.

Figure 3.9: Photograph of the current setup at FRM-II

Several additional devices such as secondary shutter, PG filter, etc. have been manufactured by the workshop of IPC. These components will be delivered end of this year and beginning of next year and have to be implemented afterwards within the electronic control system of the instrument. Motorized slit systems with integrated electronics as developed in Göttingen are ready for use at different positions of the spectrometer. These devices are implemented within

the control system of the instrument.

PUMA provides two different options for the sample stage, i.e. a double goniometer (AZ-Systems) for a top load of < 1000 kg (in combination with a +/- 20mm z-translation table < 150 kg load) or an Eulerian cradle, on a 430 mm high base module. The high flexibility concerning the usable distance to beam (300mm) allows to use complex sample environments as cryomagnets, furnaces.

Beside the standard FRM-II sample environment, PUMA provides an closed cycle cryocooler (4K - 300K) which is mountable on the xyz sample stage and optionally within the Eulerian cradle and a furnace (up to 1200 K) for the Eulerian cradle. Additionally, a cryofurnace (3K - 800K) will be delivered by the end of 2003. A high temperature furnace up to 3000K, which will be built in cooperation with the FZ Jülich and IPC is planned.

The analyser/detector unit for the single detector option of PUMA is completely tested. Moreover, The FRM-II detector group has sucessfully developed a counter module for time-resolved, stroboscopic experiments. After the system control via TACO is available, the module can be implemented within the instrument control.

The focussing PG(002) analyser (Fig. 3.10) with a motor controlled horizontal and a fixed vertical curvature is completed and can be installed at the beginning of next year.

The design of the multianalyser component for the multianalyser/multidetector option of PUMA is almost defined.

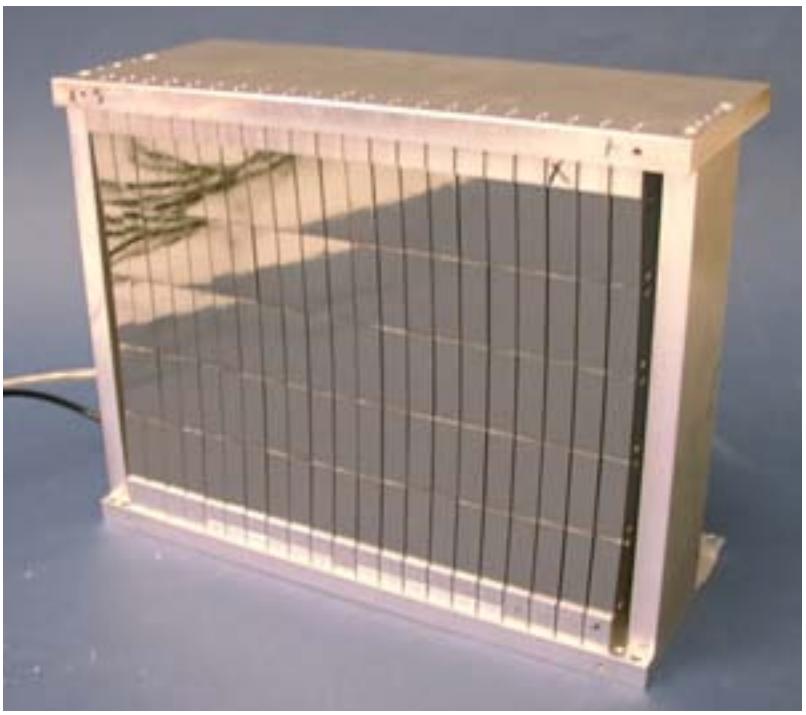

Figure 3.10: Photograph of the bending apparatus for the focussing analyser

The 11 PG(002) analyser crystals will be mounted on one common table with individual rotating devices for each analyser which again can be translated on individual linear stages. Thus, the distance sample/analyser of each individual analyser can be adjusted. The electronics group of the IPC has just finished a prototype of a multi stepper motor control module for 6 motors on a single card, thus providing a highly integrated control system for the sophisticated multianalyser system. Currently, the mechanical specifications of the multidetector unit will be developed. Two different detector options are planned: 11 single detectors, each individually movable and synchronized with the corresponding analyser blade will be used for dispersive modes of operation. An additional PSD detector is provided for the focussing mode. In cooperation with the FRM-II detector group discussions about the detector electronic control system for this option is ongoing.

In the course of this year main parts of the instrument computer network were installed. The close cooperation with the IT-Network group of the FRM-II for designing, installing and testing main parts of the instrument network is highly acknowledged.

The construction of the biological shielding around the instrument is carried out in cooperation with the mechanical design group of the FRM-II. It consists mainly of heavy concrete-filled T-shaped steel containers (height 2m, thickness 0.4m) which can flexible mounted and dismounted with the help of the crane.

3.5 RESEDA – Resonance Spinecho Spectrometer

M. Bleuel [1], **M. Axtner** [1], **R.Gähler** [2], **P. Böni** [1]

[1] Physik Department E21, TU München
[2] Institut Laue-Langevin, Grenoble

Neutron guide

Figure 3.11: Scetch of RESEDA

RESEDA, the quasielastic neutron resonance spinecho (NRSE)-spectrometer at the FRM-II is located in the neutron guide hall. The neutron guide (5b) leading to the instrument was accomplished in 2003 and is the longest polarising neutron guide in the world. Because of it´s length the bending radius is big ($r = 1640$m), so that even neutrons with a short wavelength ($\lambda = 2$Å) are transmitted to RESEDA. The polarisation is better than 96% over the whole wavelength range.

On the photo (3.12) the polarising neutron guide in its magnetic guide field is shown. A cover of 70 mm lead acts as a biological shield against the γ-radiation, which comes from absorption in the boron glass.

Neutron selector

In 2003 a reconstruction of selector shielding became necessary, because a new polarised reflectometer joined RESEDA and will use the excellent neutrons from 5b-neutron guide as well. During this reconstruction the whole instrument, including the neutron guide and all surrounding installations, was plotted in a three-dimensional model with construction program "solid works".

The new shielding is to be installed in the early spring 2004. As soon the operation of the FRM-II has started, the final adjustment of RESEDA with neutrons can begin.

Activities in 2003

The main activities in year 2003 at RESEDA were concentrated on the electric components of the instrument. The RF-circuits and the detector electronics were tested in their final position, the encoder, which determines the position of the spectrometer arms, and the NSE coils for the low resolution mode were mounted. Also the cabling of the instrument (motors, air cushions, air sensors, water, DC- and HF-supply for the Bootstrap-coils) was continued and the instrument-control-program was continuously improved.

Figure 3.12: magnetic guide field for the polarising guide

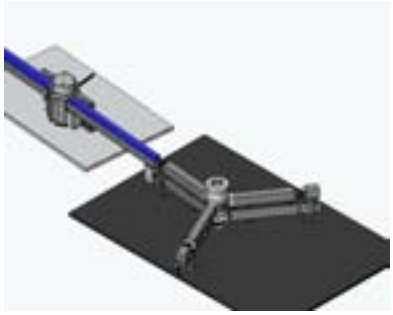

Figure 3.13: Topview of RESEDA with Selector Shielding

λ	$\lambda = 2,5 - 15$
flux at sample position	$\Phi > 10^8/cm^2s \quad (\lambda = 4)$
spin echo time	$\tau = 0,001 - 30\,ns$
length of the pseudo fields	$L = 2,6\,m$
max. (pseudo) magnetic field	$B = 1200\,G$
max. momentum transfer ($\lambda = 2.5$)	$q = 3.5^{-1}$

Table 3.1: Characteristics of RESEDA

The estimated start of the FRM-II will not be before spring of 2004. Because of this delay of at least 3 years compared to the early time table, all RESEDA activities are stretched. It is important to keep the know how and avoid a further splitting of the team.

3.6 RSSM – Backscattering Spectrometer

P. Rottländer [1], **T. Kozielewski** [1], **M. Prager** [1], **D. Richter** [1]

[1] IFF - Forschungszentrum Jülich

The backscattering spectrometer RSSM will be built at the end position of neutron guide NL6. In its standard setup it will offer an energy resolution of 0.8 μeV and an energy window of $\pm 32\,\mu$eV. A higher resolution will be optionally available. In 2003, it made great advances towards completion next year. In the following, we will give a short description of the instrument, together with an outline of the principal developments.

The first element which neutrons encounter is the ELREBO, which is a device to position a piece of a neutron guide, a beam stop, or a liquid nitrogen cooled beryllium filter in the neutron beam. The box itself is finished and vacuum tested, and the beam stop will be finished by end of 2003. The beryllium filter already is in place but with too high a nitrogen consumption and a too high final temperature of about 140 K. A redesign is on the way.

After serious problems at the University of Hannover with casting of the rotor of the home-made velocity selector which follows the ELREBO, it was decided to buy a commercial selector from Astrium, formerly Dornier. It will be delivered in July 2004. In the wavelength range of about 3 Å, this selector will be more efficient which might alleviate the cooling problems of the Be filter. However, the project of a

Figure 3.14: The intermediate version of the chopper wheel during centering of the central bushing

home-made selector will not be abandoned, but adapted for the Si(311) option (see below).

The instrument specific convergent neutron guide has a separate vacuum chamber which was finished last year. Due to problems on the side of the glass supplier, the guide elements will be delivered in March 2004 only.

At a short distance after the neutron guide, the neutrons are reflected by the phase-space transformation (PST) chopper. It is divided into six segments, three of which carry crystals of pyrolytic graphite at the circumference, the three others are empty. Neutrons coming from the chopper will be perpendicularly reflected at the monochromator. On their way back, they will pass the chopper at a segment without crystal, and hit the sample. As a major design feature of the spectrometer, the chopper also increases the intensity of the neutron beam in the desired energy range by accelerating neutrons which are too slow, and slowing down those who are too fast. For more information, see [1].

In the course of the year, the chopper wheel had to be completely redesigned, primarily due to safety reasons. The wheel now consists entirely of aluminum, where an alloy with high long-term fatigue limit has been used. Through successive design improvements, mechanical stress during rotation also has been reduced. An intermediate (Fig. 3.14) and the final version of the wheel both have been successfully spun at the speed of 4850 rpm; 4800 rpm will be the operating frequency. The chopper drive is also assembled and has entered the test and optimisation phase.

The monochromator is mounted on a drive to achieve the energy variation needed for spectroscopy. A test version of the drive with an aluminum shaft has been successfully tested for a month in the beginning of 2003. Using those experiences, the final version was built with more

Figure 3.15: Test run of the final version of the Doppler drive at 4.7 m/s

built with more sophisticated air bearings which allow for a higher manufacturing tolerance. Therefore the shaft could be made of carbon fibre compound and a more powerful motor employed. This gave an increase of the maximum attainable speed from 3.5 m/s to 4.7 m/s. The final version ran successfully for one week in November 2003. The approval of the drive will be in December 2003.

After being scattered by the sample, neutrons of the right wavelength are reflected, again perpendicularly, at the analyser crystals. Here, the instrument will offer a standard version of unpolished Si(111) crystals, with a neutron energy of 2.08 meV, an energy range of $\pm 32\,\mu$eV, and a resolution of 0.8 μeV. It will also provide a high-resolution setup with polished Si(111) crystals with a resolution of $0.45\,\mu$eV, a CaF_2 monochromator which shifts the energy window by 24μeV towards lower energies, and a version with Si(311) monochromator and analysers. It uses neutrons with a higher energy of incidence of 7.63 meV. The latter has a lower resolution but gives access to a different momentum transfer range.

The standard version of analysers and the monochromator mirror plate already were equipped with Si(111) crystals in 2002. In 2003, the first analyser shells were equipped with polished Si(111) crystals of 5×5 mm edge length. In Fig. 3.16, a quality check of the crystals is shown. This check is performed by placing a laser close to the centre of

Figure 3.16: A quality check of the high-resolution analyser. Left the very first test waver that was glued, to the right a good average image.

the analyser sphere. The laser beam is widened a little so that it illuminates an area of about 8 cm diameter. The reflected light falls on a graph paper screen which is again close to the centre. The reflections generally fall into one single place which is not much taller than twice the crystal size, except of those of the misaligned crystals.

In October 2003, the electronic department of the Research Centre Jülich finally started with the design of the instrument control system. At the same time, the instrument also started to leave first traces in the neutron guide hall in Munich: The plaster floor at the instrument site has been removed to give place for a “dancing floor”, on which the heavy components – Doppler drive and analysers – can be arranged for different setups, and for the anchoring of the gas-tight instrument chamber (Fig. 3.17). The chamber itself is already finished and will be assembled in Munich early in 2004.

The instrument will also offer a diffractometer option which allows for a good angular resolution. It will be realised by a series of position sensitive detector tubes which cover scattering angles from around 10° to 140°. This option is already constructed and awaits to be manufactured.

The standard version of the instrument is expected to be operational in the third quarter of 2004. The additional monochromators and the diffractometer option will follow until end of the year.

Figure 3.17: The instrument chamber during an inspection in March

[1] Schelten J., Alefeld B. In: Scherm R., Stiller H. H. (Editors), *Proceedings of Workshop on Neutron Scattering Instrumentation for SNQ*, volume Report Jül-1954, FZ Jülich (1984).

3.7 TOFTOF – Time of Flight Spectrometer Near Completion

T. Unruh [1], **J. Ringe** [1], **J. v. Loeben** [1], **J. Neuhaus** [1], **W. Petry** [1,2]

[1] ZWE FRM-II, TU München
[2] Physik Department E13, TU München

Several milestones could be reached on the way to the completion of the time–of–flight spectrometer TOFTOF: The chopper system has been installed and tested successfully. The 605 detectors were tested individually including the preamplifiers. The detectors and the preamplifiers were mounted on the racks and wired with the time–of–flight electronics. Last but not least a stage with the measuring cabin for the users of the instrument has been built up. The last main components of the spectrometer have now been delivered: The radial collimator, the focussing neutron guide and the shielding for the primary spectrometer. These components will finally be assembled in spring of 2004. Thus 2003 has been a successful year for the group of the TOFTOF spectrometer at FRM–II.

A picture of the instrument is displayed in Fig. 3.18. The shielding of the primary spectrometer is disassembled. Thus the view is free to the four vessels containing a total of the 7 chopper discs. It provides synchronous and asynchronous operation of each disc (diameter: 600 mm) with speeds from about 100 rpm up to 22000 rpm. The phase shift of the discs can be adjusted with an accuracy of about 0.05 degree. The speeds and phases of every disc and the gear reduction of the frame overlap chopper can be changed within the allowed limits during operation of the choppersystem without further limitations.

Figure 3.18: Front view of the time–of–flight spectrometer at FRM–II with disassembled shielding of the primary spectrometer (see text)

The flight chamber of the secondary spectrometer is positioned at the end of the primary spectrometer and is partly visible behind the chopper vessels in Fig. 3.18. This chamber also houses the racks with 605 detectors and the same number of preamplifiers. A cut–out of the detector is pictured in Fig. 3.19. On top of the flight chamber the electronics rack can be seen< which includes the time–of–flight electronics and some hardware for instrument control. The cabeling has been finished for the whole detector system which is currently being tested.

On the left hand side in Fig. 3.18 two measuring cabins are visible. The first one is for the neighbouring REFSANS instrument and the second one is for the time–of–flight spectrometer. The TOFTOF group is looking forward to furnish the cabin

and to control the first TOF experiments from there next year.

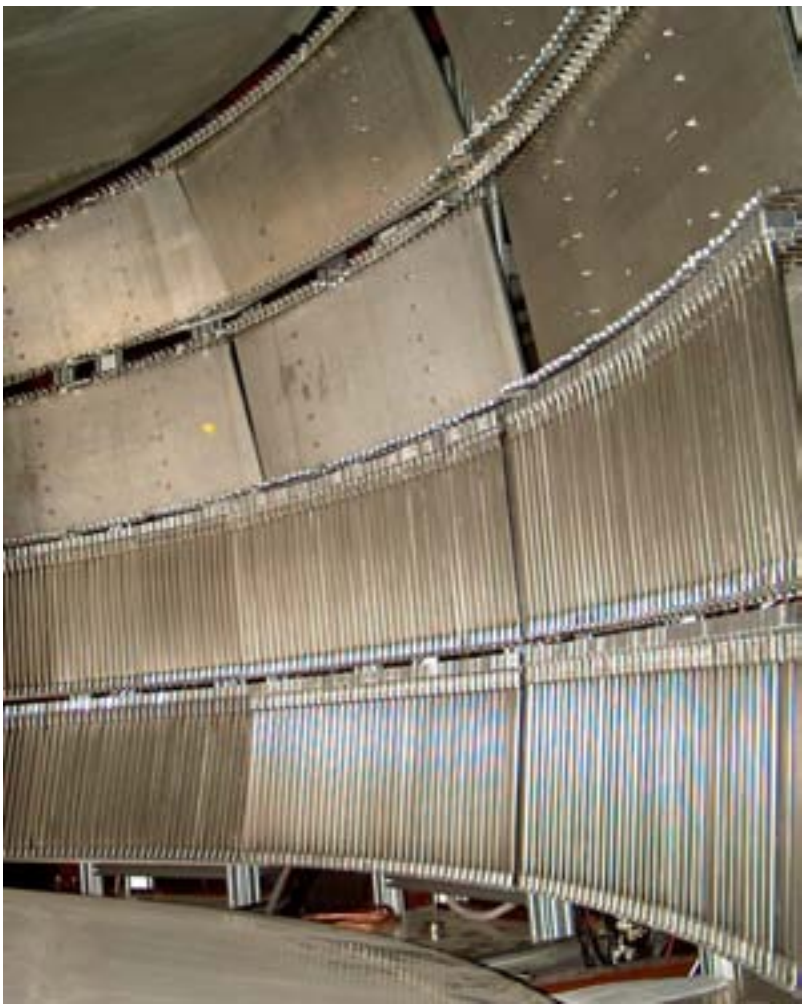

Figure 3.19: Photograph of a cut–out of the TOFTOF detector bank

4 Fundamental Physics

4.1 MAFF — Munich Accelerator for Fission Fragments

D. Habs [1,3], **R. Krücken** [2,3], **M. Groß** [1,3], **W. Assmann** [1,3], **L. Beck** [1,3], **T. Faestermann** [2,3], **R. Großmann** [1,3], **S. Heinz** [1,3], **Ph. Jüttner** [4], **O. Kester** [1,3], **H.-J. Maier** [1,3], **P. Maier-Komor** [2,3], **F. Nebel** [2,3], **M. Schumann** [1,3], **J. Szerypo** [1,3], **P. Thirolf** [1,3], **F.-L. Tralmer** [4], **E. Zech** [2,3]

[1] Ludwig-Maximilians-Universität, München
[2] Physik-Department E12, TU München
[3] Maier-Leibnitz-Labor f. Kern- und Teilchenphysik, Garching
[4] ZWE FRM-II, TU München

The **M**unich **A**ccelerator for **F**ission **F**ragments (MAFF) is a reactor-based Radioactive Ion Beam (RIB) facility which is being planned and set-up at the FRM-II mainly by the group for experimental nuclear physics (Prof. Habs, LMU) and the physics department E12 (Prof. Krücken, TUM).

The goal of this installation is the production of very intense beams of neutron-rich isotopes that will be available for a broad range of nuclear physics experiments as well as applied physics and nuclear medicine. In a first step the beam will have an energy of 30 keV (low-energy beam). In a second step also a high-energy beamline will be set up where the ions are post-accelerated to energies adjustable in the range 3.7–5.9 MeV/u. An overview of the project can be found, e. g. in [1, 2]. Here we will summarize mainly the progress within the last year.

Authorization procedure

As the FRM-II has received its final operating license in May 2003, the MAFF authorization procedure can commence. Some financial questions, however, still need to be clarified (total cost of authorization procedure).

Infrastructure

The feedthrough-plug between neutron guide tunnel and casemate

The neutron guide tunnel of the FRM-II will house the mechanics to move the target trolley and to operate the ion source changer. As the operational reliability of these components is crucial for MAFF, a manually driven backup system is considered necessary. Due to the high activity level in the tunnel, this system must be operated from outside. From the technical point of view, an obvious place is the neutron guide casemate which is connected to the neutron guide tunnel by openings in the concrete wall that were before only used by the neutron guides with the remaining space filled by shielding bricks in order to fulfill radioprotection and security requirements.

We therefore placed a special plug containing several feedthroughs alongside a neutron guide in the wall opening. The feedthroughs will contain shafts to operate the ion source trolley in case of failure of the electric drives along the beamline in the neutron guide tunnel as well as gas pipes to connect the cryopumps at the beamline to the compressors that will be placed in the casemate.

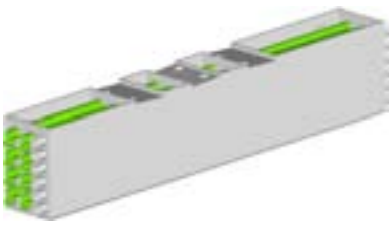

Figure 4.1: The feedthrough-plug between neutron guide tunnel and casemate.

The ion source test bench

At the former hot chemistry lab of the LMU technological laboratory an ion source test bench is being set up.

A major (financial) part of installing this test bench is the decontamination and cleaning-up of the hot lab. Since the funding has finally been provided in summer 2003, the work is meanwhile in progress. The old ventilation system has been dismantled and a new filter system is installed. The next step will be the removal of the contaminated glove boxes.

After decontamination of the lab, a mass separator which has been made available by GSI will be set up. With added diagnostics, this mass separator will be the main device for testing of different target/ion source units. Also a connection will be made to the next floor laser lab, as we are not only interested in surface ion sources but also in laser ionization. Therefore lasers in the laser lab will be used to operate a laser ion source. We will then have a full test bench available for ion sources before their use at the FRM-II in in-pile position.

Moreover, a new glove box and a welding station have been purchased and combined to an inert-gas welding station for handling radioactive materials. This station will also be placed in the ion source testing lab and will allow the assembling of ion sources containing uranium and the welding of the target container or other parts.

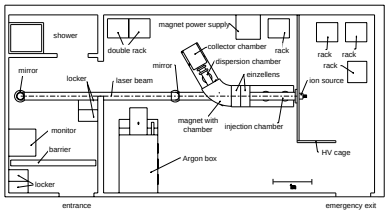

Figure 4.2: The planned layout of the ion source test lab.

Development of components

The in-pile cryopanel

A considerable fraction of the radioactivity produced in the MAFF fission target will consist of short-lived gaseous activity, like krypton or xenon fission products or the halogens bromium and iodine. It is intended to prevent migration and release of these volatile fission products by localizing them on a He-cooled cryopanel until transformation into non-volatile species by β decay. The required operational temperature below 20 K results from the vapour pressures of the gases and vapours that have to be pumped. At this temperature the usual rest gas components (except hydrogen) as well as the fission isotopes of Kr, Xe, Br, I will be frozen at remaining vapour pressures in the UHV region ($\leq 10^{-11}$ mbar). Such cryopanels will be installed in the MAFF beamtube at either side of the fission source (SR6-a and SR6-b). Limited by the inner diameter of the beamtube (250 mm) as well as by the MAFF fission source required to be moved inside the cryopanel, a compact design had to be developed.

As an adequate solution a

Figure 4.3: Prototype of the MAFF cryopanel.

double-wall tube (gap width 4 mm) with 6 spiral-like separated sections for in- and outlet of the cold He gas was designed. The cryopanel length is 1 m, the inner diameter of the He double-tube amounts to 157 mm, the minimum value needed still to be able to move the fission source inside the cryopanel. The wall thickness of 2 mm is a compromise between the safety regulations for a pressure vessel on the one hand and the minimization of the nuclear heating due to the neutron and γ flux. A passive floating heat shield will reduce the thermal heat load form the surrounding warm beam tube. Aluminum of the type 6061-T6 was chosen as material for the cryopanel because of its cryogenic specifications needed for the operation at an input temperature of 10 K, while the output temperature will be about 20 K. In addition material specifications and certificates for the use in a nuclear reactor environment already exist for Al 6061-T6.

The cryopanels will additionally provide the necessary high-vacuum conditions close to the fission source. The pumping capacity of the cryopanels is depending on the pressure and the gas type, amounting to about $12.7\ \mathrm{l\,s^{-1}\,cm^{-2}}$ for nitrogen and $5.9\ \mathrm{l\,s^{-1}\,cm^{-2}}$ for xenon. The

overall pumping capacity of the cryopanels on each side of the beam line will amount to about $8 \cdot 10^4$ l s^{-1} for nitrogen and $4 \cdot 10^4$ l s^{-1} for xenon.

In order to build up the technological knowledge for manufacturing the cryopanel via cryogenic shrinking and to allow for performance tests, a prototype has been produced by ACCEL (Bergisch Gladbach), which is shown in Fig. 4.3.

Beam Transport

The MAFF beam transport system is guiding the radioactive ion beam from the fission source, through a mass separator to the beam cooler. New simulations using the SIMION7 code, which includes fringe fields and higher order effects have been conducted. Fig. 4.4 shows on the left side a simulation result obtained with the COSY code to give an overview of the beam line.

Within the simulations for the beam transport to the mass separator several critical issues have been addressed:

1. The tube with the ion optical elements installed is bent downwards a few mm by its own weight.
2. There might be a transversal offset between the source exit hole, and the extraction lens entrance hole.
3. Some neutron and gamma absorbers must be implemented in the beam line.
4. High efficiency and low emittance are required.

Solutions to those problems have been found:

1. The bending of the tube is counterbalanced by steering voltages applied to one of the quadrupoles within each lens. Fig. 4.4 shows on the right the quadrupole prototype.
2. To be able to deal with large offsets of up to 5 mm, a segmented extraction electrode, with a 15 mm hole is used. Voltages can be applied to all four segments. In conjunction with the steering electrodes in the first triplet the offset can be corrected and the beam is focused on axis.
3. Gamma and neutron absorbing materials are placed at the foci after the first and second triplet.
4. Optimisation of the quadrupol voltages lead to 100 % transmission up to the mass separator and an emittance of 12π mm mrad at 30 keV.

The mass separator follows the layout suggested by Mattauch and Herzog. It consist of an electrostatic and a magnetic dipole for energy independent mass separation. Two masses, m_1 and m_2 (with $m_1/m_2 = 1.5$) will be selected by the separator and transported to different coolers. The simulation reveals a mass resolution of approximately 170 for the separator. The magnetic dipole is designed in a way that all masses will be focused in the same plane. A slit system will be installed there to stop the undesired masses. If a deflection voltage is applied to the slits, the beam can be bent in a way to increase the mass range

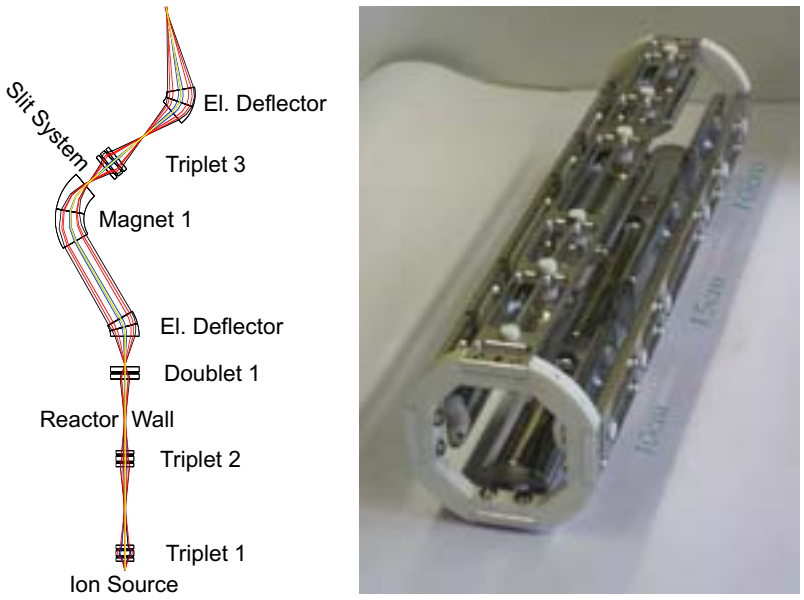

Figure 4.4: A COSY simulation of the beam line is shown on the left side. The picture on the right displays a prototype of the beam extraction quadrupole.

from $m_1/m_2 > 1.2$ to $m_1/m_2 = 1.8$.

Ion beam cooler

Instead of applying the well-established technique of Radio Frequency Quadrupoles (RFQs) where the ions are transversely confined during the cooling process by a quadratic pseudopotential we have investigated a new concept where the RFQ structure is replaced by a stack of thin Radio Frequency ring electrodes with varying inner diameters surrounding the buffer gas volume. Other than with RFQs the potential created by the RF funnel is box shaped which suggests that space charge effects limiting the maximum beam current in a RFQ should have less effect.

Following detailed Monte Carlo simulations, we have carried out first experimental investigations on the RF funnel at the IGISOL facility in Jyväskylä (Finland) with beam currents up to 20 nA. We found a very promising behaviour of the transmission characteristics since the transmission of 65 % proved to be independent of the beam intensity over all the examined range which revealed the applicability of the RF funnel as high-current cooler. This observation can on one hand be explained by the funnel electrode structure providing a high angular acceptance at the entrance and allowing for a smooth focusing of the ion beam during the cooling process. On the other hand, the box shaped pseudo potential reduces ion losses due to field distortions which concern especially particles on trajectories far off the cooler axis.

The use of RF funnels for ion guiding and focusing itself is not new and has already been applied successfully in some fields of physics and chemistry. However, up to now no RF funnels have been applied for confining low-energy ion beams at buffer gas pressures around 0.1 mbar. But nevertheless, an efficient cooling of intense low-energy beams is important for MAFF, where high-intensity high-quality beams are required.

The MAFF accelerator

The high-energy part of MAFF aims at accelerating intense radioactive ion beams of a mass-to-charge ratio < 6.5 up to energies of 5.9 MeV/u. Design goals areto provide the experiments with a high quality beam both in longitudinal and in the transverse dimension and to be able to tune finely the energy of the beam from 3.6 up to 5.9 MeV/u.

Another design goal is to achieve a very high transmission, in order to avoid high contamination of the structure and hence an

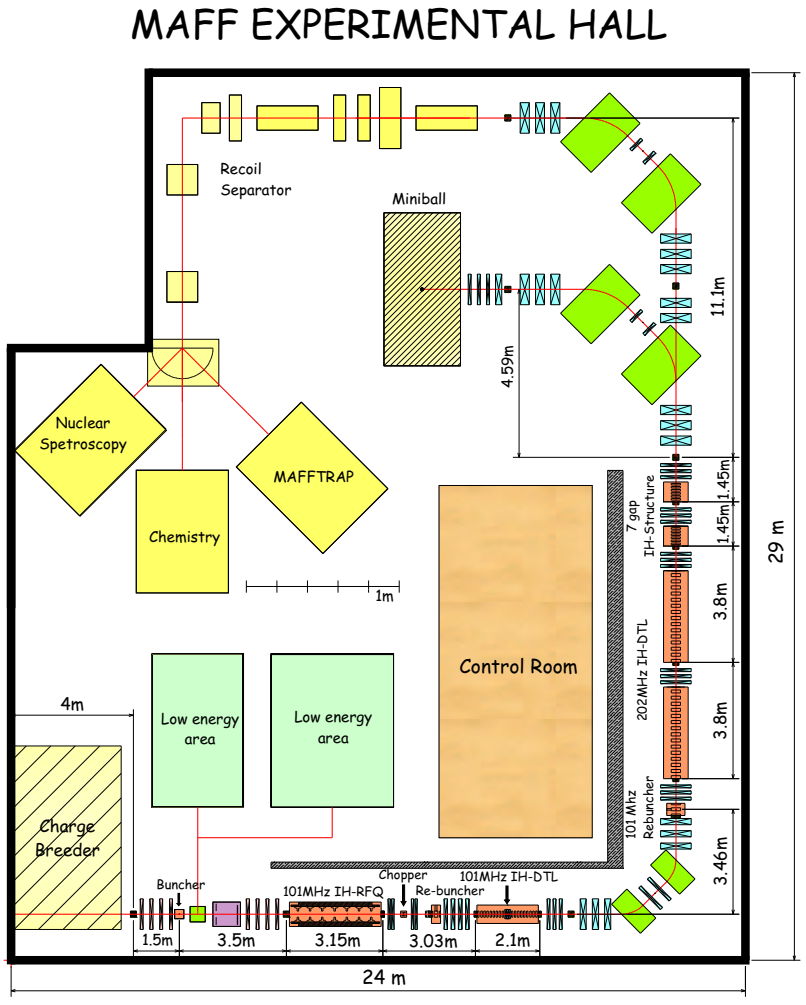

Figure 4.5: Layout of the high-energy part of MAFF in the external experimental hall.

easier maintenance of the accelerating structures.

The first part of the accelerator chain consists of a charge breeder source [3] that delivers ions with $A/q < 6.5$ and in a 101.28 MHz IH-RFQ which brings the ions up to an energy of 300 keV/u.

Currently the design has been modified in order to accommodate an external multi-harmonics buncher placed 3 meters upstream the RFQ. This device will allow a time spacing of about 80 ns between the main bunches, and it creates a bunch with a longitudinal emittance smaller than the one that is formed inside the RFQ.

The matching section downstream the RFQ consists of a chopper which cleans the beam from the small satellite bunches that are formed inside the RFQ.

The following accelerating steps are provided by a 101.28 MHZ IH-Tank that boosts the energy up to 1.45 MeV/u and three 202.56 MHz IH-Tanks which bring the beam up to the energies of 3.0, 4.2 and 5.4 MeV/u respectively [4]. There will be 2 additional short IH structures with a limited number of gaps which will be used for the fine energy variation.

The interval required for the energy variation is between 3.6 and 5.9 MeV/u so in the operation regime the final energy will be tuned from the last operating tank which delivers a final energy close to the required one and the two short cavities will be used in the accelerating and decelerating mode depending on the desired energy. In this way it is also possible to vary the final longitudinal beam parameters to achieve beam focus at the target position.

The beam is then transported to the high energy experimental area by means of two identical modular beam lines. The design goal of these beam lines are the transport of the beam without dispersion at the target point and the modularity, allowing hence a saving of the power supplies and of the other services.

MAFF-Trap

A Penning trap system similar to REXTRAP at ISOLDE (CERN) or JYFLTRAP at Jyväskylä is being built to measure nuclear masses with high precision and/or to do nuclear spectroscopy at trapped ions. The superconducting magnet has been ordered at the MAGNEX company and will be delivered mid 2004. The device will first be installed at the low-energy beamline but can later be moved to the high-energy beam.

[1] MAFF — Physics Case and Technical Description. http://www.ha.physik.uni-muenchen.de/maff/.
[2] Habs D., et al. The Munich Accelerator for Fission Fragments MAFF. Proc. EMIS-14, to be published in NIM B.
[3] Kester O., et al. In: *Ann. Rep. of the EU-RTD project "charge breeding"*, HPRI–CT–1999–50003 (2002).
[4] Pasini M., et al. Radioactive ion beam acceleration. RNB 6 Conf. Proc., to be published.

4.2 MEPHISTO – the Cold Neutron Beam Facility for Particle Physics at FRM II

C. Schanzer [1], **O. Zimmer** [1]

[1] Physik-Department, Technische Universität München, 85748 Garching

MEPHISTO is the cold neutron beam user facility for particle physics experiments at the FRM II. Its experimental zone is situated in the neutron guide hall at the end of the 116×50 mm^2 supermirror neutron guide NL3a. Some of the studies to be performed at this facility were already lined out in the last annual report. Here we briefly describe some of its features and the installation. The design of the beamline enables an easy adaptation to the actual experiment

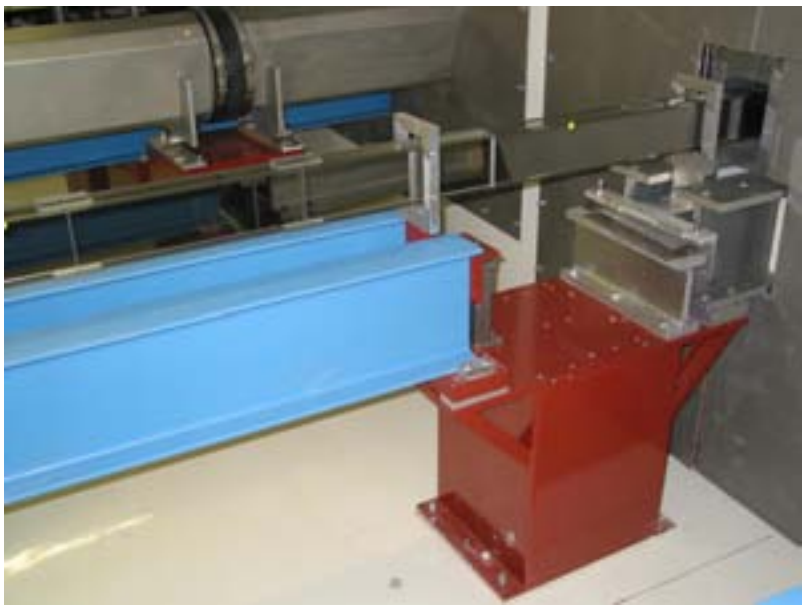

Figure 4.6: Section of the guide NL3a which will transport cold neutrons to MEPHISTO. The support socket shown is situated six meters upstream from the end of the guide. The glass elements can be easily reconfigured to accommodate a neutron polariser and choppers or a velocity selector on the socket.

without compromising a careful shielding for low radiation background.

The instrument can be operated either with polarised or non-polarised neutrons. A large-area, 40 cm long supermirror bender polariser (manufactured by Swiss Neutronics) is already available. The device possesses coatings which stay remanent even at inverted magnetic guiding field, and it is able to polarise the whole white beam. It may be installed on a support socket in the casemate six meters upstream from the end of NL3a, thus taking advantage of the heavy shielding of the casemate's wall visible on the right side in Fig. 4.6. Movable support structures and shieldings enable a reasonably simple adaptation to the change of the beam direction by about 20 mrad induced by the polariser.

A secondary beam shutter is situated in the vacuum of the beamline 10 m upstream from the end of the neutron guide (see Fig. 4.7 and 4.8). It shall enable the user to work in the experimental zone at running reactor without interfering with the other instruments. The end of the neutron guide is equipped with a flange such that the whole beamline including the tank of the beamstop can be configured to consist of a single vacuum, thus avoiding neutron windows with their inherent background due to neutron absorption and scattering. For experiments requiring ultra-high vacuum, two special flanges with very thin foils may be used instead, enabling a separation of vacua of different quality.

The heavy beam stop includes several degrees of freedom for a quick adaptation to the actual particle physics experiment, without any compromise concerning safety requirements. Neutron absorbing materials and

Figure 4.7: The secondary beam shutter (technical design: F. Tralmer). Its vacuum housing also includes two movable beam attenuators, visible behind the shutter block.

and lead shieldings for gamma-suppression are situated in a 2 m long vacuum tank, which is equipped with a CF-flange for its connection to the beamline. In a later stage, the tank will also house a little supermirror polariser and a neutron detector for monitoring the stability of the neutron polarisation during experiments without breaking the vacuum.

Figure 4.8: J. Fink mounting the shutter in the NL3a beamline.

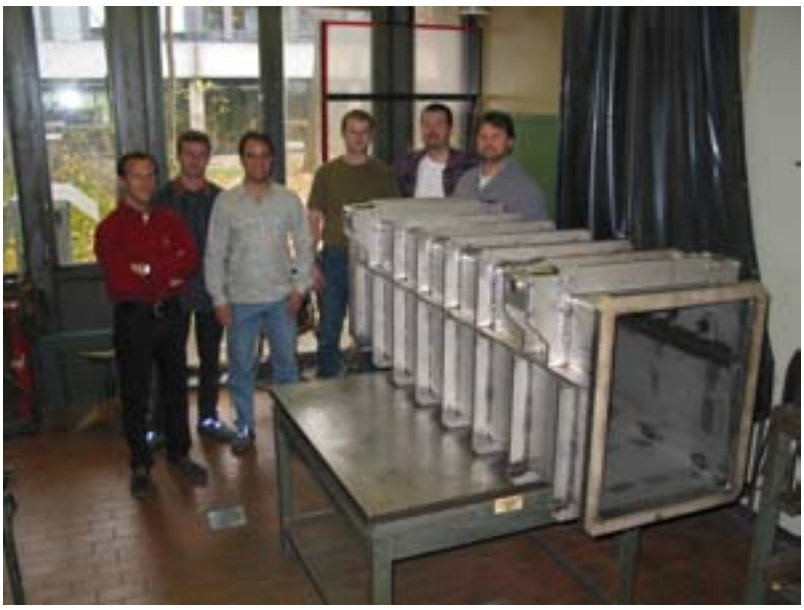

Figure 4.9: The team of the central workshop with their readily welded vacuum tank of the beamstop, a fine piece of craftsmanship. From right to left: K. Hochstetter, A. Braunschedel, T. Fechter, R. Jahrstorfer, M. Reither and M. Pfaller (M. Ducke and M. Schönberger missing on the photo).

4.3 NEPOMUC – Neutron Induced Positron Source Munich and its Experimental Facilities

C. Hugenschmidt[1], **G. Kögel**[2], **R. Repper**[1], **K. Schreckenbach**[1], **P. Sperr**[2], **B. Straßer**[1], **W. Triftshäuser**[2]

[1] ZWE FRM II, TU München
[2] Institut für Nukleare Festkörperphysik, Universität der Bundeswehr München, 85577 Neubiberg

NEPOMUC

The intense positron source is installed as an in-pile component in the tip of the declined beam tube SR11 at the new research reactor FRM-II at the Technical University of Munich. After thermal neutron capture in cadmium the absorption of the released high-energy γ-radiation in platinum generates positrons by pair production. At NEPOMUC the world highest intensity of the order of 10^{10} slow positrons per second in the primary beam is expected. The moderated positrons are extracted by electrical lenses and magnetically guided to the outside of the biological shielding of the reactor. There, an aperture, gamma-detectors and a movable beam monitor are installed in order to measure the

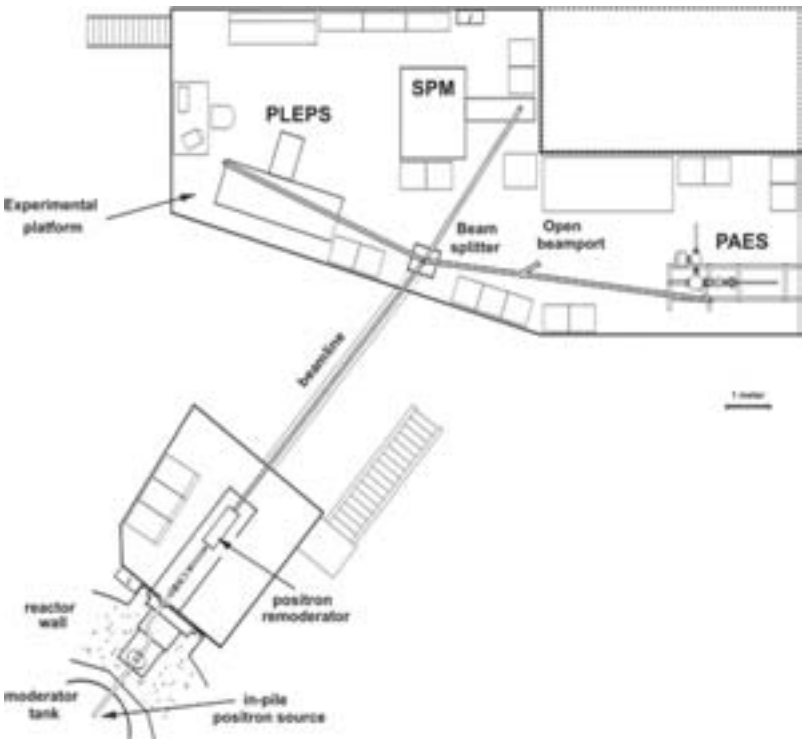

Figure 4.10: Overview of NEPOMUC and its instrumentation.

positron intensity as well as the beam profile. The following beam line guides the positrons to a beam splitter on the experimental platform.

INSTRUMENTS AT NEPOMUC

In the first arrangement, the positron beam is connected to three experiments on the platform in the experimental hall of FRM II (see 4.10). Within our collaboration a **p**ulsed **l**ow **e**nergy **p**ositron beam **s**ystem (PLEPS) and a **s**canning **p**ositron **m**icroscope (SPM) will be transferred to NEPOMUC. Both, PLEPS (4.11) and SPM (4.12) were constructed and built at the university of the Bundeswehr in Munich (UniBW). At present, these facilities are under operation with ^{22}Na positron sources with beam intensities up to 10^3 positrons per second. In order to get depth dependent information from the surface to the bulk of the material, the positron energy can be varied from a few 100 eV up to 18 keV. The lateral resolution is about 3 mm at PLEPS and of about 2 μm at the microscope. The third instrument is a facility for **p**ositron annihilation induced **A**uger **e**lectron **s**pectroscopy (PAES). The PAES facility was built up at E21/TUM and is designed for extremely sensitive studies in surface science (4.13). The Auger process is usually initiated by photo- or impact ionisation of core electrons by irradiation with X-rays or keV-electrons. An alternative technique to induce core shell ionisation is the annihilation of core electrons with slow positrons. Due to the low positron energy of some 10 eV, no background of secondary electrons is produced in the higher energy range of released Auger electrons. Besides this advantage, PAES is an exceptionally surface sensitive technique since most of the implanted positrons annihilate with electrons of the topmost atomic layer. The positron Auger electron spectrometer was extended by a separate sample lock and a sample preparation chamber. In order to prepare clean and well-defined surfaces, it is equipped with an argon sputter source and an adapted sample heater for in-situ annealing of defects particularly in the near surface region. An effusion cell was installed which consists of a tungsten foil boat with tunable sample distance. In addition, an electron beam evaporator was mounted for evaporation of low vapor pressure materials. Both, the effusion cell as well as the electron beam evaporator allow accurate deposition of adsorbates in the submonolayer range. The exact layer thickness of deposited material is determined by a piezo oscillator

Figure 4.11: Pulsed low energy positron beam system (PLEPS) under operation at UniBW.

crystal. After preparation, the sample is transferred through a gate valve into the analysis chamber by a magnetic coupled rod.

Figure 4.12: The scanning positron microscope (SPM) under operation at UniBW.

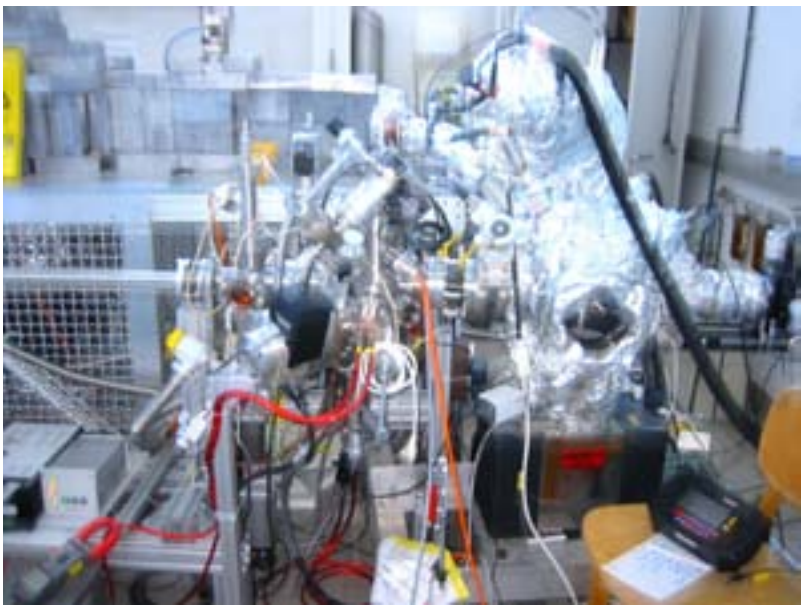

Figure 4.13: Facility for positron annihilation induced Auger electron spectroscopy (PAES) at E21, TUM.

5 Irradiation and Radiography Facilities

5.1 ANTARES – Construction of the Neutron Radiography and Tomography Facility

B. Schillinger[1,2], **E. Calzada**[1,2], **F. Grünauer**[1,2]

[1] ZWE FRM-II, TU München
[2] Physik Department E21, TU München

Overview

In 2003, the components for the neutron radiography and tomography facility ANTARES were constructed and assembled at beam line SR4b in the north-east corner of the experimental hall. The design of ANTARES has been explained in much detail in the previous annual report, so only a short overview is given here before details of the assembly are described. ANTARES consists of an external beam shutter, flight tube and block house. The external beam shutter is necessary because the UCN experiment at SR4a will insert a nozzle through the drum shutter in the biological shielding, rendering it unusable for ANTARES. Fig. 5.1 shows an overview of the facility.

Construction of the wall elements

The shielding elements and block house walls were constructed as steel casings filled with heavy concrete. The secondary shutter of density 4.5 housing and the block house elements were filled with concrete tons/m^3. As the collimated beam inside the flight tube does not touch the walls, a density of 3.5 tons/m^3 was sufficient for the walls of the flight tube housing. As the crane in the experimental hall has a nominal capacity of 10 tons only, all elements were designed for a maximum weight of about 9.5 tons. For some elements of the blockhouse wall near the beam entrance, this weight constraint could not be met, so additional removable concrete filled cylinders were constructed inside the wall volume , which were mounted after the assembly of the wall elements.

Additional problems arose because the concrete company guaranteed only for the minimum density of the concrete, but not for the nominal density. In reality, the density became higher than the calculated values, leading to a component weight of more than ten tons. Fortunately, the reactor hall crane has a special 10% overload range (of which the use is restricted to a

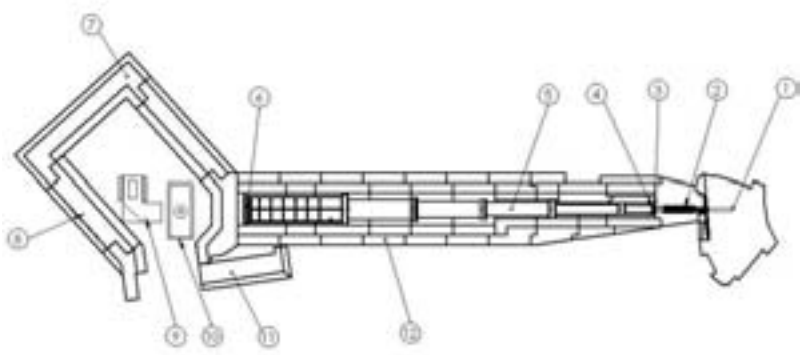

Figure 5.1: Complete layout of the facility: 1. Collimator inside of the biological shielding, 2. External vertical beam shutter, 3. Iris diaphragm, 4. Pneumatic shutter, 5. Flight tube, 6. Variable beam size limiter, 7. Measurement cabin, 8. Wall and beam stop, 9. Detector and camera system, 10. Sample manipulator, 11. Sliding door, 12. Flight tube shielding,

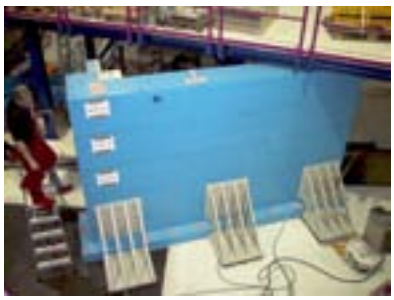

Figure 5.2: Moving the wall with air cushions

few hours per year), which was capable of handling all elements.

Mounting of the wall elements

The blockhouse walls were mounted from five horizontal segments each, weighing more than 50 tons each. The assembled walls were fitted with mounting frames for up to six air cushions (Fig. 5.2) . An external compressor was used to lift the walls and to move them into place, as the capacity of the house installations was not sufficient.

Unfortunately, several cable channels in the hall floor were only roughly covered with uneven steel plates, rendering an uneven surface and an escape path for the compressed air. They had to be covered with thin steel plates, but still, the walls could only transit the uneven regions with the aid of two steel cable tackles affixed to the reactor hall walls (Fig. 5.2).

The flight tube

As described in the last report, the flight tube consists of individual segments connected by rubber sealant rings, mounted on C-shaped brackets. The original design was taken from the vacuum housings for the neutron guides leading to the guide hall. No space was available top mount circular flanges, so the original square shape with rounded corners was altered by rounding the straight sections to a convex shape (Fig. 5.3).

Each segment has an individual vacuum connector, so single segments can be removed for experimental installations, the remaining segments can be closed off by covers. Vacuum pump and vacuum control system were salvaged from the old reactor. For the final neutron window at the end of the flight tube, a massive aluminum cover with a thin-milled window was foreseen. Static calculations predicted a material failure at the edge of the milled area, so the cover was constructed as a sandwich of a 3 mm aluminum plate, rubber seals and flange rings.

The cover stones for the flight tube housing have retractable ball casters on which they can slide from the middle, crane-accessible position to their final position under the platforms.

Figure 5.3: The flight tube with convex flanges

Mounting of the blockhouse roof

The area of the blockhouse is not accessible by the hall crane. To be able to mount the roof at all, it was constructed from small two-ton bars. The original intention had been to use a balance bar and counterweight with the hall crane, which is able to telescope towards the corner of the hall just to the beginning of the block house. Later on, a special compact truck-mounted crane was found which was just able to drive into the reactor hall in the time when the other experiments at SR-2 and SR-3 were not yet assembled, with 5 cm space left next to the already mounted measuring cabins. The roof elements were deposited on the platform for the positron experiment with the hall crane, the truck-mounted crane took over from there and deposited them in position on the blockhouse roof (Fig. 5.4).

The external beam shutter

The external shutter was constructed as a vertical concrete block containing two different collimators, driven by a hydraulic piston (Fig. 5.5) . A servo system with a position encoder and a control valve can position the shutter block to the accuracy of a tenth of a millimeter to a collimator position or to the closed position. When the position is reached, two hydraulic clamps hold the block in position, the hydraulic pump shuts off.

Figure 5.4: Mounting the blockhouse roof elements with a truck-mounted crane

A hydraulic pressure tank holds sufficient pressure to open the hydraulic clamps and close the shutter within one third of a second when magnetic valves are opened in case of power failure.

Outlook

In December 2003, The electric installation for the blockhouse was completed, so we had "first light" in the blockhouse even without neutrons. In 2004, the walls will be covered with B_4C rubber mats to reduce the activation of the steel walls, the sample manipulator will be transported to the blockhouse and the detector box will be completed. The fast experimental pneumatic shutter and the filter wheel for phase contrast tomography will be mounted as the final installations, expecting the first measurements soon after commissioning of FRM-II.

Figure 5.5: The hydraulic servo system for the beam shutter

5.2 NECTAR

T. Bücherl [1], **Ch. Lierse von Gostomski** [1], **E. Kutlar** [1], **E. Calzada** [2]

[1] Institut für Radiochemie, TU München
[2] ZWE FRM-II, TU München

General

The NEutron Computer Tomography And Radiography (NECTAR) facility is set up at the converter facility in the experimental hall (beam tube SR 10). Its uniqueness is the use of fission neutrons to radiograph samples of volumes up to 0.5 m^3 and 400 kg maximum burden. The fast neutron flux will be up to $6.4 \cdot 10^7$ cm^{-2} s^{-1} and the collimation is adjustable to L/D values of up to 300.

Figure 5.6: View in the measuring room with manipulator system for the objects (left), for the detectors (right) and provisionally mounted two-dimensional detector system (without CCD-camera).

Current status

The main components in the measuring room are the manipulator for the objects, the manipulator and storage system for the

detectors, the actually two detector system themselves and the removable and changeable collimator set in the partition wall to the neighbouring room for medical applications. All these components must be adjusted precisely to the incoming neutron beam. As most of them are heavy in weight, this cannot be performed manually within the accuracy required. Therefore a crane to be mounted on the ceiling was designed and its statics calculated. The latter is also required for its licensing.

Although the crane is not installed yet, both manipulators have been set up provisionally to verify the correct layout of the arrangement (Fig. 5.6) and to design appropriate clampings for the detector systems. To be more flexible in positioning the object manipulator, it was additionally equipped with a connection box, i.e. all cables coming from and going to the control unit are connected with the manipulator via this box.

Figure 5.7: Control unit for the manipulators.

The functionality of the control unit (Fig. 5.7) was extended by a three phase transformer, thus avoiding problems showing up when connected to electronic circuits having FI protective switches. To avoid unnecessary (neutron) activation of the object and the equipment, the effective beam cross-section will be limited by an adaptable collimator system to the real measurement geometry, i.e. the dimensions of the object and/or the active detection area. It will consist of a number of boxes made of iron which fit one into the other. The layout is shown in Fig. 5.8. The development of the LABView-based software package for control of the manipulators and detectors was continued.

Next steps

The work in 2004 will be separated into three phases. In the first phase the set up of the hardware will be completed, e.g. the crane, the detector systems, the control cabin and the collimators will be installed and all components adjusted exactly. The completion and optimization of the control software package and its integration with all other software modules (e.g. those of the detector and reconstruction software packages) is the main part of the second phase. At the end of phase two, the system is ready for operation. With the availability of fission neutrons the third phase will start. Extensive tests of the detector systems will define their characteristic parameters like the absolute detection efficiency, the spatial resolution (for the two-dimensional position

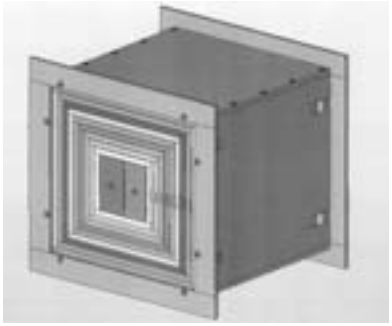

Figure 5.8: Layout of the adaptable collimator system, which will be placed in the partition wall.

sensitive detector system), the gamma-sensitivity and the neutron-gamma-discrimination ratio, respectively etc. Based on these results possibilities for further optimization will be determined and – if possible – realized.

As NECTAR is an unique system, no extensive a-priori information on its probable performance is available, i.e. the influence of beam hardening, forward scattering in the sample etc. on the resulting data for different materials must be determined first. This will be performed by using different test objects, like step wedges of many different materials. Based on this knowledge, the basics for a successful evaluation of tomographic data will be set. Tomography of many objects, different in geometry, dimension and material composition will complete the third phase and indicate the starting point for routine and research operation.

5.3 Irradiation Facilities

H. Gerstenberg [1], **X. Li** [1]

[1] ZWE FRM-II, TU München

The FRM-II will be equipped with various irradiation facilities. Due to the different tolerable sample volumes, neutron flux densities and obtainable neutron fluencies they allow in their entirety a broad scope of possible applications in basic and applied science.

In particular during the nuclear start-up phase of the FRM-II the following facilities will be available:

- a pneumatic rabbit system (RPA),
- a hydraulic rabbit system (KPA),
- a test-rig for a silicon doping facility (SDA),
- a pneumatic rabbit system (TRP) for prompt transport of irradiated samples into the neighbouring institute for radiochemistry.

In addition, at least a high speed pneumatic rabbit system will be added in the future.

All of the irradiation positions are located within the heavy water moderator tank and can be loaded and unloaded during reactor operation. A major advantage of these irradiation positions is the availability of a very pure thermal neutron field. Thus parasite threshold reactions by fast neutrons and the production of large clusters of irradiation defects are suppressed effectively.

The pneumatic rabbit system (RPA) serves typically for the activation of samples for neutron activation analysis. The pneumatic devices are operated by carbon dioxide gas in order to avoid the production of radioactive Ar-41 during the irradiation of air. The facility is composed of 6 independent irradiation channels being identical except for the vertical position within the moderator tank. Consequently the neutron flux densities in the positions vary between $5 \cdot 10^2 \mathrm{cm}^{-2}\mathrm{s}^{-1}$ and $2 \cdot 10^{14} \mathrm{cm}^{-2}\mathrm{s}^{-1}$ and the appropriate irradiation position can be chosen to fit the individual task. For radiation protection reasons the entire handling takes place in a room being exclusively used for this facility. Irradiation times can be chosen between about 20s , i.e. a significantly longer time compared to the transport time of the rabbits of a few seconds, and 5 hours. The maximum irradiation time is limited by the use of polyethylene rabbits as outer irradiation package. After irradiation the sample is first transported into a shielded cooling position where the induced gamma dose rate is measured. Finally it is transported back into the handling room (Fig. 5.9) where it is either removed from the irradiation facility by remote handling tools or alternatively sent directly to the institute for radiochemistry via a connected rabbit system (TRP).

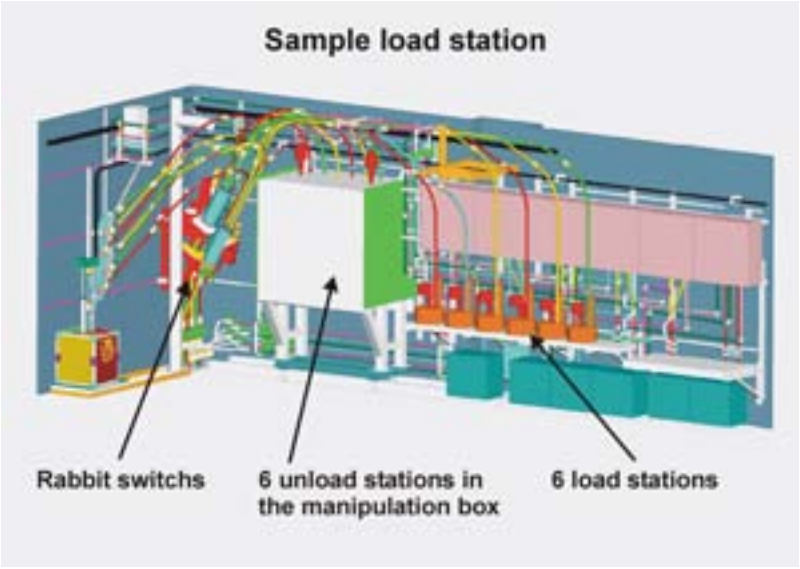

Figure 5.9: Control and handling room of the pneumatic rabbit system. Left: transfer pipe switches, middle: sample handling box, right: sample loading stations.

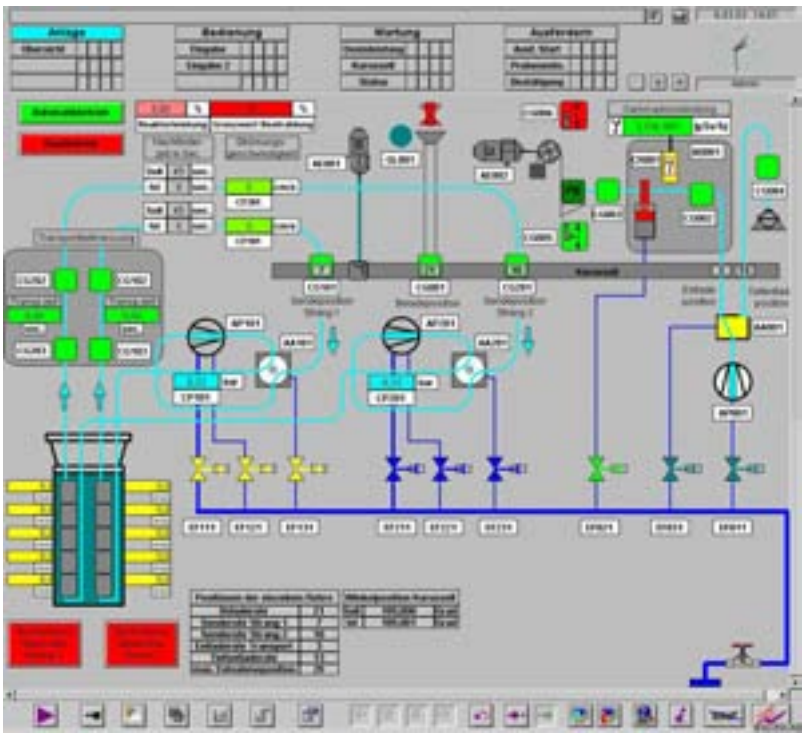

Figure 5.10: interactive control screen of the hydraulic rabbit system (KBA). The current status is displayed directly. The transfer system can be operated automatically and manually.

In contrast to the pneumatic system the hydraulic rabbit system (KBA) will be used for long term exposure or the irradiation of larger sample volumes up to approximately 35 cm^3. Consequently the samples are contained in Al rabbits during irradiation, which however are perforated in order to guarantee the cooling of the samples by pool water during irradiation. If necessary the direct contact between sample and pool water is avoided by the use of sealed quartz ampoules or small welded inner Al containers. The facility offers 2 independent identical irradiation channels each of which can be loaded by up to 5 rabbits at the same time. The driving medium of the facility is reactor pool water. The neutron flux densities have been calculated to be about $4 \cdot 10^{14} cm^{-2} s^{-1}$. Since rather high activities will have to be handled in the hydraulic rabbit system, most of the handling procedures in particular the receipt of irradiated samples and the measurement of the induced gamma dose rate is done remotely under water about 3.5 m below the reactor pool level. In addition also the loading of the samples into lead shielded transport containers takes place under water.

Both rabbit systems are controlled automatically by the SPS control system through a PC with WindowsNT operating system respectively. The current situation of each transfer system, including the position of the irradiation capsules and the status of all control valves and other important parameters such as system pressure and gamma dose rate at the sample cooling positions can be directly displayed on the screen of the control PC (Fig. 5.10). If necessary, a semi automatic control through direct operation of single components by mouse click is also possible.

The silicon doping facility (SDA) will serve for the P doping of the semiconductor Si by means of the nuclear reaction $^{30}\mathrm{Si} \xrightarrow{(n,\gamma)} {}^{31}\mathrm{Si} \xrightarrow{(\beta^-)} {}^{31}\mathrm{P}$.

This so called neutron transmutation doping offers the most homogeneous doping profile being necessary particularly in high power electronic components. In order to fulfil the requirement of homogeneity, however, it is of crucial importance to guarantee a constant neutron flux density over the entire volume of the Si ingot. Therefore the ingot is rotated during irradiation and the irradiation position has to be equipped with a specially shaped absorber (Fig. 5.11). During the nuclear start-up phase the neutron flux distribution in the Si ingot will be determined experimentally by using a simplified test rig. Then, based on this flux distribution the exact shape of this absorber made from Ni can be calculated and constructed. Once the absorber profile will be known the final Si doping facility offering a semi automatic operation will be completed. It will be suitable for Si ingots with diameters of up to 200 mm and a capacity of several tons per year.

Till the end of 2003 the hydraulic rabbit system (KBA) and the test rig of the silicon doping

system (SDA) are complete. A start-up test on them has already been carried out successfully before the commissioning of the reactor. The pneumatic rabbit system (RPA/TRP) is already in the last phase of its start-up test.

Samples with different weight and irradiation time are loaded and transferred during this start-up test of the rabbit systems under all possible conditions in order to simulate the real situations. Tests of several irradiation tasks in the same time and same transfer system are also performed. The measurements of gamma dose rate at the sample cooling positions are simulated by using a conventional calibration gamma source. If the allowed limit is overshot, the sample transfer is prevented by a interlock at the cooling positions due to the aspects of the irradiation protection.

At the test-rig of the Si doping system loading and transport of Si crystals between the irradiation position in the moderator tank and the loading place in the storage pool are tested. Flux monitors (Al, Au, Zr etc.) for the determination of the neutron flux distribution inside a Si ingot are already prepared. They will be placed at a total of 18 positions within one Si ingot during the nuclear startup.

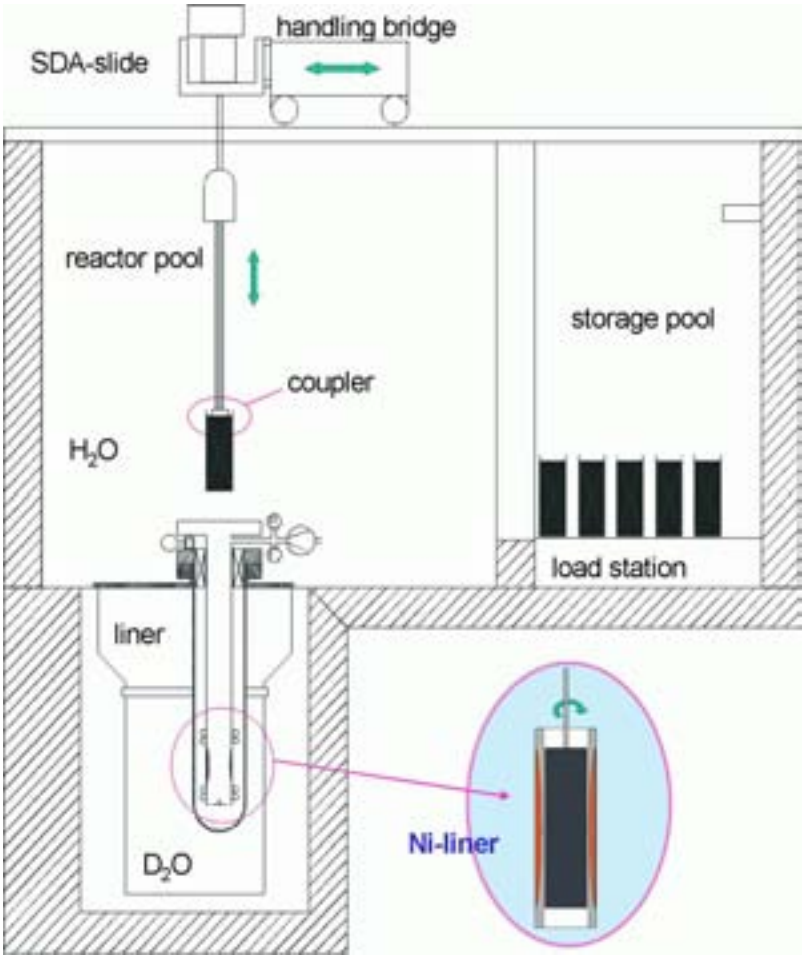

Figure 5.11: scheme of the silicon doping system.

6 New Developments

6.1 Novel Type of Neutron Image Plates Based on KCl:Eu^{2+}-LiF

M. Schlapp [1], **M. Hölzel** [1], **R. Gilles** [1], **A. Ioffe** [3], **T. Brückel** [3], **H. von Seggern** [2], **H. Fuess** [2]

[1] ZWE FRM-II, TU München/TU Darmstadt
[2] Fachbereich Materialwissenschaft, Technische Universität Darmstadt
[3] Inst. f. Festkörperforschung, Forschungszentrum Jülich

Introduction

Neutron image plates (NIPs) provide a mean for the two-dimensional, position-sensitive detection of neutrons. They combine the advantages of a large dynamic range in dose (5 orders of magnitude), a high spatial resolution (<200 μm) and a high efficiency for the detection of neutrons [1]. NIPs have found widespread application as neutron detectors for single-crystal and powder diffraction, small-angle scattering and tomography. After neutron exposure, the image plate can be read-out by scanning with a laser. Commercially available neutron image plates (NIPs) consist of a powder mixture of BaFBr:Eu^{2+} and Gd_2O_3 dispersed in a polymer matrix and supported by a flexible polymer sheet. Since BaFBr:Eu^{2+} is an excellent X-ray storage phosphor, these NIPs are prone to absorb γ-radiation which is always present as a background radiation in neutron experiments. Several ways have been proposed to make X-ray image plates sensitive to neutrons: while several groups investigated the combination of BaFBr:Eu^{2+} as phosphor and Gd_2O_3 as converter [1, 2], fewer reports were published on a possible usage of ^{6}LiF as converter [3]. Recently, we were able to demonstrate that a combination of KCl:Eu^{2+} as phosphor and ^{6}LiF as converter shows a promising potential for neutron image plates with a low γ-sensitivity [4]. In this presentation we report on the resolution of ceramic NIPs (C-NIPs) based on KCl:Eu^{2+} and LiF which were fabricated into ceramic image plates in which the alkali halides are acting as a self-supporting matrix without the necessity for using a polymeric binder. A simulation of the applicability of these NIPs as well as commercial plates for the SANS apparatus at the instrument **S**tructure **PO**wder **DI**ffractometer (SPODI) at the FRM-II will also be given.

Experimental

Ceramic neutron image plates (C-NIPs) were fabricated by pressing a mixture of 30 mol% KCl:Eu^{2+} and 70 mol% LiF with 2.5 wt% of a pressing additive (Poly-[vinyl butaryl-co-vinyl alcohol-co-vinyl acetate]) into pellets with thicknesses ranging from 250 μm to 1500 μm using uniaxial and isostatic pressure of up to 5 GPa. In order to determine the spatial resolution of these image plates, they were exposed to neutrons at the general purpose cold neutron beam at Forschungszentrum Jülich. The sharp edge of a Gd-metal sheet was used as a mask. A numerical differentiation of a scan over this edge followed by a Fast Fourier Transformation yields the Modulation Transfer Function (MTF), a measure for the contrast transfer of the original image onto the measured signal. In general, the MTF is decreasing with an increasing spatial resolution given in line pairs per mm (lp/mm), i.e. the contrast transfer from the image to the signal is diminishing with finer details. Setting the minimum contrast that two pixels must have to be distinguishable to 20%, one can determine the spatial resolution from the MTF. The new **S**tructure **PO**wder **DI**ffractometer SPODI currently under construction at the FRM-

II reactor in Garching is going to be equipped with a SANS apparatus [5]. Simulations on the properties of the instrument SPODI as well as the achievable Q-vectors of the SANS apparatus were done with the software package McStas of Risø National Laboratory.

Results and Discussion

The resolution of an image plate is determined less by the size of the read-out laser beam than by the scattering of this laser light within the image plate. Due to differences in the indices of refraction of the materials used for the fabrication of the NIP, the focused laser light is smeared over a pear-shaped volume and all information contained within this volume contributes to the detected signal proportionally to the light intensity. It is obvious that the lateral spreading of stimulation light within the NIP increases as the thickness of the image plate is increased since the photons are scattered back and forth within the plate while in thinner NIPs they are emitted either at the front or back side. In Fig.6.1 the experimentally determined MTFs of ceramic neutron image plates are depicted. One can clearly observe that the MTF is declining faster for thicker plates, i.e. the spatial resolution is decreasing with increasing thickness of the plate. It can further be found that the reduction in the resolution is largest, when the overall thickness of the plate is small while for thicker plates the effect of a loss of resolution is less pronounced. This can be attributed to the fact that although the lateral scattering of the stimulating light increases with the thickness of the plate, the intensity of the light is reduced by absorption. Since the intensity of the detected signal is directly proportional to the stimulating intensity, the light which is widely spread laterally causes only a weak contribution to the signal.

In order to ensure a high detective quantum efficiency, nearly all neutrons should be absorbed in the NIP consisting of KCl:Eu^{2+} and LiF. To achieve a high absorption and to stimulate all defects within the image plate, the thickness has to be in the range of 1000 μm. Using a contrast transfer of 20 % as a measure, one obtains a resolution of 1.5 line pairs/mm, i.e. a minimum pixel size of 670 μm. Although this value is much larger than the 200 μm resolution which can be achieved with a 135 μm thick, commercially available NIP (Fuji BAS ND) based on $BaFBr_{1-x}I_x$:Eu^{2+} and Gd_2O_3 [1, 6], one has to keep in mind that the NIPs based on KCl:Eu^{2+} and LiF exhibit a much smaller γ-sensitivity and were developed for experiments in a high γ-environment. While C-NIPs based on KCl:Eu^{2+} and LiF showed a detective quantum efficiency comparable to a Fuji BAS ND image plate, the signal after exposure to 558 keV and 618 keV γ-rays from a (n,γ)-reaction at cadmium was by one order of magnitude lower.

Due to the long distance of 5 m between the monochromator and the sample position and small (2-4 mm diameter) pin-hole slits, a low divergence of the neutron beam at SPODI is achievable. Since this

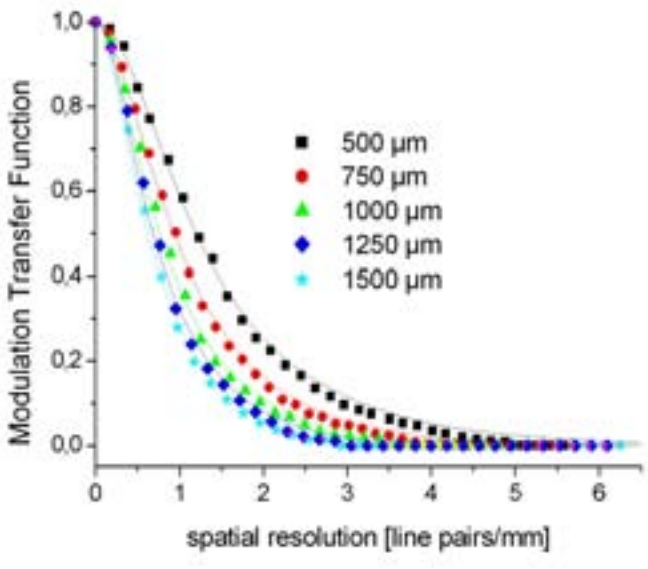

Figure 6.1: MTFs of ceramic NIPs with various thickness, setting the minimum contrast that two pixel must have to be distinguishable to 20 % (MTF=0.2), one can determine the spatial resolution of the NIP from the MTF-curve

instrument uses thermal neutrons with a wavelength between 1 and 2.5 Å, the resulting scattering angles are small compared to SANS machines using cold neutrons. This smaller angles are adapted by using a NIP as detector which has a much smaller pixel size than the detectors normally used at cold-neutron SANS machines. Fig. 6.2 exhibits the calculated maximum and minimum scattering vectors Q as well as the resolution in Q achievable with a commercially available and a ceramic neutron image plate (C-NIP) based on KCl:Eu^{2+} and LiF. Although the resolution of C-NIPs is less, it is still well below the minimum scattering vector achievable with this instrument and it can be expected that the usage of C-NIPs places less demand on shielding of the detector against a application of the NIP is the characterisation of the primary neutron beam shape and γ-background. Additionally, for short sample-detector distances, the NIP renders the detection of full Debye-Scherrer cones possible allowing a determination of the sample crystallinity and texture. This results show, that in principle particles with sizes ranging from 1 to 900 Å can be investigated by a compact SANS apparatus for thermal neutrons utilizing image plates as detector. Using a larger wavelength - a second monochromator is under planning - the achievable minimum scattering vector Q_{min} can be reduced even further.

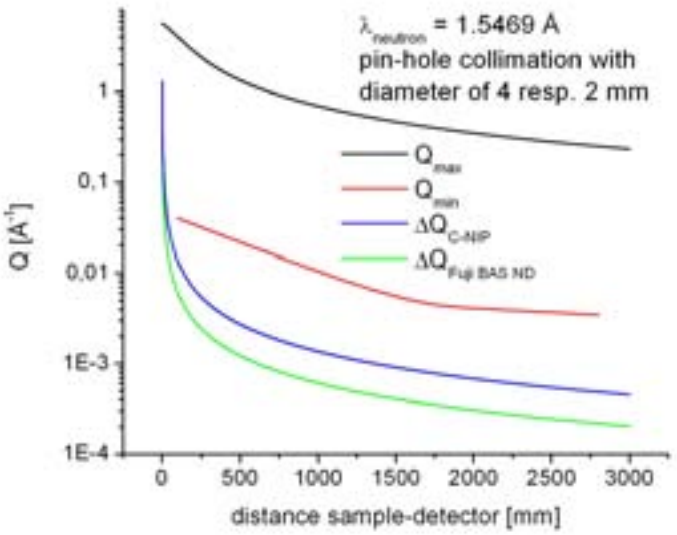

Figure 6.2: Q-range covered by the SANS apparatus at SPODI

[1] Karasawa Y., Niimura N., Tanaka I., Miyahara J., Takahashi K., Saito H., Tsuruno A., Matsubayashi M. *Physica B*, **213&214**, (1995), 978.
[2] Buecherl T., Rausch C., von Seggern H. *Nucl. Inst. & Meth. A*, **333**, (1993), 502.
[3] Takahashi K., Tazaki S., Miyahara J., Karasawa Y., Niimura N. *Nucl. Inst. & Meth. A*, **119**, (1996), 502.
[4] Schlapp M., von Seggern H., Massalovich S., Ioffe A., Conrad H., Brueckel T. *Appl. Phys. A 74 (Suppl.)*, **74**, (2002), S109.
[5] Gilles R., Krimmer B., Saroun J., Boysen H., Fuess H. *Mat. Sci. Forum.*, **378-381**, (2001), 282.
[6] Tazaki S., Neriishi K., Takahashi K., Etoh M., Karasawa Y., Kumazawa S., Niimura N. *Nucl. Inst. & Meth. A*, **424**, (1999), 20.

6.2 Response Function of a Neutron Detector for Radiation Protection Purposes

F. Grünauer [1]

[1] Physikdepartments E21, TU München

At FRM-II commercially available neutron detectors will be used for radiation monitoring and protection. These detectors are approved in the energy range of thermal to fast neutrons. Contrary to usual applications of neutron dosimetry (e.g. reactor halls), there has to be expected a major contribution of cold neutrons in the neutron-guide hall of FRM-II. It had to be examined whether this detector is suitable for cold spectra and if so, what calibration and security factors have to be applied under these special conditions. Monte Carlo calculations were carried out in order to assess the response function with respect to neutron energy and angle of incidence. It was shown, that the response function below thermal energies is rather flat. Therefore the detector can be used even in the subthermal energy range. The response of the detector is very dependent on the angle of incidence of radiation.

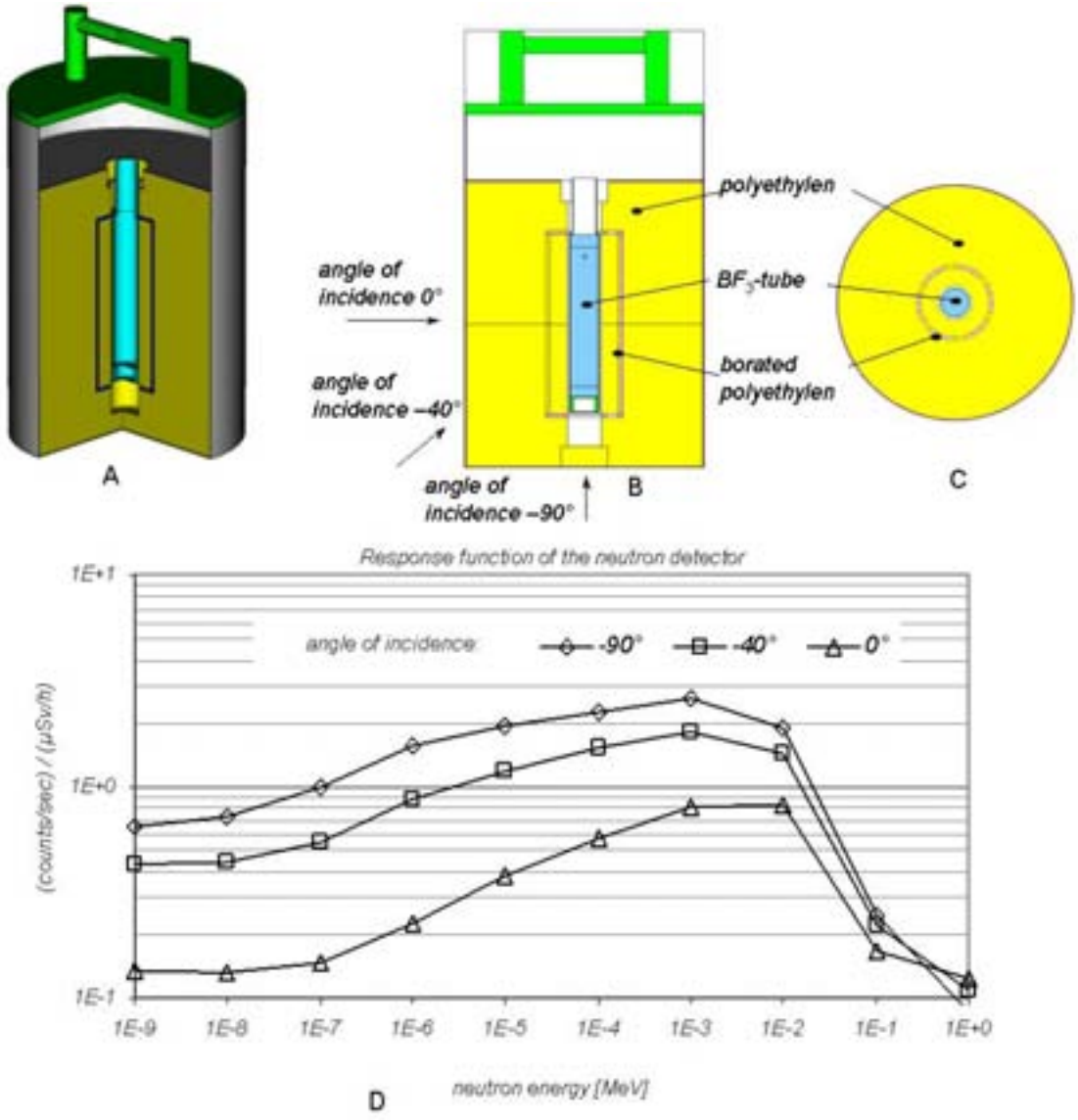

Figure 6.3: A) Monte Carlo model of the neutron detector, B) vertical cut through the detector, C) horizontal cut through the detector, D) response function of the detector

6.3 Image Deconvolution in Neutron Radiography

F. Grünauer [1]

[1] Physikdepartments E21, TU München

Nearly all neutron radiography facilities use a setup similar to a pinhole camera. Lens systems afford a very high construction effort. Generic pinhole systems provide high resolution at big L/D ratios, where L is the distance between aperture and specimen and D the diameter of a circular aperture. As the neutron fluence decreases proportional to $(D/L)^2$ a high resolution means long exposure time and a bad signal to noise ratio. It would be desirable to record images with high intensity and low resolution and to correct the resulting blur by an appropriate algorithm. Deblurring of images was tested with a $L/D = 50$ projection (Fig. 6.4 B) of a test specimen (Fig. 6.4 A), that was simulated by Monte Carlo Method. The projection is the convolution of the point spread function by the 'ideal image' (in this context, the ideal image is the projection, produced by a point source). Convolution in the spatial domain corresponds to a multiplication in the fourier domain. In principle the ideal image can be reconstructed by dividing the fourier transform of the projection by the fourier transform of the point spread function and back transforming the result to the spatial domain. However this 'invers filtering' is not successful if the image contains noise: Division by small absolute values of the point domain causes a big damage in the reconstructed image. This effect can be reduced by a Wiener filter [1], that gives a certain weight to each point in the fourier domain during the filtering process.

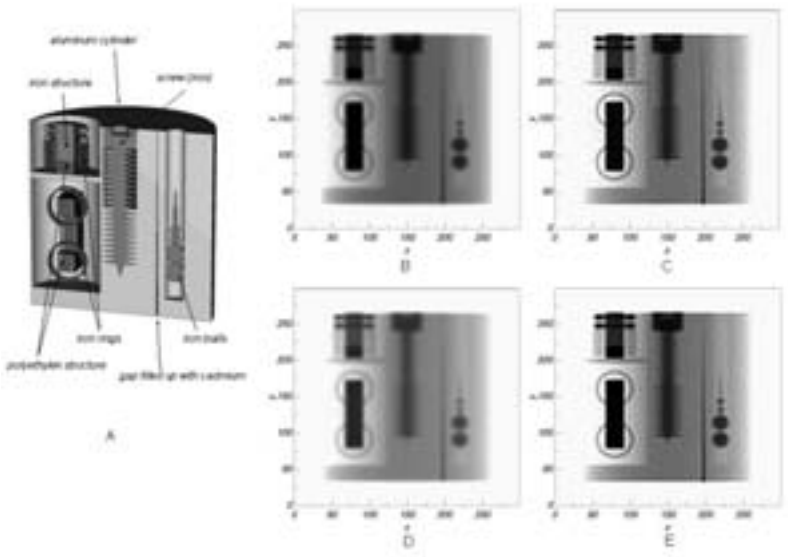

Figure 6.4: A) Test specimen, B) unprocessed projection, C) reconstruction by a Wiener filter, D) reconstruction by van Cittert algorithm, E) reconstruction by Richardson-Lucy method

The reconstruction by a Wiener filter, is shown in Fig. 6.4 C. An other approach to solve the problem of noise are iterative algorithms. The idea is to guess the 'ideal' image, to convolute it with the point spread function and to compare the result with the real image. After an appropriate adjustment of the guessed image, the procedure is started again. Fig. 6.4 D shows the result of 18 iterations of the van Cittert algorithm and Fig. 6.4 E shows the reconstruction by the Richardson-Lucy maximum likelihood algorithm. Best results are obtained by the Richardson-Lucy method. However none of the algorithms are able to recover details like the screw thread. Further improvements in the image quality can be achieved by a modification of the point spread function (see 'Coded apertures in neutron radiography' in the same report).

[1] J.C.Russ. *"The image processing handbook"* (CRC Press, Boca Raton Ann Arbor London Tokyo, 1995).

6.4 Coded Apertures in Neutron Radiography

F. Grünauer [1]

[1] Physikdepartments E21, TU München

Most neutron radiography facilities use circular single hole apertures. Such apertures provide a so called pillbox point spread function. As the point spread function has a crucial impact on the quality of reconstructed images, investigations were carried out with regard to an optimal aperture design. Many different configurations were simulated by Monte Carlo method. The test specimen is presented in 'image deconvolution in neutron radiography' in the same report. A comparison of a multiple hole aperture (fig. 6.5 E) to the 'classic' single hole aperture (fig. 6.5 A) is shown below. Both apertures have the same transmission area. The overlap of information in the projection with the multiple hole aperture was reduced by minimization of the autocorrelation function of the point spread function. The resulting image is a superposition of six images (fig. 6.5 G). For both aperture configurations the image was reconstructed by a Wiener filter. The reconstructed image, obtained with the multiple hole aperture (fig. 6.5 H), shows more details (e.g. the screw thread) and is less noisy than the reconstructed image, which stems from the single hole arrangement (fig. 6.5 D). The quality of optical systems is usually defined by the modulation transfer function [1]. Fig. 6.5 B and Fig. 6.5 F show, that the modulation transfer function has considerably less near zero zones in case of the multiple hole aperture.

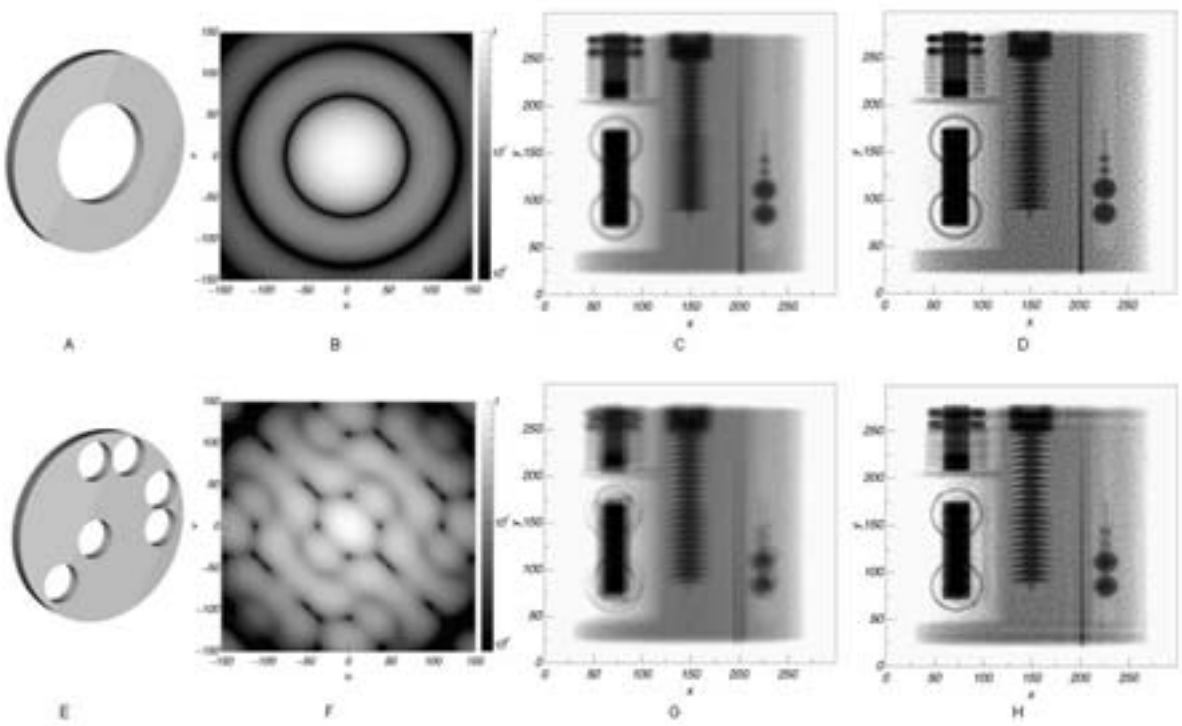

Figure 6.5: A) Single hole aperture, B) modulation transfer function for the single hole aperture, C) unprocessed projection from the single hole aperture, D) reconstructed image for the single hole aperture, E) multiple hole aperture, F) modulation transfer function for the multiple hole aperture, G) unprocessed projection from the multiple hole aperture, H) reconstructed image for the multiple hole aperture

[1] Hecht E. *"Optik"* (Addison-Wesley, Bonn München, 1989).

6.5 Non-Destructive Testing With Phase Contrast Radiography

K. Lorenz [1], **E. Steichele** [1], **E. Lehmann** [2], **P. Vontobel** [2]

[1] Physikdepartment E21, TU München
[2] Paul-Scherrer-Institut, Villigen, Schweiz

Theory

The refractive index of a material is given by the complex expression $n = 1 - \delta - i\beta$. The imaginary part of this value is responsible for the mass attenuation coefficient μ of the material which creates absorption contrast. The real part δ causes a phase shift, which leads to a deviation of the wave front. If the incoming wave is approximately a plane wave (neutrons with a high transversal spatial coherence), you get in certain object-detector-distances interference effects. Fresnel's theory for diffraction, explains the increase in contrast at edges and interfaces in the object [1] (where the gradient of the phase shift perpendicular to the neutron beam is very high; see Fig. 6.6). This additional contrast to the absorption contrast is called phase contrast.

Applications

Prof. Wellnitz, holder of the chair of conceptional lightweight construction at the FH Ingolstadt, provided us with probes of aluminum foams. In spite of the very small attenuation coefficient of aluminum, it is possible to visualize the inner structure of these foams with the help of phase contrast (see Fig. 6.7).

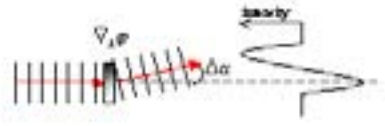

Figure 6.6: Principle

If during the casting process the outer region of a cast component solidifies quicker than the inner, the shrinking during solidification can create little holes inside the cast material. The Institut für Umformtechnik(UTG) lent us cast components with such defects inside. The size of those defects is often far too small to get enough absorption contrast to visualize them in a conventional radiography.

In association with Dr. Mollenhauer, director of the research department of the orthopedic surgery of the Friedrich-Schiller-University Jena, we use phase contrast neutron radiography to visualize the interface between an implant and the bone. By looking at this interface at different times after the implantation of the prosthesis, it is possible to study the dependence of the healing process on the surface material and the surface structure of the prosthesis.

Recent Topics of Research

A disadvantage of phase contrast radiography are the long exposure times compared to conventional radiography. This is because of the need for a neutron beam with a high transversal coherence, which is achieved by the application of small pinholes and large distances between this pinhole and the probe. This leads to a strong reduction of the beams intensity and thus to long exposure times (90min and more). A possible solution for this problem is the utilization of coded apertures [2], which replaces the single pinhole.

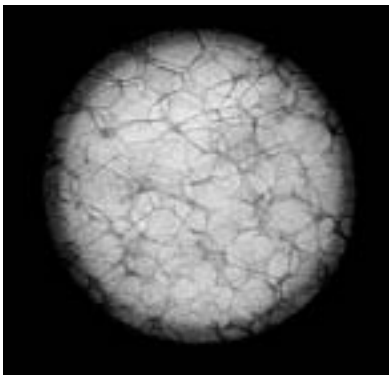

Figure 6.7: phase contrast radiography of an aluminum foam (made at the PSI in Switzerland; the diameter of the visible area is 42 mm)

The small diameter (<1mm) of the pinhole allows the application of neutron lenses with very small radii. Like this, it is possible to create lens systems with a focal length in the order of meter. With such a device, the resolution in the object plane could be improved by a factor of two or more by a given detector resolution.

By making three phase contrast radiographies in three different object-detector-distances, it

is possible to use the transport of intensity equation (TIE) to calculate the phase shift of the neutrons on their different ways through the object [3]. Doing this phase retrieval for every single projection of a tomography makes it possible to assign every voxel of the tomography a phase shift and an attenuation coefficient. Like this, it becomes possible to separate materials, with similar attenuation coefficients.

[1] Cowley J. M. *Diffraction Physics* (NHPL, 1995), 3 edition.
[2] Skinner G. K. *Nuclear Instruments and Methods in Physics Research*, **221**, (1984), 33–40.
[3] Gureyev T. E. *Optics Communications*, **147**, (1998), 229–232.

6.6 NRSE coils for MIRA

N. Arend [1], **R. Georgii** [2], **H. Wagensonner** [2], **T. Keller** [3]

[1] TU München, Department of Physics, Institute E21, 85748 Garching
[2] TU München, FRM-II ZWE, 85747 Garching
[3] Max-Planck-Institute for Solid State Research, 70569 Stuttgart

Introduction

For the multi-MIEZE (Modulation of IntEnsity by Zero Effort) [1] option of MIRA, NRSE (Neutron Resonance Spin Echo) flipper coils must be implemented. The standard design of those coils requires the neutron beam to penetrate them and therefore interact with the coil material. MIRA will operate in the cold neutron range, this must be taken into account when choosing materials and the design to avoid strong absorption and scattering.

Design efforts

The NRSE flipper coils used at other FRM-II instruments (RESEDA and TAS-NRSE) have two properties that make them unfavourable for MIRA: the DC coils are made of a 0.5 mm $\times$ 8 mm aluminum band which has an anodised Al_2O_3 coating that features a periodic structure. This structure causes significant small angle scattering at higher wavelengths. Furthermore, since the winding density is relatively low, high currents ($\approx$ 100 A) must be used to achieve the nominal DC field of 0.03 T.

In order to get around those drawbacks a new design is planned for the MIRA coils. It is based on a design proposed in [2] and developed at the MPI für Metallforschung in Stuttgart. Thin (0.5 mm) profiles made of a rigid Al alloy (see Fig. 6.8) are piled on top each other, forming the windings of the DC coil.

A considerably higher winding density (and therefore smaller current) as well as improved scattering properties can be achieved. Several approaches are being followed concerning electrical insulation (e.g. sputtered glass coating), contacts of the windings, and cooling. The design process is in progress. Significant improvements seem possible compared to the original Stuttgart design.

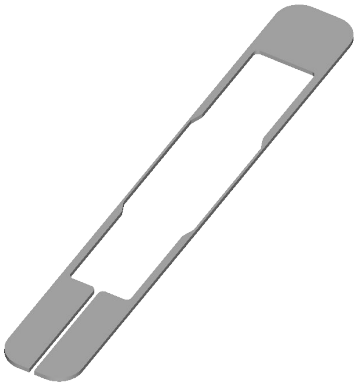

Figure 6.8: Simplified single DC coil winding (cooling channels are omitted).

B-field simulations

In order to test various designs prior to building, numerical simulations help finding design flaws and optimising the model. Fig. 6.9 shows a B-field contour plot at the center of a DC coil of $\approx$ 31 cm width (150 windings @ 2 mm profile thickness, 13 A current) based on the sketched profile.

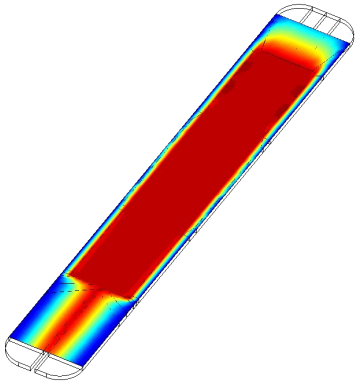

Figure 6.9: B-field contour plot of the DC coil.

The mu-metal shielding as well as cooling and other details are neglected. Deep red areas mark high, blue areas lower field magnitudes. This simulation was done using the IES© Faraday© software package.

Science with MIRAs multi-MIEZE option

A multi-MIEZE setup is capable of producing very short, well separated pulses from a constant, polarised neutron beam [1]. A four-stage setup with frequency doubling between two subsequent levels produces the beam structure shown in Fig. 6.10 (compared to a single MIEZE signal).

If an additional spin flipper coil is placed directly behind the last MIEZE level, a macroscopic spatial splitting of the spin-up (↑) and spin-down (↓) states of the neutron pulses can be achieved (Fig. 6.11) [3].

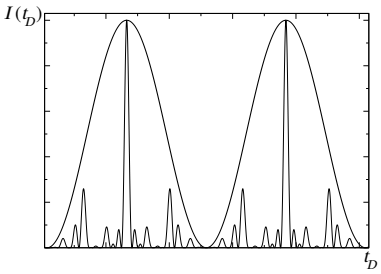

Figure 6.10: Peaks produced by a four level multi-MIEZE (sharp peaks, compared to broad single MIEZE signal).

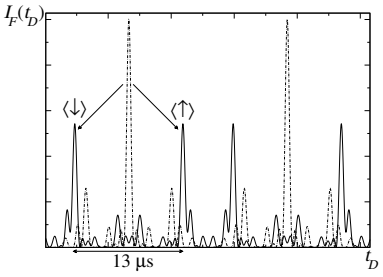

Figure 6.11: Spatial splitting of the spin-up (↑) and spin-down (↓) states.

This "longitudinal Stern-Gerlach effect" demonstrates the predictions of quantum mechanics in contrast to classical physics.

Besides the demonstration of this basic quantum-mechanical effect, the so prepared beam may serve as an experimental basis for studying interference and coherence phenomena using cold neutrons.

[1] Keller T., Golub R., Gähler R. In: Pike R., Sabatier P. (Editors), *Scattering and Inverse Scattering in Pure and Applied Science*, 1264–86 (Academic Press, San Diego, CA, 2002).

[2] Wahl M. *Aufbau einer Messanordnung zur Neutronenreflektometrie*. Master's thesis, Max-Planck-Institut für Metallforschung, Stuttgart, Germany/Institut für Theoretische und Angewandte Physik, Universität Stuttgart, Germany (2003).

[3] Arend N., Gähler R., Keller T., Georgii R., Hils T., Böni P. Classical and quantum-mechanical picture of NRSE - Measuring the longitudinal Stern-Gerlach effect by means of TOF methods (2003). Submitted to Physics Letters A.

6.7 Steps Towards Dynamic Neutron Radiography of a Combustion Engine

J. Brunner [1], **G. Frei** [2], **R. Gähler** [4], **A. Gildemeister** [3], **E. Lehmann** [2], **A. Hillenbach** [3], **B. Schillinger** [1]

[1] Physik Department E21, TU München
[2] Paul Scherrer Institut, 5232 Villigen, Switzerland
[3] Universität Heidelberg, Physikalisches Institut, 69120 Heidelberg, Germany
[4] Institute Laue Langevin, 38042 Grenoble, France

The Dynamic NR is a new technique, which is applied successfully for non-destructive testing for time dependent phenomena with a similar resolution and a similar contrast as in conventional NR. Of special interest is the investigation of the injection process in a running combustion engine under real conditions.

For obtaining a 16-bit conventional radiography image at a typical flux of 10^6 n/cm^{2}s one has to integrate scintillator light on the CCD chip typically for some seconds. Of course the sample thickness, the sample material as well as the detector efficiency determine the exact time. Additionally the readout time, depending on the dynamic range and the pixel number of the CCD, puts a lower limit to the highest achievable frame rate.

The observation of objects in the millisecond time scale is impossible with standard methods. A possible solution for repetitive processes can be stroboscopic imaging. That means a synchronization of the detector with the repetitive process and an integration of 1000 images taken at the same millisecond time window of the cycle. That way a virtual opening time of some seconds can be realized as long as the noise is constant within time (i.e. negligible readout noise) and not determined by the system.

With this method two combustion engines of aluminum towed by a electric motor were observed at ILL. The achieved spatial resolution was 1 mm because of the beam unsharpness.

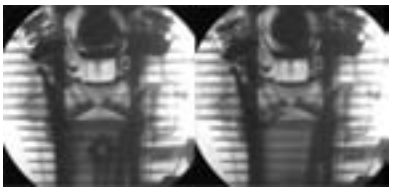

Figure 6.12: Two images of the running cycle of a motorbike at 800 rpm, 250ms with 60 image accumulations

Figure 6.13: Piston cooling of a four stroke car combustion engine can be observed well by neutron radiography, t=200ms with 120 accumulations, image size is 24cm x 24cm

This dynamic neutron investigations were performed with an detector system from PSI at a very high flux test beam line at ILL. The PSI detector consisted of a peltier cooled CCD camera using a multi channel plate as an image intensifier coupled on the CCD-chip with fiber optics.

With this equipment and the high flux thermal neutron beam of 10^9 n/cm^{2}s at ILL extremely high detection sensitivity was possible. The necessary fast triggering is done by the image intensifier. Since the scintillator decay time to 10% is 85 μs, that is the order of magnitude for the limit of the time resolution.

In the false color image Fig. 6.14 the small attenuation of the injection liquid cloud is clearly visible. The next step will be such an observation in a running engine under real conditions.

The obtained results should be a starting point to fit the different requirements of car producers in respect to fuel injection, lubricant distribution, mechanical stability and operation control. Similar inspections will be possible for all devices with repetitive operation principle. At the FRM II the ANTARES tomography station with a high neutron flux of 10^8 n/cm^{2}s and a high spatial resolution will allow such measurements soon. [1, 2]

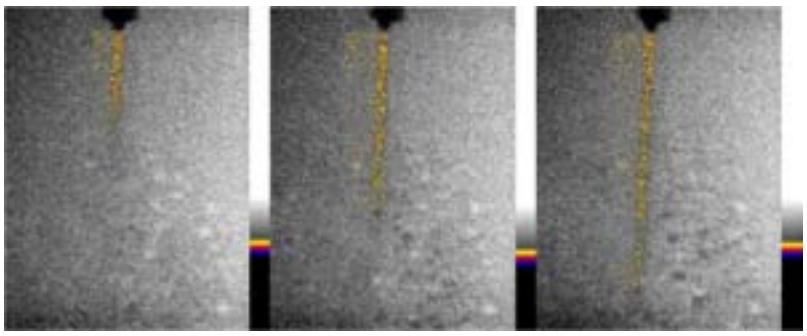

Figure 6.14: Common Rail Diesel injection nozzle (500 bar) in action, 5000 neutron radiography frames of 100ms added by software, delay to the trigger, 600μs, 700μs, 800μs, image size is 6.2cm x 8.2cm

[1] Schilllinger B. *Neue Entwicklungen zu Radiographie and Tomographie mit thermischen Neutronen*. Ph.D. thesis, Technischen Universität München (200?).
[2] Balasko M. *Physica B: Condensed Matter*, **234-236**, (1997), 1033–1034.

6.8 Development of a Fuel Element with Reduced Enrichment for the FRM-II

K. Böning[1]

[1] ZWE FRM-II, TU München

On May 2, 2003, the Bavarian State Ministry of Environment (StMLU) - on instructions received from the Federal Ministry of Environment (BMU) - awarded the FRM-II its 3rd partial nuclear license permitting nuclear startup and full power routine operation of the reactor. However, this long awaited and most welcome final license also involved the condition that the FRM-II should develop, until the end of the year 2010, a new fuel element allowing the FRM-II to continue its operation with medium enriched uranium (MEU, with a maximum of 50 % U235) instead of the present highly enriched uranium (HEU, with 93 % U235). This means that - as a first step towards this goal - an advanced fuel with a much higher density of uranium than presently available must be developed so that the reduction of enrichment could be compensated by an increase in density. Only in this way the dimensions of the fuel element can be kept unchanged, the replacement of the central part of the reactor facility can be avoided and the condition of "any penalty to the FRM-II being marginal only" can be obeyed.

After the issue of the 3rd nuclear permit an agreement between the Bavarian State Ministry of Science (StMWFK) and the Federal Ministry of Science (BMBF), which has been negotiated already two years ago and which also settled the budget requirements, has been signed on May 30, 2003. In consequence an international working group has been established at the Technische Universität München (TUM) comprising representatives of the FRM-II, of the fuel element manufacturer CERCA (France) and of the research reactor planning company Siemens/Framatome-ANP. The first meeting of this "MEU Working Group" was performed in Garching on July 29, 2003, where the break down of the project into three phases of 2 ½ years each has been agreed upon (see table 6.1).

Being well aware that this

schedule is extremely tough the working group will do everything to render this project a success. In September 2003 the BMBF issued the official notification of having allocated its share of the budget for the project phase I.

The second meeting of the MEU working group was held in Garching on October 17, 2003. The FRM-II reported on neutronics calculations which showed that an uranium density in the MEU fuel of 8.0 - 8.5 g/cm^3 will be required for a fuel element with 50 % enrichment (the present density for HEU is 3.0 g/cm^3); the maximum obtained fission density in the fuel meat will be of the order of 2.3×10^{21} fissions/cm^3. It was decided to ask CERCA to submit an offer concerning the supply of MEU and the fabrication of 4 test irradiation plates each with 8.0 density but different metallurgy and of 2 spare plates with 7.0 g/cm^3 for the case that some of the test irradiations should fail. The test irradiations will be performed at the OSIRIS materials testing reactor in Saclay which is operated by the French "Commissariat a l'Energie Atomique" (CEA) and which has already been used for the irradiation of HEU fuel plates of the FRM-II some years ago. On November 24, 2003, TUM and CERCA met with CEA at Saclay to negotiate the details of a contract concerning the irradiation of a total of 4 test plates (2 of each density) in the IRIS facility of OSIRIS, post irradiation examinations (PIEs) of probably two plates in a hot cell at Cadarache, and the final disposal of the plates which have become highly radioactive under irradiation. The final offers and updated draft contracts of CERCA and CEA are expected shortly. In order not to loose time and anticipating these contracts we have sent, on December 12, 2003, a letter of confirmation calling on CERCA to begin immediately with the production of the 50 % enriched MEU (as to be obtained from mixing 93 % and 20 % enriched uranium) and with the first steps to fabricate the irradiation test plates.

Phase I:	07.2003 - 12.2005:	Fuel development and basic questions
Phase II:	01.2006 - 06.2008:	Fuel specification and design of fuel element
Phase III:	07.2008 - 12.2010:	Fuel element fabrication and licensing

Table 6.1: Time table for the MEU fuel element development

7 Scientific Highlights

7.1 Pressure Induced Magnetic and Valence Transitions in $YbMn_2Ge_2$

M. Hofmann [1], **S.J. Campbell** [2,1], **P. Link** [1]

[1] ZWE FRM-II, Technische Universität München, 85748 Garching
[2] School of Physical, Environmental and Mathematical Sciences, The University of New South Wales, ADFA, Canberra, ACT 2600, Australia

Introduction

Rare-earth intermetallic compounds containing ytterbium exhibit a wide range of interesting and unusual physical and magnetic properties. This occurs mainly as a result of their mixed valence states (II/III) or changes from one valence state to the other. Applied pressure is likely to cause changes in the valence character of systems exhibiting intermediate valence and is therefore correspondingly expected to influence the magnetic behaviour [1]. This was highlighted in recent pressure magnetisation measurements [2] which revealed anomalous changes in the magnetic behaviour of $YbMn_2Ge_2$ around a critical pressure of about 1.25 GPa. At ambient pressure the Yb mean valence was estimated to be ≈ 2.35 in this compound [3, 4] and therefore it is expected that only the Mn sublattice will order magnetically.

We have previously demonstrated that $YbMn_2Ge_2$ crystallizes in the tetragonal $ThCr_2Si_2$ type structure; it has a planar antiferromagnetic structure below $T_{N1} \approx 510$K, transforming to a canted antiferromagnetic structure below $T_{N2} \approx 185$K [5]. Our recent neutron and x-ray diffraction experiments reveal that $YbMn_2Ge_2$ under pressure exhibits distinct changes in the magnetic structure along with a sharp decrease in the a-lattice parameter above 1.5 GPa [6]. In addition we also observe reversible peak splitting characteristic for a valence transition of first order around the critical pressure range $p \approx 1.25$ GPa.

Valence Transition

Figure 7.1 shows the variation of the unit cell volume of $YbMn_2Ge_2$ as a function of pressure as determined from our

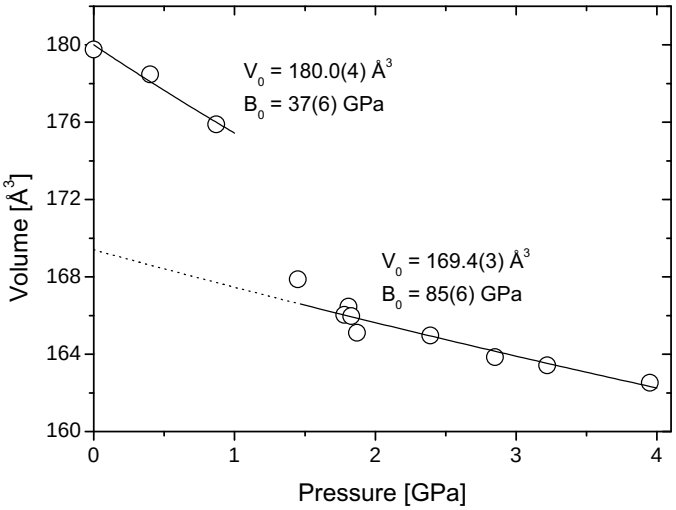

Figure 7.1: The variation of the unit cell volume of $YbMn_2Ge_2$ with pressure as determined by the x-ray diffraction measurements at ambient temperature (the lines are fits to the data as discussed in the text).

x-ray diffraction investigation at ambient temperature [6]. The key feature is the step like behaviour of the volume at around p ≈ 1–1.5 GPa. This is caused primarily by a significant decrease in the a-lattice parameter (≈ 3%) with the c-lattice parameter found to vary only slightly over the entire pressure range. Given that the dimensions of the basal plane in this tetragonal $ThCr_2Si_2$ - type structure are determined primarily by the radii of the rare earth atoms and that, in general, applied pressure favours change in the valence character of compounds containing Ce, Eu and Yb e.g. [1], this pronounced decrease in the lattice parameter provides evidence for a pressure-induced valence transition from a divalent-like Yb ionic state to a Yb^{3+} state in $YbMn_2Ge_2$. This behaviour fits in well with the significant changes in magnetic properties evident at pressure p ≈ 1.25 GPa in the magnetisation measurements of Fujiwara et al [2].

In order to derive the bulk modulus using Murnaghan's equation of state [7], because of the strong variation in the volume, we distinguish between lower and higher pressure regions separated at ≈ 1 –1.5 GPa. As shown in Figure 7.1, between 0 GPa and 1 GPa $YbMn_2Ge_2$ has a much smaller value for B_0 = 37(6) GPa with V_0 = 180.0(4) Å^3, than at pressures above p ≈ 1.5 GPa where the fit yields B_0 = 85(6) and V_0 = 169.4(3) Å^3. This latter value of V_0 is close to the value V = 167.9 Å^3 [4] calculated for a hypothetical trivalent $YbMn_2Ge_2$ state, thus indicating a valence change to almost trivalent Yb between p ≈ 1 GPa and 1.5 GPa. This is consistent with recent L_{III}-edge measurements on $YbMn_2Ge_2$ which indicate a first-order transition p ≈ 1.25 GPa at which pressure the Yb mean valence changes abruptly from 2.4 to a mean valence of about 2.85 at p = 1.3 GPa [8].

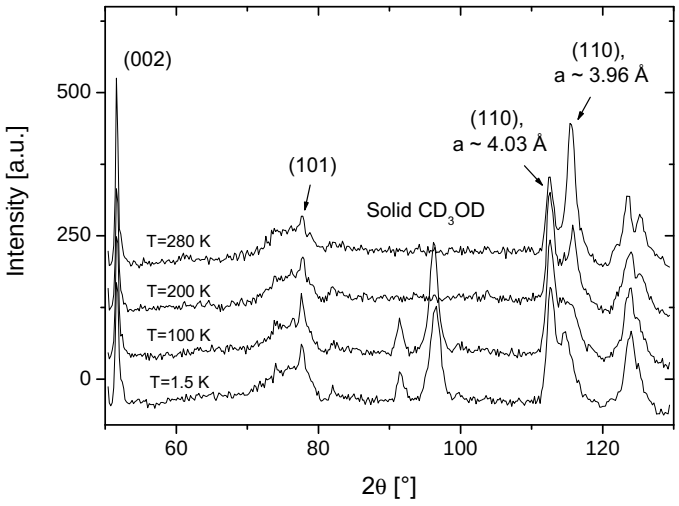

Figure 7.2: Neutron diffraction patterns of $YbMn_2Ge_2$ at p ≈ 1.35 GPa between T = 1.5 - 280 K. Indicated are the (110) reflections with lattice spacings a(2+) ≈ 4.03 Å and a(3+) ≈ 3.96 Å as discussed in the text.

Further evidence for this valence transition is found in the analysis of our neutron diffraction data which were obtained at p ≈ 1.35 GPa (figure 7.2). The experiments were carried out on the G6.1 diffractometer at LLB, Saclay. As shown in figure 7.2, at T = 280 K we observe peak splitting of the main structural peaks; in particular we observe two (110) reflections which indicate the presence of two phases with different a-lattice constants, e.g. a(2+) ≈ 4.03 Å and a(3+) ≈ 3.96 Å. As stated above a change in the rare earth ionic radii will affect mainly the basal plane, the larger lattice spacing a(2+) ≈ 4.03 Å, therefore corresponds to a valence state of divalent character while the smaller lattice spacing, a(3+) ≈ 3.96 Å, is consistent with trivalent Yb. Based on the relative peak intensities, the fractions of the Yb^{2+} like and the Yb^{3+} phases are estimated as 35 % and 65 % respectively. On lowering the temperature the phase fraction of trivalent $YbMn_2Ge_2$ decreases to 40 % with the change found to be reversible with temperature.

Magnetic structure at high pressure

The neutron diffraction pattern of $YbMn_2Ge_2$ at ambient pressure (figure 7.3) shows the characteristic crystallographic features of the tetragonal $ThCr_2Si_2$ structure. As well, the magnetic reflection (101) is clearly discernible, as expected for the planar antiferromagnetic arrangement of the Mn moments at ambient temperature [3]. The refined magnetic moment at T = 290 K is 2.5 μ_B, increasing to 3.4 μ_B at T = 1.5 K consistent with our earlier findings [3]. The lattice parameters of $YbMn_2Ge_2$ at T = 290 K are a = 4.083 Å and c = 10.902 Å [9].

By comparison, at an applied pressure p $\approx$ 2.7 GPa the (101) reflection - the main magnetic reflection in the planar antiferromagnetism of $YbMn_2Ge_2$ - is excluded from the diffraction pattern and disappears almost completely. As well, the appearance of an additional magnetic reflection at $2\theta \approx 123$ indicates a new magnetic ordering scheme. This reflection can be indexed as (111) on the basis of a primitive tetragonal cell. The resulting structure closely resembles the magnetic structure of $YbMn_2Si_2$ (of trivalent Yb) at ambient conditions. Indeed $YbMn_2Ge_2$ at a pressure of 2.7 GPa is found to exhibit similar lattice constants and, more importantly, similar Mn-Mn bond distances to those of trivalent $YbMn_2Si_2$ at room temperature (d_{Mn-Mn} = 2.768 Å in $YbMn_2Ge_2$ and d_{Mn-Mn} = 2.757 Å in $YbMn_2Si_2$). In this latter structure, ferromagnetically coupled Mn layers are coupled antiferromagnetically along the c-axis [10] with the moment direction along the z direction. Analysis of the neutron diffraction pattern of $YbMn_2Ge_2$ (at T = 280 K and at a pressure of p = 2.7 GPa) in terms of the collinear antiferromagnetic structure of trivalent $YbMn_2Si_2$ yields a moment value of $\mu \approx 1.3\ \mu_B$ with refined lattice constants of a = 3.940 Å and c = 10.786 Å.

The current investigations demonstrate clearly the extra insight which variable temperature neutron diffraction measurements carried out under pressure can provide in the study of compounds exhibiting valence changes. Our continuing studies of a series of Yb and Eu based compounds indicate clearly the potential and prospects for incorporating pressure-cell measurements into the routine investiga-

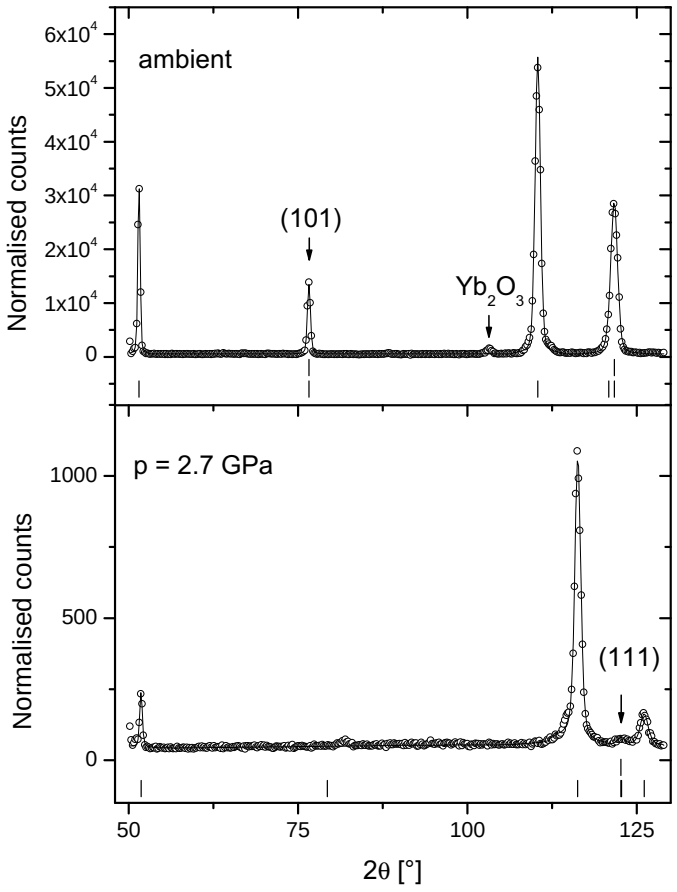

Figure 7.3: Neutron diffraction patterns of $YbMn_2Ge_2$ at: (upper) ambient pressure and temperature; (lower) 2.7 GPa; T = 280 K. The lines are Rietveld refinement fits to the data with the markers indicating the peak position of the nuclear (bottom) and magnetic (top) reflections of $YbMn_2Ge_2$. The small peak at $\approx$ 82 in the pattern at 2.7 GPa results from an instrumental effect.

tions available to users at FRM-II.

SJC acknowledges the support of the Alexander von Humboldt Foundation during renewal of his Research Fellowship at FRM-II, Technische Universität München.

[1] Thompson J., Lawrence J. In: Schneider K., Eyring L., Lander H., Choppin G. (Editors), *Handbook on the Physics and Chemistry of Rare Earths*, volume 19 (Elsevier, 1994).
[2] Fujiwara T., Fujii H., Uwatoko Y., Koyami K., Motokawa M., Shigeoka T. *Acta Phys. Pol.*, **34**, (2003), 1541.
[3] Hofmann M., Campbell S. J., Edge A. V. J. *Appl. Phys.*, **74**, (2002), S713.
[4] Szytula A., Penc B., Jezierski A., Hofmann M., Campbell S. J. *Acta Phys. Pol.*, **34**, (2003), 1561.
[5] Hofmann M., Campbell S. J., Szytula A. *J. Alloys Comp.*, **311**, (2000), 137.
[6] Hofmann M., Campbell S. J., Link P., Goncharenko I., Knorr K. *Physica B.*
[7] Murnaghan F. D. *Finite Deformation of an Elastic Solid* (Dover, New York, 1967).
[8] Fujiwara T., Uwatoko Y., Fujii H., Koyami K., Motokawa M., Shigeoka T. *J. Magn. Magn. Mater.* In press.
[9] Hofmann M., Goncharenko I., Link P., Campbell S. J. (in preparation 2004).
[10] Hofmann M., Campbell S. J., Edge A. V. J., Studer A. J. *J. Phys.: Condens. Matter*, **13**, (2001), 9773.

7.2 Critical Exponents in MnSi

R. Georgii[1], **P. Böni**[2], **D. Lamago**[1], **S. Stüber**[1], **S. V.Grigoriev**[3], **A.I. Okorokov**[3], **H. Eckerlebe**[4], **P.K. Pranzas**[4], **B. Roessli**[5], **W.E. Fischer**[5]

[1] ZWE FRM-II, TU München
[2] E21, Physik-Department, TU München
[3] Petersburg Nuclear Physics Institute, Gatchina, St.Petersburg 188300, Russia
[4] GKSS Forschungszentrum, 21502 Geesthacht
[5] Laboratory for Neutron Scattering, ETH Zürich & Paul Scherrer Institute, CH-5232 Villigen PSI, Switzerland

The chiral fluctuations in the weak itinerant magnet MnSi were studied by means of small angle neutron scattering with polarized neutrons (see JB 2002 for details). Due to the lack of a centre of symmetry the magnetic moments are arranged along a left-handed spiral due to the Dzyaloshinskii-Moriya (DM) interaction. The experiments show that the incommensurate magnetic peaks evolve with increasing temperature into diffuse scattering that is mainly concentrated in a ring with the radius $q_c = 0.039$ Å^{-1} centred at the position of the direct beam $q = 0$.

For the determination of the critical exponents we started to interpret the data by extracting difference spectra of the two beam polarisations. Therefore, the effect of background scattering is eliminated and only the full anti-symmetric part of the magnetic cross section is considered. The spectra are integrated along a ring of constant q for both polarisations independently (i.e. the integration is performed along a half circle of 180^0) and the intensity is plotted against q. The resulting structure is fitted with a Lorentzian peak. The two parameters of this fit, the width and the intensity, are plotted against the temperature as shown in Figure 7.4. From these two plots the following critical exponents can now be extracted using $T_c = (28.7 \pm 0.05)$ K for all fits:

As the imaginary part of the paramagnetic susceptibility is proportional to the neutron magnetic scattering function we can derive the critical parameter γ for $T \geq T_c$ directly from the intensity

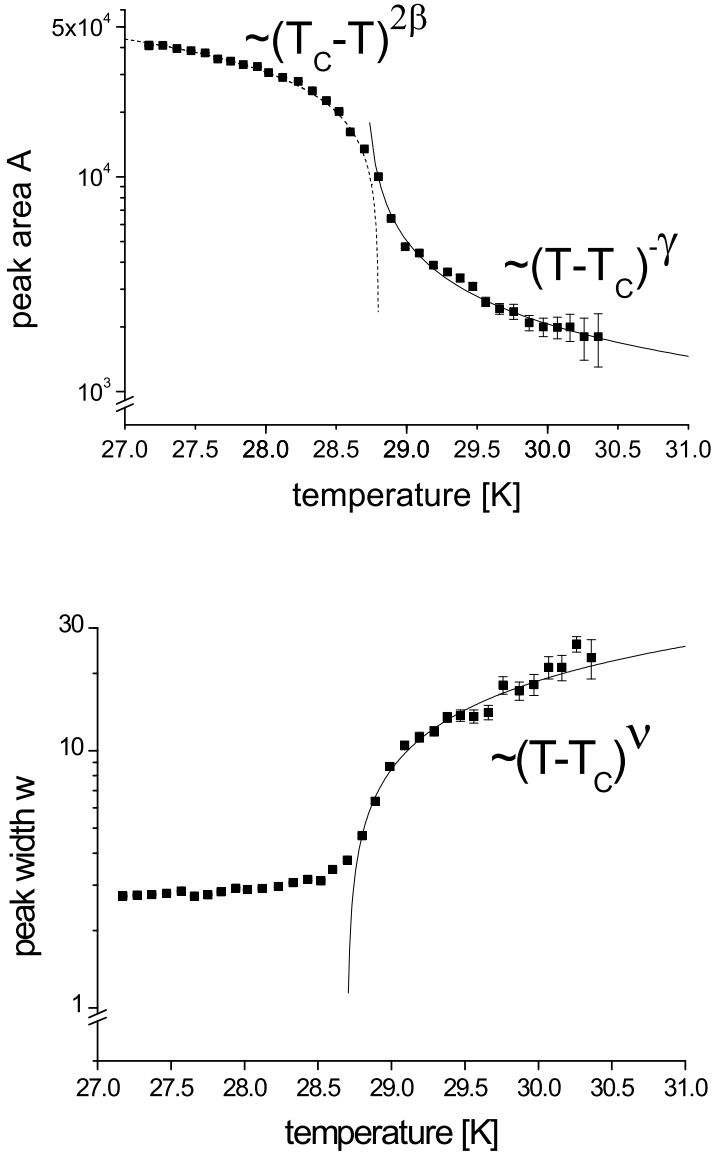

Figure 7.4: The intensity (a) and width (b) of the Lorentzian fits versus the temperature. From the intensity plot below T_c the critical exponent γ for the magnetisation M and above T_c the critical exponent β for the paramagnetic susceptibility χ is obtained. From the width one gets the critical exponent ν for κ, the inverse of the correlation length.

plot. For MnSi we obtain a value $\gamma = 0.61 \pm 0.01$.

As the intensity of the scattering in the ordered phase is proportional to the square of the magnetisation we get the critical parameter 2β for $T \leq T_c$ from the intensity plot. For MnSi we obtain $\beta = 0.218 \pm 0.016$. The width of the peak is proportional to the inverse of the correlation length, therefore we obtain ν from the width of the peak. We find $\nu = 0.541 \pm 0.011$.

These results are so far only preliminary as we intend to remeasure MnSi for obtaining better statistics and also need to include the effects of the finite instrument resolution. But a few conclusions can already be drawn: While the values for β and ν are similar to the values of other magnetic systems [1] the value for γ clearly is smaller. Another interesting observation is that for $d = 2$ we get for $\gamma + 2\beta - d \cdot \nu = -0.036 \pm 0.017$, indicating a two-dimensional magnetic system.

[1] B.D. Gaulin M. C., Mason T. *Physica B*, **156&157**, (1989), 244.

7.3 Dipolar Anisotropy of Spin Waves in Heisenberg Ferromagnet EuS Investigated by Small-angle Polarized Neutron Scattering

D. Lamago [1,4], **O. Okorokov** [2], **S. Grigoriev** [2], **P. Böni** [1], **R. Georgii** [1], **H. Eckerlebe** [3], **P. K. Pranzas** [3]

[1] Physikdepartment E21, TU München
[2] Petersburg Nuclear Physics Institute, Gatchina, 188350, Russia
[3] GKSS-Forschungszentrum, Max-Planck-Str.,21502 Geesthacht, Germany
[4] ZWE FRM-II, TU München

Introduction

Spin dynamics have been studied in the isotropic ferromagnet EuS by means of small-angle polarized neutrons scattering in the temperature range 14 $K \leq T_C =$ 16.6 $K \leq 35K$ in external magnetic fields of H=0-250 mT inclined about $\varphi = 45^\circ$ relative to the incident beam. Isotropic ferromagnets have been subject of extensive studies. Due to its strongly localized moments and low anisotropy fields, EuS is a very good realization of a Heisenberg ferromagnet. In addition EuS is of particular interest because of the large moment of the Eu^{2+} ions of $7\mu_B$ leading to the strong dipolar interactions, which are not negligible in comparison with the exchange interaction.The goal of this research has been to investigate the influence of the dipole-dipole interaction on the critical behaviour of the system at temperatures above the Curie temperature ($T_C = 16.5\ K$).The technique apply for this experiment make use of the asymmetry of the small-angle scattering of polarized neutrons[1, 2] .

Theoretical Foundation

According to [2] one can observe the left-right asymmetry of polarized neutron scattering by measuring the difference in the intensities of the neutrons which are scattered through a small angle θ and which are originally polarized along the magnetization of the sample and opposite to it: $\Delta\ I(\theta) = I(\theta, P_0) - I(\theta, -P_0)$, where P_0 is the initial polarization. This quantity can be written in the form [3]:

$$\Delta I(\theta) \approx \int A_m^2 (em)(eP_0) S^a_{q,\omega} + A_m \alpha M (P_0 m_\perp) \phi_{q,\omega} d\omega \tag{7.1}$$

The first term describes the magnetic scattering while the second describes an interference of magnetic and nuclear scattering. $A_m = \gamma e^2 / m_e C^2$ is the amplitude of the magnetic scattering of the atom. α is the expectation value of the nuclear amplitude, $e = \mathbf{q}/q, m = \mathbf{M}/M$, $\mathbf{M}$ is the magnetization of the sample and $m_\perp = m - e(em)$. The function $S^a_{q,\omega}$ describes the antisymmetric spin correlations and $\phi_{q,\omega}$ is the dynamic nuclear structure factor.

In the case of small-angle scattering where ω is very small compared to the energy of incident neutrons, the scattering by spin waves can be separated experimentally from the contribution of magnetic nuclear scattering. For this purpose one should perform the measurement of $\Delta I(\pm\theta, P_0)$ with the polarization directed along and opposite to the magnetization of the sample and form the difference $\Delta I_A = \frac{1}{2}[\Delta I(\theta, P_0) - \Delta I(-\theta, P_0)]$.

Experiments And Results

The SAPNS experiments were performed using the SANS-2 of the research reactor FRG-1 at the GKSS-Forschungszentrum in Geesthacht(Germany). All measurements were conducted using polarized neutrons ($P_0 =$ 0.95) of fixed wavelength $\lambda =$ 5.8 ($\Delta\lambda/\lambda = 0.1$) with angular divergence of 10 mrad. The scattered neutrons were detected by a position sensitive detector 258 $\times$ 258 mm^2. The isotopically enriched sample ^{153}EuS was composed of roughly 100 single crystals, aligned such that the overall mosaic was $\eta \approx 0.75^\circ$. The sample was mounted inside a cry-

omagnet inclined by an angle $\varphi = 45^\circ$ relative to the incident beam and providing a field up to 250 mT. The scattering intensity were measured in the temperature range from $T = 14\ K$ to $T = 50\ K$. With the described experimental setup one can observe the left-right asymmetry of neutron scattering and thus investigate the critical dynamics by triple-spin correlations in the magnetic field and measure with high accuracy the parameters of spin waves in ferromagnetic phase [4, 5].

The two-spin correlation

In the measurements shown in Fig. 7.5 and 7.6 one can notice the changes in both the quasi-elastic and the inelastic scattering contributions due to the critical spin fluctuations and to the spin-wave excitations respectively.

The measured intensity of the scattered neutrons is well described by the Ornstein-Zernicke expression:

$$I(q) = A(q^2 + \kappa^2)^{-1}, \tag{7.2}$$

where A is the scattering amplitude and κ is the inverse correlation length. Fig. 7.5 shows the temperature dependence of the correlation length $R_C = \frac{1}{\kappa}$. For temperatures above T_C and up to the highest temperatures of our experiments, the line shapes are well described by the spin correlation theories. R_C increases while temperature approaches the Curie temperature $T_C = 16.5\ K$ from above and decreases with further lowering of the temperature. The correlation length decreases with increasing magnetic field as shown in Fig. 7.6. The behaviour of R_C can be explained through the strong field regime, which is determined according to Ref.[6] by the condition $T_C(\kappa_C a_0)^z = g\mu H$. Here z is the critical field exponent and a_0 is a constant of order of 1 Å. From the field dependence of the correlation length at T_C the value of the parameter $\frac{1}{z} = 0.65 \pm 0.02$ was evaluated. The deviation from the theoretical value ($1/z = 0.4$) of a pure Heisenberg ferromagnet is attributed to the dipolar interactions.

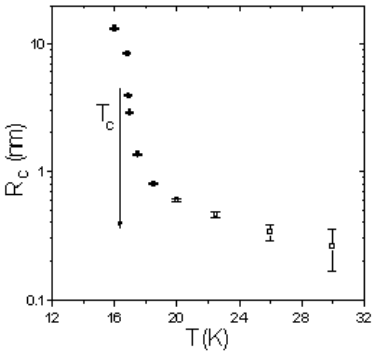

Figure 7.5: Influence of temperature on the correlation length

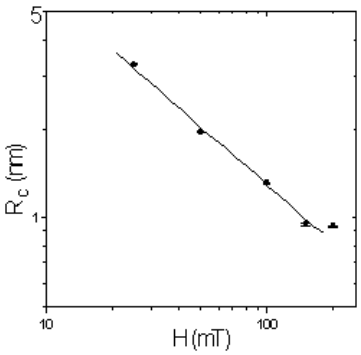

Figure 7.6: Magnetic field dependence of the correlation radius at the Curie temperature

[1] Okorokov A. I. *Physika B*, **204-205**, (2000), 276–278.
[2] Okorokov A. *JETP Lett.*, **48**, (1986), 8.
[3] Gukasov A. *Physika B*, **267-268**, (1999), 97–105.
[4] Toperverg B., Deriglazov V., Mikhailova V. *Physika B*, **183**, (1993), 326.
[5] Deriglazov V. *Physika B*, **180-181**, (1992), 262–264.
[6] Maleyev S. *Physics Review*, **8**, (1987), 323.

7.4 Submicrometer X-ray Tomography with Doubly Asymmetrical Bragg Diffraction at SLS

M. Stampanoni [1], **G. L. Borchert** [2], **P. Rüegsegger** [3], **R. Abela** [1], **J. Rebelo-Kornmeier** [2]

[1] SLS PSI, Villigen, Schweiz
[2] ZWE FRM-II, TU München
[3] IBT ETH, Zürich, Schweiz

Introduction

Microtomography is a challenging research domain being approached with neutron as well as X-ray techniques. By exploiting the high intensity of third-generation synchrotron sources and combining hard X-ray microscopy with tomographic techniques, it is possible to obtain volumetric information of a sample in the micrometer or even sub-micrometer scale with minimal sample preparation. The challenge to trespass the threshold of one micrometer spatial resolution with hard X-rays has spurred the development of detectors optimized for spatial resolutions to the detriment of efficiency. In fact, state-of-the-art devices, which convert X-rays to visible light with a thin scintillator and project them onto the CCD with a microscope optics, claim a spatial resolution around 1 micrometer with efficiency of less than 1% at 30 keV [1]. This, of course, implies very large exposure time. As a consequence, the scientific development aims to perform tomographic scans (usually 500-1000 two-dimensional radiographic projections have to be acquired) with sub-micrometer resolution within minutes. At the Materials Science Beamline 4S of the SLS we installed a novel detector, called Bragg Magnifier and described in detail in Ref. [2], which efficiently acquires distortion-free, magnified hard X-ray projection images of a sample with spatial resolutions around 250 nm.

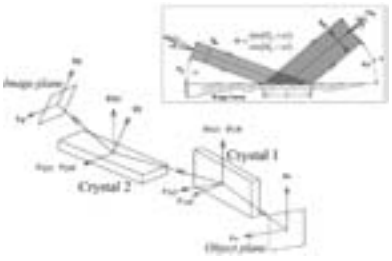

Figure 7.7: X-ray optics of the Bragg magnifier showing the main crystals and the objects and image planes. ”O” describes the incident beam coordinates, ”H” the diffracted one. Inset: coplanar, asymmetric one-dimensional Bragg diffraction; m is the magnification factor.

Working principle

The Bragg Magnifier performs two-dimensional magnification in the X-ray regime exploiting the well know principle of asymmetrical Bragg diffraction from two crossed flat crystals, see inset of Fig. 7.7. The intensity distribution of the beam containing absorption information about the sample is collected by the optics and enlarged according to X-ray dynamical diffraction theory. Let us define the magnification factor as m = $\sin(\theta_B + \alpha)/\sin(\theta_B - \alpha)$ where θ_B is the Bragg angle and α is the asymmetry angle, i.e. the angle between the crystal surface and its lattice planes. It can be shown [3] that the angular divergence of the incident (ω_O) and diffracted (ω_H) beam are related to each other by $\omega_H = 1/|m| \cdot \omega_O$ For S_O and S_H being the spatial cross-sections of the incident and diffracted beam, Liouville's theorem requires that $S_O \cdot \omega_O = S_H \cdot \omega_H$ and hence$S_H = |m| \cdot S_O$.Therefore if $|m| > 1$ the range of total reflection for the emergent beam is $1/|m|$ times smaller than that of the incident beam, while its spatial cross section is $|m|$ times greater (Fankuchen effect). This allows enlarging the radiographic projection of the sample.

Figure 7.8: X-ray optics of the Bragg Magnifier. Both crystals in Kirkpatrik-Baez geometry as well as the entrance of the 1:1 tandem optics are clearly visible.

Realization and first experiments

Si(220) crystals with an asymmetry angle of $\alpha = 8°$ have been chosen as X-ray optics. They are fixed on high-precision goniometer heads which allow pitching and rolling within an angular reproducibility of 2" as well as rocking with an angular resolution of 0.05". The magnified X-ray image is collected by an high-efficiency position sensitive detector and converted to visible light by a 35x35 mm2 CsI(Tl) scintillator of 300 micrometer thickness. The generated light is projected by an high-efficiency 1:1 tandem optics onto a high performance CCD. The new CCD camera features a 2048x2048 full frame Atmel THX7899M chip with a full well capacity of more than 250'000 electrons. Pixel frequency is 3.3 MHz, resulting in a readout time of 320 ms for a 2k x 2k image. The CCD-chip is Peltier and water cooled to -24 °C , dark-current is 6 e^-/pix/s at -22°C and the RMS noise in dark is 29 e^- The effective dynamic range is > 5000:1. Sub-area readout or on-chip binning allows frame rates up to 4-5 Hz for exposure time of 50 ms. Fig. 7.8 shows the Bragg Magnifier installed at the micro-tomography station of the Materials Science Beamline 4S.

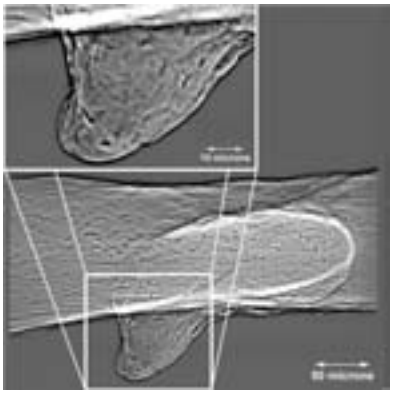

Figure 7.9: High-resolution radiography of a human bone trabecula. Magnification is 50x50 and the field of view is 575 x 575 μm^2.

Tuning the X-ray energy from 21.1 keV up to 22.75 keV and rocking both crystals accordingly, we obtained magnification factors ranging from 20x20 to 100x100. By setting the energy to 22.34 keV, the Bragg Magnifier produces a magnification of approximately 50x50 resulting in a theoretical pixel size of 280x280 nm^2. With these parameters we acquired a radiography of a human bone trabecula, which is shown in Fig. 7.9.

In the inset of Fig. 7.9, Fresnel fringes can clearly be observed. These are principally due to the coherent nature of the beam. As a consequence, and according to theoretical predictions [4], the image has to be interpreted as an edge-enhanced projection.

From the field of materials science we studied a sample of carbon fibre reinforced material to be used in space craft application. With the same settings of the parameters we acquired 500 two-dimensional projections of the sample in equidistant angular intervals from 0°to 180°. The exposure time was 5 seconds for each projection resulting in a total scan time of approximately 40 min. Flat and dark field corrected data have been reconstructed with a standard filtered-backprojection algorithm [5]. The resulting three-dimensional image is shown in Fig. 7.10.

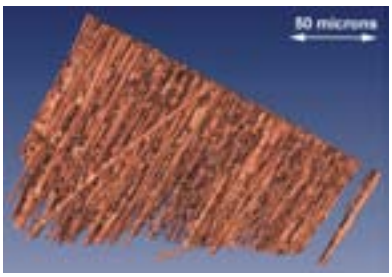

Figure 7.10: A three-dimensional reconstruction of the carbon fibre reinforced sample. The fibres with a diameter of 4μm are clearly resolved.

Conclusion and outlook

The reliability of double asymmetrical Bragg diffraction from flat crystals has been demonstrated and the Bragg Magnifier produces very good X-ray images. Its basic principle is applicable at lower energies, and this even with fewer difficulties since the crystals acceptance is higher, increasing the flexibility of the instrumentation. With the concrete perspective to reach voxel's size around 100 nm^3, completely unexplored dimensions will be accessible to computer tomography.

[1] Koch A., et al. *J. Opt. Soc. Am. A*, 15.
[2] Stampanoni M., et al. *J. Appl. Phys.*, **92**, (2002), 7630–7635.
[3] Caciuffo R., et al. *Physics Reports*, 152.
[4] Spal R. *Phys. Rev. Lett*, **86**, (2002), 3044.
[5] Kak A. X., Slaney. *Principles of Computerized Tomographic Imaging* (IEEE, New York, 1988).

7.5 Short-time Stroboscopic Neutron Imaging on a Rotating Engine

B. Schillinger [1,2], **H. Abele** [4], **J. Brunner** [1,2], **G. Frei** [3], **R. Gähler** [5], **A. Gildemeister** [4], **A. Hillenbach** [4], **E. Lehmann** [3], **P. Vontobel** [3]

[1] ZWE FRM-II, TU München
[2] Phsikdepartment E21, TU München
[3] Paul-Scherrer-Institut, Villigen PSI, Switzerland
[4] Universität Heidelberg, Faculty for Physics, Germany
[5] Institut Laue-Langevin, Grenoble, France

Abstract

Todays neutron sources do not deliver sufficient flux to examine singular short-time events in the millisecond range by neutron radiography. However, periodic processes can be examined if a triggered accumulating detector collects information of identical time windows and positions over several cycles of the process. At the intense neutron beam H9 of ILL Grenoble, an electrically driven BMW engine was examined at 1000 rpm with time resolution of 200 microseconds.

Detection systems

So far, the only feasible detection systems found are interline frame transfer CCDs or CCD cameras with gated image intensifiers, in combination with a neutron sensitive scintillation screen and mirror.

For interline frame transfer CCD cameras, the CCD chip area consists of alternate light sensitive pixel columns and masked vertical shift registers. Image information from the light sensitive pixels can be transferred into the masked, light-insensitive shift register with a single clock cycle, enabling for exposure times in the range of ten microseconds. This process can be repeated several times (with flushing the image pixels between exposures) before the whole image information is read out via the shift registers. The advantage of this method is that no additional noise is introduced by an image intensifier, the disadvantage is that the number of on-chip accumulations is limited. Additional frame accumulations can be done off-line in the computer, but their statistics is limited by the digitization process of the individual frames.

With gated image intensifiers, theoretical gating times of down to 3 ns can be achieved, however the decay time to 10% of the employed scintillator is 85 microseconds, limiting the achievable time resolution. The advantage of intensified CCDs is their higher pixel capacity which enables for the accumulation of several hundred gating periods before readout. They are limited by the additional quantum noise generated by the electron multiplication in the intensifier. Up to now, there is no clear superiority of one system visible.

For both systems, less than one percent of the total neutron fluence is used for imaging, resulting in very high activation of the sample. A different approach is being tried with a chopper wheel in Japan, which drastically reduces activation, but is rather inflexible in adjusting the time window.

Measurements

The beam line H9 behind the Lohengrin experiment at ILL Grenoble is the most intense neutron radiography beam in the world, with a flux of $2 * 10^9$ n/cm^{2}s and a collimation of L/D=110. ILL, Universität Heidelberg, Paul-Scherrer-Institut and TU München collaborated on the measurement of an electrically driven four-piston BMW engine. The engine was driven by a 2 kW electro motor, mounted on a vertical translation stage. Since water cooling was not possible, the spark plugs were removed to reduce drag and heat production.

The detection system was a MCP intensified CCD camera PI-max with a Peltier cooled chip (1300 * 1024 pixels) with 16 bit digitization. The usable dynamic range is limited by the inherent noise of the intensifier.

The full cycle of this four-stroke engine running at 1000 rpm was split into 120 individual frames over 2 rotations, 150 individual images were recorded as an on-chip accumulation of a 200 microseconds exposure each. In this way, the total exposure time for the full run was in the order of 18 minutes only. The field of view was 24 cm * 24 cm. The observation area could be varied by displacement of the full set-up.

Figure 7.11 shows one frame of the recorded movie, showing valves, pistons, piston rods, piston pins and piston rings. Of special interest is the visualization of the oil cooling of the piston bottoms. Since the pistons are only connected to the engine body via the piston rings with very low heat dissipation, a continuous oil jet is directed from below at the piston bottoms, lowering the piston temperature by more than 200 degrees C. In the movie, the oil jet of 1-2 mm diameter is clearly visible. Around the upper turning point of the piston, the dome-like spread of the oil at the underside of the piston can be observed.

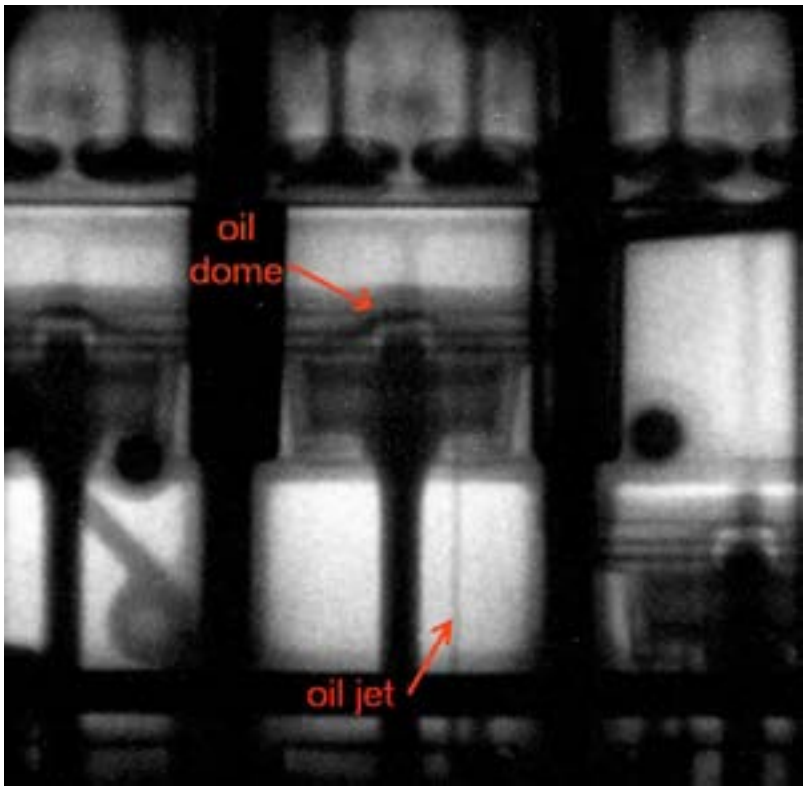

Figure 7.11: Single frame of a sequence of images of a running car engine, rotated at 1000 rpm. All components are clearly visible (valves, cylinder head, connecting rod, piston, piston pin, piston ring). Of highest interest in this run was the oil injection from below for cooling the piston.

Outlook

Further measurements will be done in 2004, using a single-piston diesel engine to examine the injection process. As soon as FRM-II is operational, measurements will commence in Garching as well, trading beam intensity for better collimation. Future measurements will focus especially on the oil cycle for the lubrication of the bearings of cam shaft and crank shaft. To overcome the limitation in time resolution given by the scintillator, new scintillation materials must be examined for feasibility for short-time neutron radiography. The neutron quantum statistics and the quantum noise of the image intensifier will be the final limitation of achievable time resolution, though it is by far not met yet.

8 Events, People and Figures

8.1 1st FRM-II Workshop on Neutron Scattering -Advanced Materials- 21.7-24.7 Burg Rothenfels am Main

R. Georgii [1], **P. Böni** [2], **A. Meyer** [3], **W. Petry** [1], **R. Röhlsberger** [3]

[1] ZWE FRM-II, TU München
[2] Physik-Department E21, TU München
[3] Physik-Department E13, TU München

Resume

On 21.7-24.7 the 1st FRM-II Workshop on Neutron Scattering –Advanced Materials– took place at the Burg Rothenfels am Main. About 45 participants mainly from the FRM-II instrumentation group and the institutes E13 and E21 of the Physics Department, but also guests from as far as Australia (Prof. Steward Campbell) enjoyed the very romantic scenery of the medivial castle above the picturesque Main valley. This exceptional surrounding, together with the superb food and the beautiful Burgkeller of the castle led to extensive scientific discussions besides the more then 30 talks given during the three days. A very broad range of talks from various fields as magnetism over viscous melts to nuclear and fundamental physics demonstrated the very rich field for the use of the neutrons as probes from large scales to microscopic scales. According the participants this workshop helped to get an overview of the science, which will be performed at the FRM II and should be repeated in regular terms.

8.2 Public Relations

V. Klamroth [1]

[1] Technische Universität München, Presse & Kommunikation, Bereich Garching

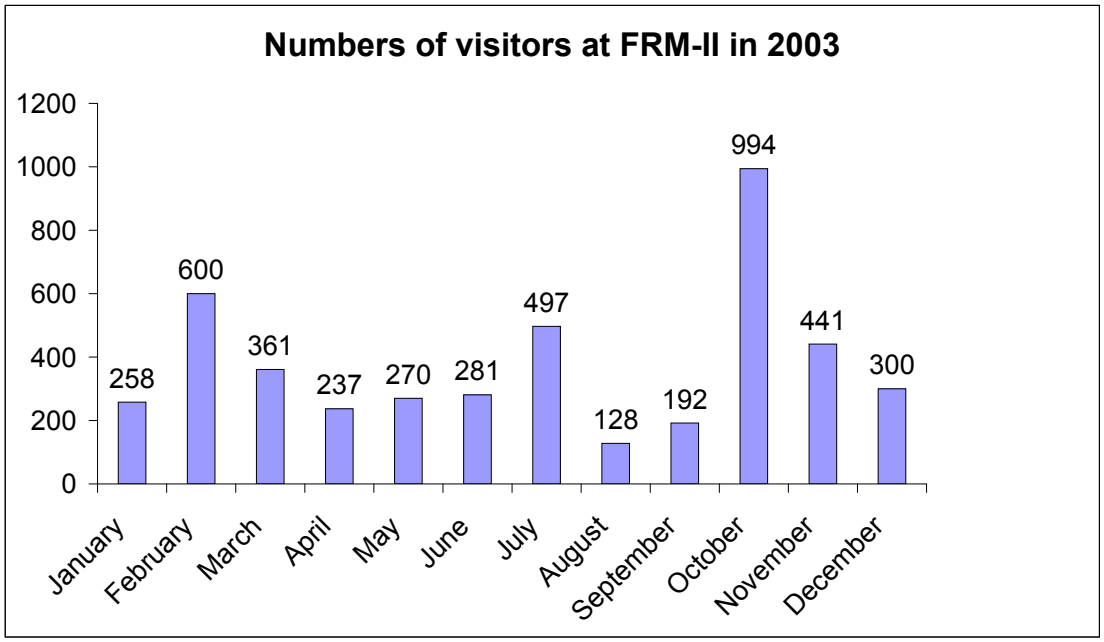

The major event in 2003 was the visit of the Bavarian Prime Minister Dr. Edmund Stoiber giving the official starting signal for the FRM-II in presence of the Bavarian Minister of Science and the Minister of Environmental Affairs on 4th of June. About 40 journalists, photographers, cameramen and other media representatives came to Garching to cover this event. Already the official permission of the Federal Ministry of Environmental Affairs in the middle of April had had a large attraction for the media. Numerous requests from national and international journalists had to be answered. This high media interest in the FRM-II last on for the rest of the year. The main questions concerned the start of operation and the use of the neutron source. In addition there were many requests for pictures and interviews with scientists.

The number of visitors in Garching was even higher than in the year 2002. More than 4,500 persons visited the FRM-II. Yet alone, 630 visitors came to the FRM-II at the open day in October, a Saturday where all scientific institutes on the Campus in Garching were open to the public.

Staff of the FRM-II engaged with dedication as guides all over the year. This service to the public is even more creditable as the strict access regulations to the reactor and the long security procedures for visitors require a high level of patience.

Numerous politicians from different parties including members of the federal parliament were gathering information about the FRM-II and came to Garching. The large audience at the public lecture of Prof. Petry in the Bavarian representation in Berlin demonstrated the high interest in

the new neutron source all over Germany.

The Bavarian Minister of Science showed the FRM-II to the Minister of Education of Luxembourg as an example of the successful Bavarian science politics. In a special issue of the engineer journal "Technik in Bayern" we presented the broad spectrum of the use of the new neutron source.

As required by law, the leaflet "Rundherum sicher" ("All around safe") including arrangements in case of emergency was delivered to the inhabitants of the nearby villages and students and employees on the campus in August. The leaflet also describes the safety of the reactor and shows by means of appropriate comparisons how low the radioactive release from the reactor is compared to natural radioactivity. The German version of this leaflet can be ordered at the visitor's office (Tel 289-12147) or directly downloaded from http://www.frm2.tum.de/publikationen. There is also an English version available.

8.3 Committees

Strategierat FRM-II

Chairman

Prof. Dr. Gernot Heger
Institut für Kristallographie
RWTH Aachen

Members

Ministerialdirigent Jürgen Großkreutz
Bayrisches Staatsministerium für Wissenschaft, Forschung und Kunst

Dr. Rainer Köpke
Bundesministerium für Bildung und Forschung

Prof. Dr. Georg Büldt
Institut für Biologische Informationsverarbeitung
Forschungszentrum Jülich

Prof. Dr. Dosch
Max-Planck-Institut für Metallforschung

Prof. Dr. Dieter Richter
Institut für Festkörperphysik
Forschungszentrum Jülich

Prof. Dr. Dirk Schwalm
Max-Planck-Institut für Kernphysik, Heidelberg

Prof. Dr. Helmut Schwarz
Institute for Chemistry
Technische Universität Berlin

Prof. Dr. Dr. Michael Wannenmacher
Radiologische Klinik und Poliklinik
Abteilung Strahlentherapie
Universität Heidelberg

Dr. Heinz Voggenreiter
Senior Manager
Corporate Research and Technologie
EADS, Paris

Prof. Dr. Götz Eckold
Institute of Physical Chemistry
Universität Göttingen
(Speaker Instrumentation advisory board)

Guests

Prof. Dr. Dr. Wolfgang A. Hermann
Präsident der Technischen Universität München

Dr.-Ing. Rainer Kuch
Zentrale Verwaltung
Technische Universität München

Dr. Michael Klimke
Zentrale Verwaltung
Technische Universität München

Prof. Dr. Winfried Petry
ZWE FRM-II
Technische Universität München

Prof. Dr. Klaus Schreckenbach
ZWE FRM-II
Technische Universität München

Guido Engelke
ZWE FRM-II
Technische Universität München

Dr. Viola Klammroth
ZWE FRM-II
Technische Universität München

TUM advisory board

Chairman

Prof. Dr. Ewald Werner
Lehrstuhl für Werkstoffkunde und -mechanik
Technische Universität München

Members

Prof. Dr. Peter Böni
Physik Department E21
Technische Universität München

Prof. Dr. Andreas Türler
Institut für Radiochemie
Technische Universität München

Prof. Dr. Markus Schwaiger
Nuklearmedizinische Klinik und Poliklinik
Klinikum rechts der Isar
Technische Universität München

Prof. Dr. Bernhard Wolf
Heinz Nixdorf-Lehrstuhl für medizinische Elektronik
Technische Universität München

Prof. Dr. Arne Skerra
Lehrstuhl für Biologische Chemie
Technische Universität München

Guests

Dr. Markus Busold
University Management
Technische Universität München
(until October 2003)

Dr. Michael Klimke
University Management
Technische Universität München
(since October 2003)

Guido Engelke
ZWE FRM-II
Technische Universität München

Prof. Winfried Petry
ZWE FRM-II
Technische Universität München

Prof. Klaus Schreckenbach
ZWE FRM-II
Technische Universität München

Instrumentation advisory board

Chairman

Prof. Dr. Götz Eckold
Institut for Physical Chemistry
Georg-August-Universität Göttingen

Members

Prof. Dr. Dieter Habs
Sektion Physik
Ludwig-Maximilian-Universität München

Prof. Dr. Peter Böni
Physik Department E21
Technische Universität München

Prof. Dr. Dirk Dubbers
Physikalisches Institut
Universität Heidelberg

Dr. Hans Graf
Abteilung NE
Hahn-Meitner-Institut, Berlin

Prof. Dr. Andreas Magerl
Chair for Crystallography and Structural Physics
Friedrich-Alexander-Universität Erlangen-Nürnberg

Prof.Dr. Gottfried Münzenberg
Gesellschaft für Schwerionenforschung mbH, Darmstadt

Prof. Dr. Wolfgang Scherer
Lehrstuhl für Chemische Physik
Universität Augsburg

Dr. habil. Dieter Schwahn
Institut für Festkörperforschung
Forschungszentrum Jülich

Prof. Dr. Markus Schwaiger
Lehrstuhl für Nuklearmedizin
Technische Universität München

Prof. Dr. Andreas Türler
Institut für Radiochemie
Technische Universität München

Dr. habil. Regine Willumeit
GKSS Forschungszentrum, Geesthacht

Guests

Dr. Markus Busold
University Management
Technische Universität München (until October 2003)

Dr. Michael Klimke
Zentrale Verwaltung
Technische Universität München (since Ocotber 2003)

Dr. Klaus Feldmann
BEO-PFR
Forschungszentrum Jülich

Ministerialdirigent Jürgen Großkreutz
Bayrisches Staatsministerium für Wissenschaft, Forschung und Kunst

Prof. Dr. Gernot Heger
Institut für Kristallographie
RWTH Aachen

RR Felix Köhl
Bayerisches Staatsministerium für Wissenschaft, Forschung und Kunst

ORRin Birgit Schmid
Bayerisches Staatsministerium für Wissenschaft, Forschung und Kunst

Dr. Jürgen Neuhaus
ZWE-FRM-II
Technische Universität München

Prof. Dr. Winfried Petry
ZWE-FRM-II
Technische Universität München

Guido Engelke
ZWE FRM-II
Technische Universität München

Prof. Dr. W. Press
Institut Laue Langevin
Grenoble, France

Prof. Dr. Klaus Schreckbach
ZWE FRM-II
Technische Universität München

Prof. Dr. Tasso Springer

8.4 Staff

Board of Directors

Scientific director
Prof. Dr. W. Petry

Technical director
Prof. Dr. K. Schreckenbach

Administrative director
G. Engelke

Experiments

Head
Prof. Dr. W. Petry

Secretaries
E. Doll
W. Wittowetz

Coordination
Dr. J. Neuhaus

Instruments
N. Arend
H. Bamberger

M.Bleuel
J. Brunner
K. Buchner
E. Calzada
D. Etzdorf

Figure 8.1: Experiments staff

J. Franke (MPI-Stuttgart)
Dr. R. Georgii
Dr. R. Gilles
F. Grünauer
Dr. E. Gutsmiedl
F. Hibsch
Dr. M. Hofmann
Dr. M. Hölzel (TU Darmsatdt)
Dr. K. Hradil (Univ. Göttingen)
Dr. C. Hugenschmidt
Dr. T. Keller (MPI-Stuttgart)
Dr. V. Kudryaschov
B. Krimmer (TU-Darmstadt)
D. Lamago
Dr. P. Link
R. Lorenz
T. Mehaddene
Dr. M. Meven
M. Misera
M. Mühlbauer
A. Müller
Dr. B. Pedersen
R. Repper
J. Ringe
Dr. P. Rühm (MPI Stuttgart)
Dr. B. Schillinger
Dr. M. Schlapp (TU Darmstadt)
H. Schneider (Univ. Göttingen)
G. Seidl
Dr .T. Unruh
H. Wagensonner
Dr. W. Waschkowski
Dr. U. Wildgruber
(MPI-Stuttgart)

Detectors and electronic
Dr. K. Zeitelhack
S. Egerland
Dr. A. Kastenmüller
D. Maier
M. Panradl

Sample environment
Dr. J. Peters
H. Kolb
A. Pscheidt
A. Schmidt
S. Sedlmair
J. Wetzlaff

Neutron optics
Prof. Dr. G. Borchert
C. Breunig
H. Hofmann
E. Kahle
Dr. S. Massalovitch
C. Schanzer
A. Urban

Instrument control and software
J. Krüger
J. Dettbarn
S. Galinski
H. Gilde
S. Praßl
S. Roth

Networking and computers
J. Beckmann
J. Ertl
S. Krohn
R. Müller
J. Mittermaier
J. Pulz
F. Zoebisch

Public relations
Dr. W. Waschkowski
Dr. V. Klamroth (ZV, TUM)
K. Schaumlöffel
J. Jeske
I. Maier

Guests
Prof. S. Campbell (Univ. NSW Australia)

Administration

Head
G. Engelke

Secretary
C. Zeller

Members
B. Bendak
B. Gallenberger
I. Heinath
H. Niedermeier
R. Obermeier

Figure 8.2: Administration staff

Reactor operation

Head
Prof. Dr. K. Schreckenbach

Secretaries
K. Lüttig
M. Neuberger
S. Rubsch

Visitor service
J. Jeske
I. Maier

Management
Dr. H. Gerstenberg (irradiation and sources)
Dr. J. Meier (reactor projects)
Dr. C. Morkel (reactor operation)

Shift members
F. Gründer
A. Bancsov
A. Benke
M. Danner
M. Flieher
H. Groß
L. Herdam
K. Höglauer
T. Kalk
G. Kaltenegger
U. Kappenberg
F. Kewitz
M. G. Krümpelmann
J. Kund
A. Lochinger
G. Mauermann
A. Meilinger
M. Moser
L. Rottenkolber
G. Schlittenbauer
N. Wiegner

Technical services
N. Waasmaier
J. Aigner
D. Bahmet
F. Doll
H. Gampfer
W. Glashauser
J. Groß
G. Guld
F. Hofstetter
M. Kleidorfer
W. Kluge
H. Kollmannsberger
J.-L. Krauß
R. Maier
K. Otto
A. Schindler
R. Schlecht jun.
J. Schreiner
H. Sedlmeier
C. Strobl
G. Wagner
A. Weber
J. Wetzl
C. Ziller

Electrics and electronics
R. Schätzlein
G. Aigner
W. Buchner
Ü. Sarikaya
H. Schwaighofer

Figure 8.3: Reactor operation staff

Irradiation and sources
Dr. H. Gerstenberg
J.-M. Favoli
Dr. E. Gutsmiedl
Dr. X. Li
C. Müller
M. Oberndorfer
D. Päthe
W. Lange
G. Langenstück
W. Waschkowski

Reactor projects
Dr. J. Meier

Documentation
V. Zill
J. Jung

Instrument Safety
R. Lorenz

Technical design
F.-L. Tralmer
J. Fink
H. Fußstetter
J. Jüttner
K. Lichtenstein
P. Mross
M. Ullrich

Workshops
C. Herzog
U. Stiegel
A. Begic
M. Fuß
A. Huber
A. Scharl
R. Schlecht sen.
M. Tessaro

Radiation protection
Dr. H. Zeising
S. Dambeck
W. Dollrieß
Dr. H. Gerstenberg
H. Hottmann
Dr. J. Meier
B. Neugebauer
F. M. Wagner
S. Wolff
H.-J. Werth

Chemical laboratory
Dr. F. Dienstbach
T. Asam
C. Auer
R. Bertsch

Reactor physics

Prof. Dr. K. Böning
Dr. A. Röhrmoser
N. Wieschalla

Security department

L. Stienen
J. Stephani

8.5 Publications

[1] Arend N., Gähler R., Keller T., Georgii R., Hils T., Böni P. *Classical and quantum-mechanical picture of NRSE - Measuring the longitudinal Stern-Gerlach effect by means of TOF methods. Physics Letters A.* Submitted.

[2] Asthalter T., Sergueev I., Franz H., Petry W., Messel K., R.Verbeni. *Glass dynamics and scaling behavior under pressure using quasielastic nuclear forward scattering. Hyperfine Interactions*, **C5**(29-32).

[3] Attié D., Cordier B., Gros M., Laurent P., Schanne S., Tauzin G., von Ballmoos P., Bouchet L., Jean P., Knödlseder J., Mandrou P., Paul P., Roques J.-P., Skinner G., Vedrenne G., Georgii R., von Kienlin A., Lichti G., Schönfelder V., Strong A., Wunderer C., Shrader C., Sturner S., Teegarden B., Weidenspointner G., Kiener J., Porquet M.-G., Tatischeff V., Crespin S., Joly S., André Y., Sanchez F., Leleux P. *INTEGRAL/SPI ground calibration. Astron. & Astrophys.*, **411**, (2003), L71–L79.

[4] Bader A., Faschinger W., Hradil K., Kumpf C., Schallenberg T., Schumacher C., Geurts J., Neder K., Molenkamp L. W. *Two-step relaxation of ZnSe grown on (001) GaAs. J. Appl. Phys.* In print.

[5] Bleuel M., Demmel F., Gähler R., Golub R., Habicht K., Keller T., Klimko S., Köper I., Longeville S., Prokudaylo S. In: Mezei F., Pappas C., Gutberlet T. (Editors), *Neutron-spin-echo-spectroscopy*, Lecture Notes in Physics (Springer, 2003).

[6] Böning K., Waschkowski W., Schreckenbach K. *Konzept und Sicherheit des FRM-II. Technik in Bayern*, **4**, (2003), 12 – 13.

[7] Böning K., Neuhaus J. *The Neutron Beams of TUM's FRM-II.* To appear in the Compendium on Purpose-Designed Research Reactor Features of the International Atomic Energy Agency (IAEA), Vienna, manuscript 9 pages.

[8] Brunner J., Frei G., Lehmann E., Vontobel P., Schillinger B. *Steps towards dynamic neutron radiography of a combustion engine. PSI Scientific Report*, **III**, (2003), 164.

[9] Cadogan J. M., Ryan D. H., Moze O., Suharyana, Hofmann M. *Magnetic ordering in $ErFe_6Sn_6$. J. Phys.: Condens. Matter.*, **15**, (2003), 1757.

[10] Chatake T., Ostermann A., Kurihara K., Parak F. G., Niimura N. *Hydration in proteins observed by high-resolution neutron crystallography. Proteins*, **50**, (2003), 516–523.

[11] Ehrhardt H., Campbell S. J., Hofmann M. *Magnetism of the nanostructured spinel zinc ferrite. Scripta Materialia*, **2003**, (2003), 1141.

[12] Engler N., Ostermann A., Niimura N., Parak F. G. *Hydrogen atoms in proteins: Position and dynamics. Proc. Natl. Acad. Sci. USA*, **100**, (2003), 10243–10248.

[13] Engler N., Prusakov V., Ostermann A., Parak F. *A water network within a protein: temperature-dependent water ligation in H64V-metmyoglobin and relaxation to deoxymyoglobin. Eur. Biophys. J.*, **31**, (2003), 595–607.

[14] Faestermann T., Assmann W., Beck L., Bongers H., Carli W., Groß M., Großmann R., Habs D., Hartung P., Heinz S., Jüttner P., Kester O., Krücken R., Maier H.-J., Maier-Komor P., Nebel F., Ospald F., Pasini M., Rudolph K., Schumann M., Szerypo J., Thirolf P. G., Tralmer F., Zech E. *The Munich Accelerator for Fission Fragments (MAFF).* In: *Proc. 6th Int. Conf. on Radioactive Nuclear Beams (RNB6)* (Argonne, Illinois, 2003). To be published in Nucl. Phys. A.

[15] Frank A. I., Balashov S. N., Bondarenko I. V., Geltenbort P., Høghøj P., Masalovich S. V., Nosov V. G. *Phase modulation of a neutron wave and diffraction of ultracold neutrons on a moving grating. Physics Letters A*, **311**, (2003), 6–12.

[16] Frey F., Weidner E., Pedersen B. *Tieftemperaturmessungen zur Strukturuntersuchung an dekagonal en Quasikristallen.* In preparation.

[17] Georgii R., Böni P., Pleshanov N. *Polarised reflectometry with MIRA at the FRM-II. Physica B: Cond. Matt.*, **335**, (2003), 250–254.
[18] Georgii R., Böni P., Pleshanov N. *The VCN reflectometer for MIRA at the FRM-II. Langumir*, **19**, (2003), 7794–7795.
[19] Georgii R., Böni P., Lamago D., Stuber S., Grigoriev S., Malyeev S. *Critical scattering of MnSi. Physica B.* Accepted.
[20] Gilles R., Mukherji D., Genovese D. D., Strunz P., Barbier B., Kockelmann W., Rösler J., Fuess H. *Misfit Investigations of Nickel-base Superalloys. Materials Science Forum*, **426-432**, (2003), 821.
[21] Habicht K., Keller T., Golub R. *The resolution function in neutron spin echo spectroscopy with three axis spectrometers. J. Appl. Cryst.*, **36**, (2003), 1307.
[22] Habicht K., Golub R., Keimer B., Mezei F., Keller T. *Phonon lifetime measurements with neutron resonance spin echo at BENSC - anharmonic lattice dynamics*. In: *Proceedings SCNS* (ILL, 2003).
[23] Habicht K., Golub R., Keller T. *Resolution issues for neutron spin echo spectroscopy on triple axis spectrometers*. In: *Proceedings SCNS* (ILL, 2003).
[24] Habicht K., Golub R., Gähler R., Keller T. In: Mezei F., Pappas C., Gutberlet T. (Editors), *Neutron-spin-echo-spectroscopy*, Lecture Notes in Physics (Springer, 2003).
[25] Habs D., Groß M., Assmann W., Ames F., Bongers H., Emhofer S., Heinz S., Henry S., Kester O., Neumayr J., Ospald F., Reiter P., Sieber T., Szerypo J., Thirolf P., Varentsov V., Wilfart A., Faestermann T., Krücken R., Maier-Komor P. *The Munich Accelerator for Fission Fragments MAFF. Nucl. Instr. and Meth. B*, **204**.
[26] Herrmann R. A., Pedersen B., Scherer W., Shorokhov D. *Hyperconjugative Delocalization in Silatranes*. Submitted to Chem. Comm.
[27] Hoelzel M., Danilkin S., Ehrenberg H., Toebbens D. M., Udovic T. J., und H. Wipf H. F. *Effects of high-pressure hydrogen charging on the structure of austenitic stainless steels. Mat. Sci. & Eng. A.* Submitted.
[28] Hoelzel M., Gilles R., Schlapp M., Boysen H., Fuess H. *Monte Carlo simulations of various instrument configurations of the new Structure Powder Diffractometer (SPODI). Physica B.* In print.
[29] Hofmann M. *Zerstörungsfreie Materialprüfung. Technik in Bayern*, **7. Jhg**(4), (2003), 18.
[30] Hofmann M., Campbell S. J., Kaczmarek W. A., Welzel S. *Mechanochemical Transformation of α-Fe_2O_3 to $Fe_{3-x}O_4$ - Microstructural Investigation. J. Alloys Comp.*, **348**, (2003), 278.
[31] Hofmann M., Campbell S. J., Link P., Goncharenko I., Knorr K. *Pressure Induced Magnetic and Valence Transition in $YbMn_2Ge_2$. Physica B.* In press.
[32] Hofmann M., Campbell S. J., Edge A. V. J. *Valence and magnetic transitions in $YbMn_2Si_{2-x}Ge_x$. J. Mag. Mag. Mater.* In press.
[33] Hugenschmidt C., Straßer B., Schreckenbach K. *Investigation of the Annealed Copper Surface by Positron Annihilation Induced Auger Electron Spectroscopy. Radiat. Phys. Chem.*, **68**(3-4), (2003), 627–629.
[34] Hugenschmidt C., Liszkay L., Egger W. *Investigation of Laser Treated AlN by Positron Lifetime Measurements*. In: *Proceedings of the 3rd International Workshop on Positron Studies of Semiconductor Defects PSSD-2002* (Sendai, Japan, 2003).
[35] Hugenschmidt C., Kögel G., Repper R., Schreckenbach K., Sperr P., Triftshäuser W. *Positron Source Based on Neutron Capture. Radiat. Phys. Chem.*, **68**(3-4), (2003), 669–671.
[36] Hugenschmidt C., Kögel G., Repper R., Schreckenbach K., Sperr P., Straßer B., Triftshäuser W. *NEPOMUC - The New Positron Beam Facility at FRM II. Mat. Sci. Forum*. In press.
[37] Kardjilov N., S.Baechler, Basturk M., Schillinger B., et al. *New features in cold neutron radiog-*

raphy and tomography - Part II: applied energy-selective neutron radiography and tomography. *Nucl. Instrum. Meth. A*, **501**, (2003), 536–546.

[38] Keller T., Keimer B., Habicht K., Golub R., Mezei F. In: Mezei F., Pappas C., Gutberlet T. (Editors), *Neutron-spin-echo-spectroscopy*, Lecture Notes in Physics (Springer, 2003).

[39] Korsounski V., Neder R., Hradil K., Barglik-Chory C., Müller G., Neuefeind J. *Investigation of nanocrystalline CdS-Glutathione particles by radial distribution function*. *J. Appl. Cryst.*, **36**, (2003), 1389–1396.

[40] Lamago D., Dameris M., Schnadt C., Eyring V., Brühl C. *Impact of large solar zenith angles on lower stratospheric dynamical and chemical processes in a coupled chemistry-climate model*. *Atmos. Chem. Phys.*, **3**, (2003), 1981–1990.

[41] Lehmann E., Frei G., Hartmann S., Vontobel P., Brunner J., Schillinger B., Abele H., Gildemeister A., Gähler R. *Dynamic imaging with a triggered and intensified system at a high intense neutron beam*. *PSI annual report 2003*. In print.

[42] Liszkay L., Kögel G., Sperr P., Egger W., Hugenschmidt C., Triftshäuser W. *Positron Beam Splitter at the High Intensity Positron Beam in Munich*. *Mat. Sci. Forum*. In press.

[43] Longeville S., Doster W., Diehl M., Gähler R., Petry W. *Neutron Resonance Spin-Echo: Oxygen transport in crowded protein solutions*. *Lecture Notes in Physics*, **601**, (2003), 325–335.

[44] Major J., Dosch H., Felcher G. P., Habicht K., Keller T., te-Velthuis S. G. E., Vorobiev A., Wahl M. *Combining of neutron spin echo and reflectivity: a new technique for probing surface and interface order*. *Physica B*, **336**, (2003), 8.

[45] Molls M., Kneschaurek P., Waschkowski W. *Tumortherapie mit schnellen Neutronen*. *Technik in Bayern*, (4).

[46] Moze O., Hofmann M., Cadogan J. M., Buschow K. H. J., Ryan D. H. *Magnetic order in RCr_2Si_2 intermetallics*. *European Physical Journal B*. In press.

[47] Mukherji D., Strunz P., Genovese D. D., Gilles R., Rösler J. *Investigation of microstructural changes in Inconel 706 at high temperatures by in situ SANS*. *Metallurgical Transaction*, **34**, (2003), 2781.

[48] Mukherji D., Gilles R., Barbier B., Genovese D. D., Hasse B., Strunz P., Wroblewski T., Fuess H., Rösler J. *Lattice misfit measurements in INCONEL 706 containing coherent γ' and γ'' precipitates*. *Scripta Materialia*, **48**, (2003), 333.

[49] Neder R. B., Korsounski V., Hradil K., Barglik-Chory C., Müller G. *Defect structure of glutathione stabilized CdS nanoparticles*. *J. Appl. Cryst.* Accepted for publication.

[50] Niimura N., Chatake T., Ostermann A., Kurihara K., Tanaka T. *High resolution neutron protein crystallography. Hydrogen and hydration in proteins*. *Z. Kristallogr.*, **218**, (2003), 96–107.

[51] Pasini M., Kester O., Habs D., Groß M., Sieber T., Maier H.-J., Assmann W., Krücken R., Faestermann T., Schempp A., Ratzinger U., Safvan C. P. *Radioactive Ion Beam Acceleration at MAFF*. In: *Proc. 6th Int. Conf. on Radioactive Nuclear Beams (RNB6)* (Argonne, Illinois, 2003). To be published in Nucl. Phys. A.

[52] Petry W. *Advanced Neutron Instrumentation at FRM-II*. *atw 48*, **5**, (2003), 315–318.

[53] Petry W. *Neutronen für Lebensqualität*. *Technik in Bayern*, **4**, (2003), 8–10.

[54] Rajevac V., Hoelzel M., Danilkin S. A., und H. Fuess A. H. *Phonon dispersion in austenitic stainless steels Fe-18Cr-12Ni-2Mo and Fe-18Cr-16Ni-10Mn*. *J. Phys. C: Cond. Matter.* Submitted.

[55] Rekveldt M. T., Bouwman W. G., Kraan W. H., Uca O., Grigoriev S. V., Habicht K., Keller T. In: Mezei F., Pappas C., Gutberlet T. (Editors), *Neutron-spin-echo-spectroscopy*, Lecture Notes in Physics (Springer, 2003).

[56] Roth S., Burghammer M., Gilles R., Mukherji D., Rösler J., Strunz P. *Precipitate scanning in Ni-base γ/γ' superalloys*. *NIM B*, **200**, (2003), 255.

[57] Schillinger B. *Neutronen sehen, was Röntgenstrahlen verborgen bleibt*. *Technik in Bayern*, **4**,

(2003), 14–15.

[58] Schlapp M., Hoelzel M., Gilles R., Ioffe A., Brueckel T., Fueß H., von Seggern H. *Neutron image plates with low γ-sensitivity*. In: *Proceedings of ECNS* (2003). Submitted to Physica B.

[59] Schlapp M., Bulur E., von Seggern H. *Photo-stimulated luminescence of calcium co-doped BaFBr:Eu2+ x-ray storage phosphors*. *J. Phys. D: Appl. Phys.*, **36**, (2003), 103–108.

[60] Schmidt M., Hofmann M., Campbell S. J. *Magnetic Structure of Strontium Ferrite $Sr_4Fe_4O_11$*. *J. Phys.: Condens. Matter.*, **15**, (2003), 8691.

[61] Stampanoni M., Borchert G., Abela R., Rüegsegger P. *A Bragg Magnifier With Sub-µm Resolution Using High Energy Synchrotron Light*. In: *AIP Conf. Proc.*, volume 652, 112 (2003).

[62] Stampanoni M., Borchert G., Abela R., Rüegsegger P. *Nanotomography based on double asymmetrical Bragg diffraction*. *Applied Physics Letters*, **82**, (2003), 2922–2924.

[63] Stampanoni M., Borchert G., Abela R., Rüegsegger P. *Nanotomography based on double asymmetrical Bragg diffraction*. *Virtual Journal of Nanoscale, Science & Technology*, **7**(18).

[64] Stampanoni M., Borchert G., Rüegsegger P., Abela R. *Submicrometer X-ray tomography with double asymmetrical Bragg diffraction*. *PSI Scientific Report Annex VII*, 52–54.

[65] Strunz P., Gilles R., Mukherji D., Wiedenmann A. *Anisotropic SANS data evaluation: a faster approach*. *J. Appl. Cryst.*, **36**(854).

[66] Strunz P., Mukherji D., Gilles R., Rösler J., Wiedenmann A. *Small-Angle Neutron Scattering: a Tool for Microstructural Investigation of High-Temperature Materials*. *Materials Science Forum*, **426 - 432**, (2003), 755.

[67] Szytula A., Penc B., Jezierski A., Hofmann M., Campbell S. J. *Electronic Structure of $YbMn_2X_2$ (X = Si,Ge) Compounds*. *Acta Phys. Pol.*, **34**, (2003), 1561.

[68] Waschkowski W., Lange W., Böning K. *Fast Neutrons for Tumor Treatments and Technical Applications at the FRM-II*. To appear in the Compendium on Purpose-Designed Research Reactor Features of the International Atomic Energy Agency (IAEA), Vienna, manuscript 9 pages.

[69] Weidner E., Pedersen B., Frey F., C. P. *High-resolutuion x-ray studies on martian pyroxenes*. In preparation.

[70] Wronkowska A., Wronkowski A., Bukalek A., Stefanski M., Arwin H., Firszt F., Legowski S., Meczynska H., Hradil K. *Investigation of $Cd_1 - xMn_xTe$ crystals by means of ellipsometry and auger electron spectroscopy*. *Applied Surface Science*, **212**, (2003), 110–115.

[71] Wu E., Campbell S. J., Kaczmarek W. A., Hofmann M., Kennedy S. *Nanostructured $(Co_xFe_{1-x})_{3-y}O_4$ Spinel - Mechanochemical Synthesis*. *Z. Metallkunde*. In press.

[72] Wurst K., Schweda E., Bevan D. J. M., Mohyla J., Wallwork K. S., Hofmann M. *Single-crystal structure determination of $Zr_{50}Sc_12O_{118}$*. *Solid State Science*, **15**, (2003), 1491.

[73] Zeising H. *FRM-II: Uses of the neutron source for research, medicine and industry*. Conference transcript of the 5th international symposium on radiation protection of the TÜV academy (2003).

[74] Zeising H.-W. *Internal radiation protection at the "neutron research source FRM-II"*. Conference transcript of the 12th expert talk "Monitoring the environmental radiation".

Imprint

Publisher:
Technische Universität München
Neue Forschungsneutronenquelle
ZWE-FRM-II
Lichtenbergstr. 1
85747 Garching
Germany
Phone: +49 89-289-14965
Fax: +49 89-289-14995
Internet: http://www.frm2.tum.de
email: userinfo@frm2.tum.de

Editors:
J. Neuhaus
B. Pedersen

Photographic credits:
All images: TUM

Design:
B. Pedersen, TUM
J. Neuhaus, TUM
C. Simon

Typesetting(LaTeX 2_ε):
B. Pedersen, TUM